

---

**ORGANIZED MATERIALS  
FOR TRIGGERED DRUG RELEASE**

---

by

**Aoife Rock B.Sc. (Hons).**

**This Thesis is Submitted for the Degree of  
Master of Science in Chemistry by Research.**

**Supervisor: Dr. R. J. Forster.**

**School of Chemical Sciences, Dublin City University.**

**November 1998.**

## DECLARATION

---

I hereby certify that this material, which I now submit for assessment on the programme of study leading to the award of Master of Science in Chemistry by Research, is entirely my own work and has not been taken from the work of others save and to the extent that such work has been cited and acknowledged within the text of my work.

Signed: Aoife Rock ID No.: 95970738  
Aoife Rock

Date : 8/2/99

## ABSTRACT

---

The aim of this project was to investigate the possibility of achieving pH triggered drug release through electrostatic repulsion of charged functionalities within ordered polymer films. As a general introduction to the focus of the research, Chapter 1 outlines the various approaches currently in use or under development in the field of drug delivery. The two principle methods of forming monolayer assemblies and the electrochemical techniques used to characterize the structures are also described.

Chapter 2 details the investigations into the effect of pH on Langmuir monolayers of *cis*-11-Eicosenoic acid (EA). Results show that electrostatic repulsion between deprotonated acid groups causes the monolayer to expand, suggesting that pH-induced structural changes may influence the films permeability. However, due to monolayer instability, EA was unsuitable for the production of Langmuir-Blodgett films (LB) and efforts were focused on 10, 12-Tricosadiynoic acid (TDA).

Chapter 3 describes the fabrication of polymeric LB films of TDA on Indium-Tin oxide (ITO) coated glass substrates. Capacitance studies reveal that a compact monolayer with an estimated dielectric constant of 4.8 is formed. Diffusion of the hydrophilic  $\text{Fe}(\text{CN})_6^{3-}$  complex through the polymer is impeded further suggesting that the layer is compact.

Chapter 4 deals with the permeation studies conducted on Self-Assembled Monolayers of Thiocetic Acid (TA). The shorter, less dense TA monolayers were found to be permeable, in the protonated state, to the  $\text{Ru}(\text{NH}_3)_6^{3+}$  and  $\text{Fe}(\text{CN})_6^{3-}$  probes studied. Upon ionization, an apparent reduction in monolayer permeability was observed, but only in the case of the negatively charged complex suggesting that electrostatic repulsion between the charged monolayer and the similarly charged probe screened it from the monolayer interior.

There are two important conclusions to this work; First, if such an approach is to become viable it will be essential to strike a compromise between monolayer association and the degree of freedom necessary for rearrangement. Second, as a consequence of the surface charge density required to expand the film, the application of such a system will be limited by the charge of the compound to be released.

## ACKNOWLEDGEMENTS

---

Sincere thanks to my supervisor Dr. Robert Forster for all his help and support throughout the course of this project. I'd also like to extend my thanks to Dr. Dermot Diamond (for kindly allowing me the use of his LB trough) and to the ever-obliging Technical Staff of the School of Chemical Sciences.

On a more personal level, a big thanks to the postgrads and postdocs in Chemistry, both past and present, and in particular the lads in the lab (WG30) plus a few honorary members who have been great company over the years.

Last but by no means least, I wish to thank my family, who have always been there for me - I could not have done it without you!

Thanks,  
Aoife.

# CONTENTS

---

Declaration .....	ii
Abstract .....	iii
Acknowledgements .....	iv

List of Abbreviations .....	viii
List Of Symbols & Units .....	ix

## Chapter 1

### Organized Materials for Controlled Drug Release

<b>1.1 Introduction.....</b>	<b>2</b>
1.1.1 Controlled Drug Release .....	3
(i) Polymeric Delivery Systems .....	3
(ii) Colloidal Delivery Systems .....	6
1.1.2 Pulsed Drug Release .....	9
(i) Triggered Release Systems .....	9
(ii) Self-regulating Systems .....	11
1.1.3 Triggered Release from Organized Materials .....	12
<b>1.2 Monolayer Forming Techniques.....</b>	<b>14</b>
1.2.1 Langmuir-Blodgett Films .....	14
(i) The Langmuir-Blodgett Trough .....	15
(ii) Surface Pressure-Area Isotherms .....	15
(iii) Deposition of Langmuir-Blodgett Films .....	17
1.2.2 Self Assembly .....	18
<b>1.3 Electrochemical Characterization .....</b>	<b>20</b>
1.3.1 Cyclic Voltammetry .....	21
(i) The Estimation of Standard Rate Constants .....	23
(ii) The Estimation of Diffusion Coefficients .....	25
(iii) Double-layer Capacitance .....	25
Models for the Double-layer Structure .....	25
Double-layer Structure of a Monolayer Modified Surface .....	29
Evaluation of $C_{dl}$ by Cyclic Voltammetry .....	30
1.3.2 Chronoamperometry .....	31
(i) The Determination of Electrode Area .....	32
(ii) The Determination of Diffusion Coefficients .....	32
(iii) The Evaluation of $C_{dl}$ .....	33
1.3.3 Sampled Current Voltammetry .....	34
(i) The Evaluation of Standard Rate Constants .....	36

---

1.3.4 AC Impedance.....	37
(i) The Theory of AC Impedance.....	37
(ii) The Principle of Equivalent Circuits.....	39
(iii) The Interpretation of Impedance Spectra.....	42
<b>1.4 Concluding Remarks.....</b>	<b>44</b>
<b>1.5 References.....</b>	<b>45</b>

## **Chapter 2**

### **Preliminary Investigations into the Formation of Organized Polymeric Films: *Cis*-11-Eicosenoic Acid.**

<b>2.1 Introduction.....</b>	<b>49</b>
<b>2.2 Experimental.....</b>	<b>51</b>
2.2.1 Materials/Reagents.....	51
2.2.2 Monolayer Formation.....	51
2.2.3 LB Film Deposition.....	51
<b>2.3 Results &amp; Discussion.....</b>	<b>53</b>
2.3.1 Calibration with Arachidic Acid.....	53
(i) Surface Pressure-Area Isotherms.....	53
(ii) Deposition.....	53
2.3.2 Langmuir Films of Eicosenoic acid.....	55
(i) Surface Pressure-Area Isotherms.....	55
Pure Water Subphase (pH 5.5).....	55
The Effect of Subphase pH on the $\pi$ -A Isotherms.....	56
The Effect of Subphase Composition on the $\pi$ -A Isotherms.....	58
(ii) Deposition.....	61
<b>2.4 Conclusions.....</b>	<b>64</b>
<b>2.5 References.....</b>	<b>65</b>

## **Chapter 3**

### **The Formation, Polymerization and Characterization of 10,12-Tricosadiynoic Acid Monolayers.**

<b>3.1 Introduction.....</b>	<b>67</b>
3.1.1 Polymerization of Diacetylenes.....	68
3.1.2 LB Films of Diacetylenic Acids.....	69
<b>3.2 Experimental.....</b>	<b>74</b>
3.2.1 Materials/Reagents.....	74
3.2.2 Preparation of TDA Monolayers.....	74
3.2.3 Permeation Studies.....	76

---

<b>3.3 Results &amp; Discussion</b> .....	<b>77</b>
3.3.1 Surface Pressure-Area Isotherms .....	77
(i) TDA Monolayers .....	77
(ii) Effect of pH on TDA Monolayers.....	78
3.3.2 Formation of PTDA Films .....	82
(i) Deposition of TDA Monolayer Followed by Polymerization .....	83
(ii) Polymerization of TDA Monolayer Followed by Deposition .....	86
3.3.3 Capacitance Measurements .....	91
(i) Cyclic Voltammetry.....	92
(ii) Chronoamperometry .....	93
(iii) AC Impedance.....	94
(iv) The evaluation of $C_M$ and $\epsilon$ .....	96
3.3.4 Permeation Studies .....	98
<b>3.4 Conclusions</b> .....	<b>99</b>
<b>3.5 References</b> .....	<b>101</b>

## Chapter 4

### The Formation and Characterization of Self-Assembled Thioctic Acid Monolayers.

<b>4.1 Introduction</b> .....	<b>103</b>
4.1.1 Capacitance Studies .....	104
4.1.2 Permeation Studies .....	107
<b>4.2 Experimental</b> .....	<b>119</b>
4.2.1 Materials/Reagents .....	119
4.2.2 Instrumentation.....	119
4.2.3 Preparation of Gold Electrodes .....	119
4.2.4 Modification of Gold Electrodes .....	120
<b>4.3 Results &amp; Discussion</b> .....	<b>121</b>
4.3.1 Self-Assembly of Thioctic Acid Monolayers .....	121
4.3.2 Capacitance Measurements.....	122
(i) Evaluation of Monolayer Capacitance and Dielectric Constant.....	124
(ii) Determination of Surface $pK_a$ from $C_{dl}$ .....	126
4.3.3 Permeation Studies .....	130
(i) Cyclic Voltammetry.....	132
(ii) Sampled Current Voltammetry .....	137
(iii) Chronoamperometry .....	140
(iv) Effect of pH on Response of $Fe(CN)_6^{3-}$ .....	142
(v) AC Impedance .....	145
<b>4.4 Conclusions</b> .....	<b>148</b>
<b>4.5 References</b> .....	<b>150</b>

## LIST OF ABBREVIATIONS

---

<b>Abbreviation</b>	<b>Description</b>
LB	Langmuir-Blodgett
SAM	Self-Assembled Monolayer
CV	Cyclic Voltammetry/Voltammogram
CA	Chronoamperometry
SCV	Sampled Current Voltammetry
PZC	Potential of Zero Charge
PAD	Plane of Acid Dissociation
SCE	Saturated Calomel Electrode (NHE -0.2412 V)
EA	Eicosenoic Acid
TDA	Tricosadiynoic Acid
TA	Thioctic Acid
ITO	Indium-Tin Oxide
ESP	Equilibrium Spreading Pressure
GIT	Gastrointestinal Tract
RES	Reticuloendothelial System

## LIST OF SYMBOLS & UNITS

---

Symbol	Description/Units
A	i. Geometric Area of the Electrode ( $\text{cm}^2$ ) ii. Mean Area per Molecule ( $\text{\AA}^2$ )
$A_i$	Mean Molecular Area Corresponding to Initial Increase in Surface Pressure ( $\text{\AA}^2$ )
$A_0$	Limiting Molecular Area ( $\text{\AA}^2$ )
C	Capacitance (F)
$C_{dl}$	Interfacial Capacitance ( $\mu\text{F cm}^{-2}$ )
$C_{GC}$	Gouy-Chapman (Diffuse Layer) Capacitance ( $\mu\text{F cm}^{-2}$ )
$C_H$	Helmholtz (Compact) Capacitance ( $\mu\text{F cm}^{-2}$ )
$C_M$	Monolayer Capacitance ( $\mu\text{F cm}^{-2}$ )
$C_i$	Concentration of Species i ( $\text{mol cm}^{-3}$ )
$C_i^*$	Bulk Concentration of Species i ( $\text{mol cm}^{-3}$ )
$C^*$	Bulk Concentration of both Oxidant and Reductant in AC Impedance ( $\text{mol cm}^{-3}$ )
$D_i$	Diffusion Coefficient of Species i ( $\text{cm}^2 \text{s}^{-1}$ )
d	Monolayer Thickness (m)
E	Potential (V)
$E_{app}$	Applied Potential (V)
$E^{o'}$	Standard Potential (V)
$E_b$	Base Potential (V)
$E_p$	Peak potential (V)
$\Delta E_p$	Separation in Peak Potential (V)
$\Delta E$	Pulse or AC Amplitude (V)
F	Faraday's Constant ( $96485 \text{ C mol}^{-1}$ )
$f$	Fraction of Molecules in Deprotonated state
$i$	Current (A)
$i_a$	Anodic Current (A)
$i_c$	Cathodic Current (A)
$i_{dl}$	Double-Layer Capacitance Current (A)
$i_F$	Faradaic Current (A)
$i_{lim}$	Mass Transfer Limiting Current (A)
$i_p$	Peak Current (A)
$j$	$(-1)^{1/2}$
$k^0$	Standard Heterogeneous Rate Constant ( $\text{cm s}^{-1}$ )
$k_{app}$	Apparent Heterogeneous Rate Constant ( $\text{cm s}^{-1}$ )
$n$	Number of Electrons per Mole involved in a Reaction
O	Oxidant
R	i. Gas Constant ( $8.314 \text{ J mol}^{-1} \text{ K}^{-1}$ ) ii. Resistance ( $\Omega$ ) iii. Reductant

---

$R_{CT}$	Charge Transfer Resistance ( $\Omega$ )
$R_U$	Uncompensated Solution Resistance ( $\Omega$ )
$T$	Temperature (K)
$t$	Time (s)
$V$	Voltage (V)
$X$	Ratio of Current at Potential E to $i_{lim}$ in SCV
$z$	Electrolyte Charge
$Z$	Impedance Vector ( $\Omega$ )
$Z'$	Real Part of Impedance ( $\Omega$ )
$Z''$	Imaginary Part of Impedance ( $\Omega$ )
$Z_w$	Warburg Impedance ( $\Omega$ )
$\Gamma_T$	Surface Concentration ( $\text{mol cm}^{-2}$ )
$\alpha$	Transfer Coefficient
$\beta$	Distance Dependant Tunnelling Parameter ( $\text{\AA}^{-1}$ )
$\epsilon$	Relative Permittivity or Dielectric Constant
$\epsilon_0$	Permittivity of Free Space ( $8.854 \times 10^{-12} \text{ F m}^{-1}$ )
$\phi$	Electrostatic Potential (V)
$\gamma$	$(D_O/D_R)^{1/2}$
$\lambda$	Wavelength (nm)
$\pi$	i. Mathematical Constant (3.14159) ii. Surface Pressure (mN/m)
$\pi_C$	Collapse Pressure (mN/m)
$\theta$	Phase Angle (deg)
$\sigma$	Warburg Coefficient ( $\Omega \text{ s}^{-1/2}$ )
$\tau$	i. Experimental Timescale (s) ii. Sampling Time in SCV (s)
$\tau'$	Time Delay before Current Sampling in SCV(s)
$\upsilon$	Scan Rate ( $\text{V s}^{-1}$ )
$\omega$	Angular Frequency, $2\pi F$ ( $\text{s}^{-1}$ )
$\xi$	Dimensionless Rate Parameter in SCV
$\psi$	Dimensionless Rate Parameter in CV

---

# **CHAPTER 1**

## **Organized Materials for Triggered Drug Release**

---

## 1.1 INTRODUCTION

Each drug has a concentration range above which it is toxic, but below which it is ineffective. Therefore, from a therapeutic point of view, the drug should be delivered at a rate that would give the optimal therapeutic concentration while minimizing unfavourable side effects.

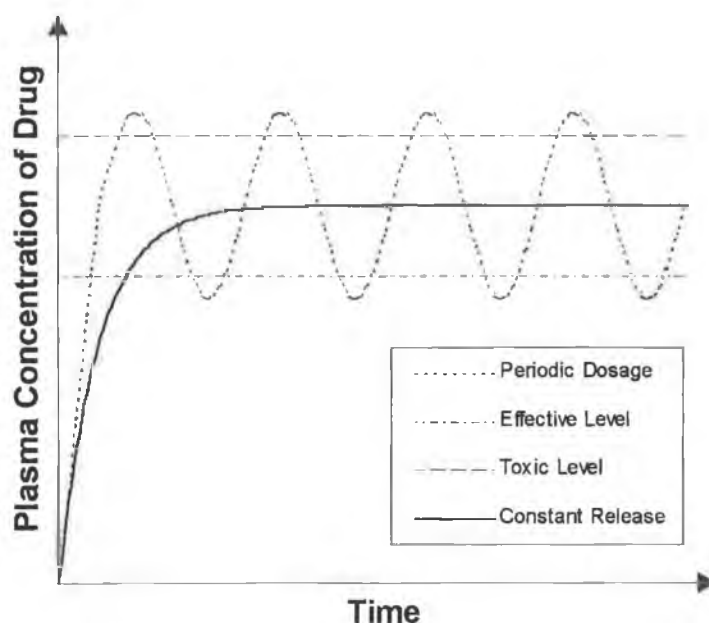


**Figure 1.1** Plasma concentration versus time for constant-release systems and traditional periodic dosing.

However, traditional drug therapies result in oscillating blood drug levels as the drug concentration rises, peaks and declines causing alternating periods of ineffectiveness and possible toxicity. For most drugs, conventional methods of formulation are usually quite effective. However, some drugs are unstable and toxic, possess a narrow therapeutic range, exhibit extreme solubility problems, require localization to a particular site in the body, require strict compliance or long-term use. In such cases, a method of continuous administration of the drug is desirable to maintain fixed plasma drug levels. Anticancer drugs, for example, possess quite a narrow therapeutic margin and when delivered by conventional methods produce adverse systemic reactions. By maintaining plasma concentration in the therapeutically

appropriate range the harmful side effects can be reduced. In recent years there has been intensive interest in developing more sophisticated drug delivery systems with improved safety and efficacy. The costs involved in the research and development required to bring new drugs to the market are so prohibitive that novel approaches that could reduce the risks associated with currently available drugs and develop more effective means of drug delivery are of great importance.

### **1.1.1 Controlled Drug Release**

Research in the area of drug delivery focused initially on controlled release systems which deliver the drug at a predetermined rate (constant if desired) over extended periods (+12 h.). These sustained release preparations maintain the drug concentration within the desired therapeutic range. Generally controlled release systems are based on either polymers or colloids.

#### **(i) Polymeric Delivery Systems**

Controlled release systems constructed using polymers, are available in a variety of formulations. The delivery systems are classed according to the mechanism by which the polymer releases the drug, that is by diffusion control, chemical control or solvent activation.<sup>1</sup>

There are two types of diffusion controlled systems; reservoir systems, where the drug is surrounded by a non-degradable, rate-limiting, polymeric membrane or capsule, and matrix systems, where the drug is uniformly distributed within the polymer matrix. If the polymer is biodegradable then the release mechanism is both diffusional and chemical. In the case of nonporous polymeric films the drug diffuses through the polymer phase. Microporous polymers allow the drug diffuse through water filled pores. In each case, release rates are controlled by the nature of the polymeric material.

In chemically controlled systems, water or enzymes either degrade the polymer which encapsulates the drug (erodible systems), or they cleave the bond between the drug and the polymer backbone (polymer-bound systems). Erodible polymer systems display either surface erosion characteristics,<sup>2</sup> where the release rate is proportional to

the erosion rate, or bulk erosion characteristics<sup>3</sup> where the release rate depends on the matrix volume. The lability of the bonds and the hydrophobicity of the monomers influence the rate of polymer degradation. Therefore, by forming copolymers with varying ratios of monomers, different degradation rates and release rates can be achieved.

In solvent activated systems, the drug is entrapped in the polymer until external solvent causes swelling of the polymer or water imbibement creates sufficient osmotic pressure to force the drug's release. Osmotically controlled release systems use either the drug itself or an accompanying salt as the osmotic agent.

In addition to the above mechanisms, there are ways in which the drug release can be augmented. Some polymer systems, for example, can be externally activated to release more drug when required by magnetism<sup>4</sup> or ultrasound.<sup>5</sup>

A number of sustained release systems have been investigated over the past decade, some have reached the market place and are now established methods of drug delivery, others are still in the developmental stage.<sup>6, 7, 13-15</sup> Specially-designed tablets which enable the constant release of the drug as it passes through the gastrointestinal tract (GIT) have been developed. The osmotic tablet,<sup>6</sup> has been shown to release a number of drugs effectively e.g., nifedipine used in treating heart disease. Various approaches have been employed to sustain drug release, for example binding of charged drugs to ion-exchange resins,<sup>7</sup> or the encapsulation of drugs within erodible polymers.<sup>1</sup> These systems provide constant release of the drug over longer periods and so reduce the number of pills needed to be taken. Bio or muco-adhesive systems that affect transit time of the drug as it passes through the GIT are also of interest. Bioadhesive polymers fix the system at a specific location of the GIT, where the drug may be preferentially absorbed or induce local therapeutic effects. By interacting directly with the intestinal mucosa at the site of adhesion drug absorption is also improved. The mucoadhesive polymer polycarbophil led to the improved intestinal absorption of the peptide drug DGAVP *in vivo*.<sup>8</sup> However, long-term bioadhesion by means of non-specific mucoadhesion is limited by the rapid turnover of the intestinal mucus, and so the concept of specific (receptor-mediated) adhesion is currently under study.

Various drug coatings have been used to by-pass certain parts of the GIT and hence certain peptidases. Coatings composed of acid-resistant acrylic resins by-pass

the stomach and release the drug in the small intestine.<sup>9</sup> Polymer coatings containing azoaromatic groups form tough water impervious films that remain intact in the stomach and small intestine, but which are reduced by indigenous microflora in the large intestine.<sup>10</sup>

Biodegradable polymers, e.g., polyesters<sup>11</sup> and polyanhydrides<sup>12</sup> have been of great interest in controlled release technology. The ability of these polymers to be reabsorbed by the body eliminates the need for surgical removal of the device when drug delivery is complete. Injectable nanospheres and implants have been developed from biodegradable polymers for use in slow release systems.<sup>13</sup> Polymeric nanospheres when injected intravenously exhibit increased blood circulation times compared to vesicular carriers. When injected into muscle or fat tissue the nanospheres release drugs over long periods. Implants have been used for the slow release of drugs at the target site.<sup>14, 15</sup> By using biodegradable implants a high local concentration can be achieved without the dissipation of the drug throughout the whole physiological system, thereby reducing systemic toxicity and increasing drug potency.<sup>16</sup>

Transdermal patches have been developed to slowly deliver drugs through the skin in small doses. Since only a limited number of drugs possess the appropriate permeability characteristics (i.e., a significant water and oil solubility and a low molecular weight), various procedures are currently under study to enhance transdermal drug delivery (e.g., combining the drug with chemical enhancers, or by using physical means such as phonophoresis (the application of ultrasound to facilitate permeation through the skin), iontophoresis (the use of electric current to force the flux of ionized drugs through existing pathways in the skin, i.e., hair follicles and sweat glands) and electroporation (the use of short pulses, a few milliseconds in length, with an intensity of a few hundred volts to open additional pores). Avoidance of hepatic first-pass metabolism is the essential benefit of transdermal delivery.<sup>17</sup> However, there are disadvantages associated with the transdermal route such as the high inter-subject variability in skin permeation. Burning and heat denaturation can also be problematic when using iontophoresis and phonophoresis, and strict control over pH and ionic strength is required for iontophoresis.

## (ii) Colloidal Delivery Systems

Colloidal drug delivery systems are vesicular dosage forms in the nanometre size range.<sup>18</sup> Liposomes are the most widely studied of these vesicles. They consist of one or more concentric spheres of lipid bilayers surrounding aqueous compartments. Since their discovery in the 1960s, liposomes have been considered as ideal candidates for drug delivery. They are capable of loading hydrophilic, hydrophobic and amphiphilic drugs in their aqueous and bilayer phases and are composed of materials which are biocompatible, biodegradable and normally non immunogenic. It was hoped these vesicles would protect the encapsulated drug from enzymatic degradation and other deactivation processes.

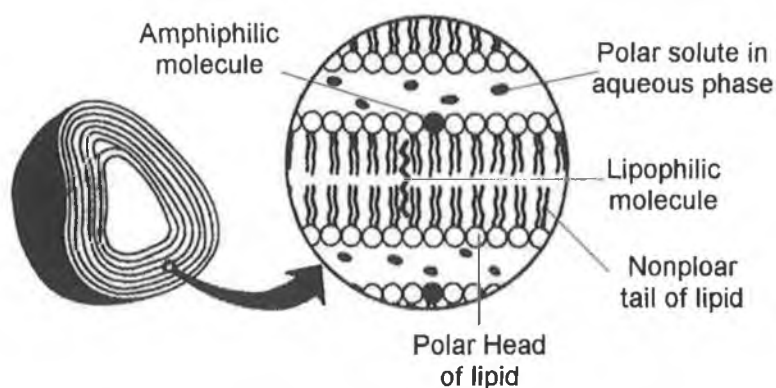


**Figure 1.2** Illustration of liposome showing interaction with hydrophilic, lipophilic and amphiphilic drugs. Adapted from Ref. [19].

Liposomes were first designed as drug carriers for targeting purposes, concentrating the drug at the site of action while simultaneously diverting it from sites where it might be toxic, e.g., teratogenic compounds used to treat cancers are steered clear of the reproductive system. However, the rate at which liposomes are eliminated by the reticuloendothelial system (RES), (within second/minutes of intravenous injection) presented a major obstacle for the delivery of drugs to cells and tissues of organs other than the RES.<sup>20</sup> In order to accumulate liposomes in areas other than the liver and spleen they must be actively targeted. Targeting is based on ligand-receptor chemistry and is achieved by covalently binding the appropriate ligand to the liposome surface. However, binding of the liposome to the target site depends on it remaining in the circulation system long enough to encounter the target site and

so uptake by the RES still posed a problem. Efforts have been made to reduce the affinity of liposomes to the RES by varying the lipid composition and liposome size. Optimization of these two parameters prolongs circulation times and enhances the active targeting of liposomes to other areas.<sup>21</sup> Stealth liposomes that possess a protective carbohydrate coating have been developed.<sup>22</sup> The coating mimics the surface of red blood cells and hence avoids detection and uptake by the RES.

The colloidal instability of liposomes in the circulating blood has prompted many groups to investigate the use of polymeric liposomes made from synthetic lipids which have polymerizable groups in their fatty acid chains or polar headgroups.<sup>23</sup> Unfortunately, the enhanced stability offered by these structures is at the expense of biodegradability, and so precludes them for use *in vivo*. Initial attempts to prepare biodegradable polymerized liposomes used reversibly polymerizable dimercaptolecithin.<sup>24</sup> Stable yet biodegradable polypeptide vesicles, formed by the polycondensation of long-chain  $\alpha$ -amino acid esters may also prove to be suitable carriers for the systemic delivery of drugs,<sup>25</sup> the possibility of designing systems based on polypeptides which degrade only in the presence of certain enzymes would be extremely advantageous in terms of specific release and biocompatibility.

Another problem associated with liposomes, is that when the liposome binds to its target cell it has to cross the vascular epithelium. There are several mechanisms by which liposomes may be internalized but unfortunately the major pathway results in their degradation, following internalization by the lysosomes of the cell. To overcome this difficulty, liposomes with various types of triggered release mechanisms have been developed, e.g., pH-sensitive, temperature-sensitive or target-sensitive liposomes. The released drug can then enter the cell by normal transport processes. However extracellular release, subjects the drug to possible metabolic degradation prior to cellular uptake. Also, the changes in lipid composition necessary to prolong circulation times, often result in a reduced sensitivity to the appropriate environmental change. Thus, liposomes with both a reduced affinity to RES, and a target-triggered release mechanism, have yet to be developed.

Liposomes have been successfully used as sustained release dosage forms when injected subcutaneously. When used topically, liposomes are thought to influence the transport of some drugs through the skin compared with traditional creams. Some

studies show an increase in flux,<sup>26, 27</sup> although in many studies no increase in drug transport was observed.<sup>28, 29</sup> Investigations into whether intact liposomes can actually penetrate into the stratum corneum have been carried out. Again the results varied, some reports showed penetration into the skin,<sup>18</sup> the rate of which depended on the physiochemical properties of both the liposome and the drug. Others showed that while there was no penetration, the deposition of drug was facilitated when incorporated in the liposome.<sup>30</sup> Since the conditions varied enormously from case to case, one can only conclude that the interaction of liposomes with the stratum corneum, depends on the liposome size, lamellarity and composition (i.e., the type of phospholipids used).

The use of liposomes in oral formulations has also been investigated. Many drugs, both hydrophilic (e.g., insulin<sup>31</sup>) and lipophilic (e.g., indomethacin<sup>32</sup>) were studied. It was envisaged that liposomes could possibly protect the drugs from luminal degradation and transfer them from the mucosal to the serosal side of the GI barrier, avoiding intracellular degradation by direct release into the blood/lymph. This would significantly enhance the systemic bioavailability of poorly absorbed or labile drugs, e.g., peptides and hydrophilic antibiotics, following oral administration. However, to date the oral administration of liposomes has not been feasible since they are not stable enough to resist luminal or intracellular degradation. The research has shown that liposomes are sensitive to bile salts and generally release their contents in the intestine.<sup>33</sup> In the rare event that they escape luminal destruction, studies have shown that only a small portion become endocytosed by the intestinal cells. Following endocytosis, the liposomes are digested and their contents released intracellularly. There has been no evidence to suggest that intact liposomes can gain access to the blood/lymph.<sup>34</sup>

By utilizing sustained release formulations it is possible to achieve invariant systemic drug concentrations. However, in certain situations it is not beneficial to continually release the drug, therefore attempts have been made to develop more advanced delivery systems that release the encapsulated drug in response to a specific physical or chemical stimulus. These systems supply the drug on demand and so overcome the tolerance problems associated with constant release. Stimuli-responsive systems may be externally modulated or self-regulated. The self-

regulatory system approaches the ideal delivery system. By releasing the drug in response to physiological signals, they mimic the way that the body regulates metabolite concentrations in response to other metabolites.

### **1.1.2 Pulsed Drug Release**

Stimuli-responsive polymers are currently receiving considerable attention as materials for the development of intelligent drug delivery systems. Using devices constructed from these materials, external regulation of drug release is feasible. More sophisticated, self-regulatory systems are capable of modulating drug delivery in response to physiological conditions. These pulsatile systems increase the therapeutic efficacy of the drug, by decreasing side effects, dosage and frequency of administration.

#### **(i) Triggered Release Systems**

Stimuli-sensitive polymers experience changes in either their structure or their chemical properties in response to changes in environmental conditions or external forces. A number of stimuli, including pH, temperature, magnetic fields, electrical currents, and ultrasound have been shown in experimental systems to provide increased delivery. However, most of them require either a nondegradable polymer or the incorporation of an additional substance (e.g., magnetic beads, enzymes) within the polymer matrix.

By introducing magnetic beads into the polymer matrix and applying a magnetic field, the beads can be made to squeeze the drug out through the polymer.<sup>35</sup> Parameters that affect the release rate include the strength and frequency of the applied magnetic field, the polymer composition, and the strength and orientation of the polymer-embedded magnets.

The use of ultrasound to externally augment drug release rates on demand has also been explored. Reversible increases in release rates of biodegradable and nonerodible polymer systems were observed.<sup>5</sup> The release rates increased in proportion to the intensity of the ultrasound. Ultrasonic waves cause thermal effects and induce temporary alterations<sup>36</sup> in the physical structure of the skin thereby increasing drug absorption. However, the physiological effect of long-term exposure

to ultrasound has yet to be examined before ultrasound-responsive delivery systems become practical.

A novel polymeric system,<sup>37</sup> which rapidly changes from a solid state to a liquid state in response to small electric currents that disintegrate the solid polymer complex into two water-soluble polymers, has been developed.

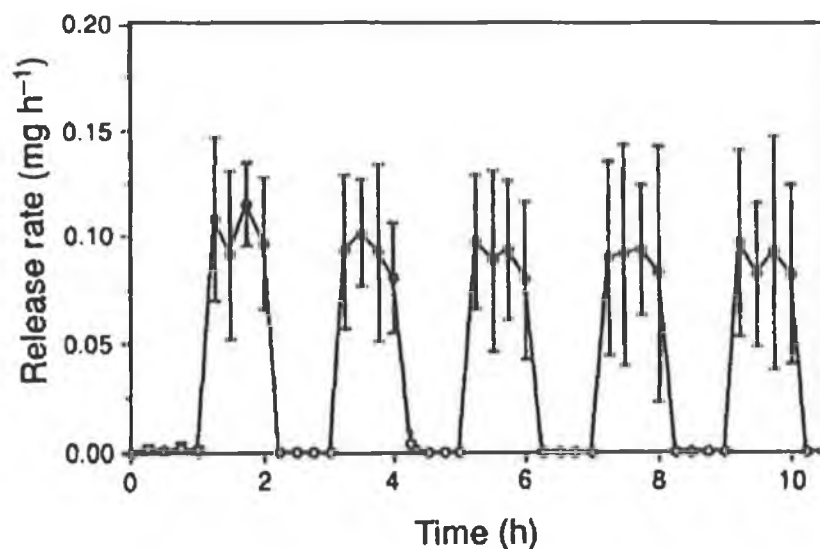


Figure 1.3 Insulin release rate (normalized to mg h<sup>-1</sup> per 160 mg device) from insulin-loaded matrix of poly(ethyloxazoline)-poly(methacrylic acid) complex with the application of step-function electric current in 0.9% saline solution. ●, current on (5mA); O, current off. Taken from Ref. [37].

When the current is applied, hydroxyl ions produced by electrolysis of water increase the local pH. This process causes a disruption in the hydrogen bonding between the two polymers causing the complex to disintegrate. Using this system the modulated release of insulin was achieved.

Changes in physiological temperature or pH are often associated with many diseases, e.g., tumor growth is accompanied by an abnormal rate of metabolism which leads to unusual local temperatures and pH. Many researchers have exploited these stimuli to trigger drug release. pH-sensitive polymer matrices contain weak acid or base functionalities which on protonation cause the polymer to swell by coulombic repulsion.<sup>38</sup> This swelling results in the increased permeability of the encapsulated drug. The temperature-responsive swelling and shrinking of hydrogels has been used

to achieve a similar on-off regulation of drug release.<sup>39</sup> However, before release systems based on environmental changes can become viable delivery devices, the pH or temperature sensitivity must be enhanced to exploit the small changes that physiological abnormalities produce.<sup>40</sup> Changes in pH are also encountered on passage through the digestive tract and a number of companies are working on formulations which release drugs only in the colon (e.g., for treating Crohn's disease). Drug targeting to the colon can be achieved by coating granules with a pH-sensitive polymer. The coating material should dissolve only at pH 7.5 whereafter the drug is released. Drug release has been achieved by exploiting the pH sensitivity of partially esterified copolymers of methyl vinyl ether and maleic anhydride. Disks of the copolymer containing hydrocortisone were coated with a hydrogel containing an immobilized urease. When exposed to urea the enzyme produce ammonium hydroxide and carbonate which raised the local pH and accelerated the polymers surface erosion and drug release.<sup>41</sup>

## **(ii) Self-regulating Systems**

Often, ailments are accompanied by changes in concentration or the appearance/disappearance of more subtle chemical markers. Many groups have exploited enzymes as transducers which synchronize the matrix response to the marker of interest. For example, glucose-dependent insulin release has been achieved by incorporating the enzyme glucose oxidase into pH-sensitive polymer membranes.<sup>42</sup> The gluconic acid, produced by the glucose oxidase catalyzed oxidation of glucose, lowers the pH within the polyamine membrane. Electrostatic repulsion between the positively charged amine groups causes the membrane to expand thereby increasing the rate of insulin delivery. As the physiological glucose concentration decreases (i.e., in response to the released insulin), the membrane contracts and the rate of insulin delivery decreases. In this manner, the membrane controls the insulin delivery rate in response to the glucose concentration. In a similar approach, the pH-dependent solubility of insulin controls its release.<sup>43</sup> The decrease in pH in the polymer microenvironment, due to the enzyme catalyzed formation of gluconic acid, causes an increase in the solubility of the encapsulated insulin, which in turn increases

its release rate. Obviously, factors such as the stability of the insulin and enzymes and the response time of the system will dictate how well these systems work in practice.

The above mentioned enzyme-responsive polymer delivery systems are important examples of intelligent drug delivery systems. They are capable of sensing when and how much of the encapsulated drug to release. However, the rupture of a self-regulatory membrane could potentially cause overdose. Therefore, precautionary measures such as the incorporation of a tough outer-guard membrane or the subdivision of the reservoir will be required if usable devices based on these membranes are to be developed.

### **1.1.3 Triggered Release from Organized Materials**

The objective of this project is to develop advanced encapsulation materials capable of regulating drug release. Of particular interest is the fabrication of drug coatings from organized high-density polymer films. The structure of the polymer film, formed by the polymerization of two-dimensional molecular assemblies, is precisely controlled at a molecular level, unlike the highly disorganized and entangled structure of conventional polymers. Very often incomplete mixing or encapsulation can alter concentration gradients and change the biodegradation and release rates of conventional polymers. The problems of irreproducibility and localized/variable release rates typically associated with these systems, could be effectively eliminated by employing ordered polymer systems of uniform thickness. Colloidal systems by nature are quite ordered structures but unfortunately their leaky, low drug carrying capacity has hampered their use in many situations. An ordered polymer film that prevents diffusion of the encapsulated drug when it is not required but which is capable of undergoing a reversible change in permeability would revolutionize drug delivery. The reversible change in film permeability, brought about by a rearrangement in film structure on exposure to a specific external stimulus, would ultimately result in the release of the encapsulated drug. In order to trigger structural changes within the film, the ordered polymer is required to have a built-in sensitivity to its chemical environment. For example, if fabrication of films that undergo pH induced structural change is desired, then the monomers used to produce such films

must contain either acid or amine functionalities that will deprotonate/protonate depending on the pH of the contacting solution. By designing films capable of switching the release of an encapsulated drug on and off in a controlled manner, it ought to be possible to maintain the drug concentration within the patient close to its minimum effective level. Two distinct techniques are used to form these highly organized materials. The first approach involves polymerizing monolayers formed by the Langmuir-Blodgett technique, the second involves the self-assembly of ordered monolayers.

## 1.2 MONOLAYER FORMING TECHNIQUES

The two principle methods used to form monomolecular films, are the Langmuir-Blodgett and Self-Assembly methods.<sup>44, 45</sup> In 1937 Irvine Langmuir and Katharine Blodgett<sup>46, 47</sup> developed a procedure for transferring water-surface monolayers to solid substrates. Using the Langmuir-Blodgett (LB) technique they were able to form molecular assemblies with controlled thickness and well-defined orientation. Later in 1980, Sagiv<sup>48</sup> demonstrated that monolayers like those formed by Langmuir and Blodgett could be produced by utilizing the specific interaction between the amphiphilic molecules and a substrate. Although the early work on silanes led to unstable layers due to hydrolysis, more recently thiol and disulphide based systems have led to a renewed interest because of their long-range order and stability. Through the self-assembly of these compounds, the construction of stable, ordered monolayer structures on solid surfaces with controlled chemical features, such as charge and hydrophobicity is possible.

### 1.2.1 Langmuir-Blodgett Films

Langmuir films consist of surfactant molecules that assemble at the pre-existing interface between two phases, typically water and air, that differ in their degree of hydrophilicity. The interface can be either liquid-liquid or liquid-gas, water is the most hydrophilic medium, while the most hydrophobic media are gases. Langmuir-Blodgettry is the technique developed to transfer the monolayer film assembled at the interface to a solid substrate. Good monolayer-forming materials are required to be amphiphilic in nature. Amphiphilic molecules contain two distinct regions, one hydrophilic and the other hydrophobic. The hydrophilic part is attracted to polar media (e.g., water) and the forces acting on it are predominantly ionic. The hydrophobic part is less water soluble and the forces acting on it are predominantly van der Waals. Surface-active molecules are trapped at the interface as a result of these two very different types of interactions within the one molecular structure.

### **(i) The Langmuir-Blodgett Trough**

A typical Langmuir-Blodgett (LB) trough consists of a compartment with a movable barrier enclosing the Langmuir film and enabling the monolayer to be compressed on the subphase surface. The body and the barrier are made from teflon. The compartment contains a pressure sensor and a removable dipper mechanism. The basis of pressure measurement is a Wilhelmy plate suspended at the air-liquid interface. The surface tension of the liquid, which is defined as the work required to expand the surface isothermally by unit area, pulls the Wilhelmy plate into the bulk of the subphase. The force acting on the paper is measured by means of an electronic microbalance. The tendency of surface-active molecules to accumulate at the interface favours expansion of the interface and lowers the surface tension. This reduction in surface tension is known as surface pressure, and is expressed as milliNewtons per metre, mN/m. For any given substance, it depends on the area of water surface divided by the number of molecules. Therefore, it is possible to monitor surface pressure as a function of the area occupied per molecule providing that the number of molecules deposited on the surface is known. Characteristics of a monolayer on the subphase surface are studied by measuring the changes in surface tension upon monolayer compression. A plot of surface pressure as a function of area occupied per molecule, known as a  $\pi$ -A isotherm is recorded. The shape of this isotherm is characteristic of the molecules making up the film. It often contains sharp bends or kinks indicative of phase transitions within the two-dimensional layer.

### **(ii) Surface Pressure-Area Isotherms**

In a typical experiment, a dilute solution ( $0.1-1 \text{ mg ml}^{-1}$ ) of an amphiphilic molecule in a volatile water immiscible solvent such as chloroform, is introduced dropwise onto the surface of a polar liquid subphase, with the aid of a microsyringe. The subphase is usually ultra-pure water, although other high surface tension liquids such as ethylene glycol, glycerol and mercury have been used. The solvent evaporates to leave a monolayer of molecules which is regarded as a two-dimensional gas, where distances between the molecules are large and interactions are small. A surface monolayer will only be achieved if the hydrophilic and hydrophobic

interactions in the molecules are balanced. No hydrophobic part results in the molecule being dragged into the subphase and dissolved. Molecules with no hydrophilic groups tend to form thicker multilayer films on the subphase surface.

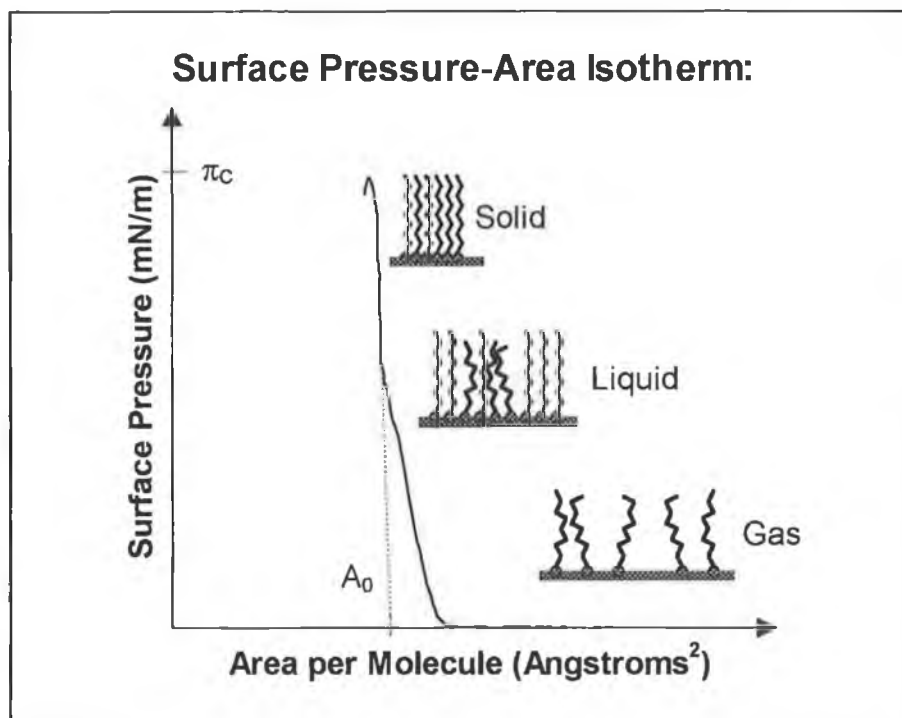


**Figure 1.4** Typical Surface pressure-Area isotherm showing molecular orientations.

As illustrated in Figure 1.4, following initial deposition onto the subphase surface, the molecules behave like a two-dimensional gas. As the film is gradually compressed some ordering takes place and the molecules behave as a two-dimensional liquid. In the liquid phase the monolayer is coherent, except that the molecules have more degrees of freedom than in the solid phase due to the larger areas occupied. With continued compression, the increased surface pressure causes additional ordering and the molecules are orientated in a quasi 'solid' state. In the solid state the molecules are closely packed and uniformly orientated. The solid state is characterized by a steep approximately linear relationship between surface pressure and area per molecule. By extrapolating this line back to  $\pi=0$  we obtain a value for the limiting molecular area,  $A_0$ . Further compression of the barrier results in the monolayer collapsing due to mechanical instability and film incompressibility. The forces exerted upon the monolayer become too strong for confinement in two dimensions and so

molecules are ejected out of the monolayer plane. The collapse pressure ( $\pi_c$ ) is the maximum pressure to which the monolayer can be compressed without detectable expulsion of the molecules from the Langmuir film. Its value depends on the chemical substance, temperature and the rate of compression. Once the collapse pressure is reached the film irreversibly loses its monomolecular form. Improved film quality can be obtained by annealing the film, i.e., compressing and expanding it a number of times below  $\pi_c$ . This encourages more efficient packing and a shift to lower molecular areas is observed.

### **(iii) Deposition of Langmuir-Blodgett Films**

Depositing an LB film involves attaching a suitable substrate to the dipper which is then mechanically lowered into the subphase breaking through the compressed Langmuir film. Provided the hydrophobicity of the substrate surface is correct the Langmuir film attaches itself to the substrate coating it with a monomolecular layer. The compressed monolayer can be transferred to a variety of solid substrates although most depositions have involved hydrophilic substrates. A hydrophobic substrate (e.g., silanized glass, polystyrene, freshly etched silicon) will result in deposition on the first immersion, the hydrophobic groups of the molecule adhering to the substrate. With a hydrophilic substrate (e.g., glass, quartz, aluminium) no deposition will occur until the first immersion since the hydrophobic groups are repelled by the substrate as it is immersed in the water. Subsequent monolayers can be deposited thus allowing multilayer films to be fabricated. For good deposition, the monolayer must be kept at constant surface pressure when transfer is occurring. This is achieved by closing the barrier under pressure control while dipping takes place. In some systems reactive deposition occurs in which the molecules adsorb spontaneously on the substrate at the same speed that a new clean area becomes available as a result of substrate withdrawal.

## 1.2.2 Self Assembly

Self-assembly is defined as the formation of orientated monolayer films on a surface by the spontaneous adsorption of molecules from a solution directly onto a solid substrate and stabilizing lateral interactions, e.g., alkyltrichlorosilanes on glass, alkylcarboxylic acids on aluminium, alkylthiols on gold, organic disulphides on gold. By introducing various functional groups at the terminal position of the surface-active molecule, monolayer systems with functional surfaces can be fabricated. The main advantage of this technique is that the only process required is simply the submersion of the appropriate substrate in a dilute solution ( $\sim 1$  mM) of an active surfactant in an organic solvent. Immersion times vary from several minutes to several days depending on the surfactant. Bonding interactions, registry between the head group and the substrate, and intermolecular interactions between adjacent adsorbate molecules all influence the kinetics of monolayer assembly. The approach works well for molecules with a strong binding functionality and a structure that packs well in two-dimensions. Another advantage of this method is that self-assembly takes place on surfaces regardless of their shape and is therefore not restricted to the large, flat substrates typically used in LB transfer experiments. The adsorption is thought to be a two-phase process, the rapid physisorption of an imperfect monolayer followed by a slower process of consolidation and chemisorption. As the head group chemisorbs onto the surface the strong exothermic molecular-substrate interaction pins the head group to a specific site on the surface through a chemical bond that can be covalent, polar covalent or ionic. As a result of the exothermic head group-substrate interactions, the molecules try to occupy every available binding site on the surface. The spontaneous molecular adsorption brings the molecules close enough together to allow the short range, dispersive, London-type, van der Waals forces to become important. When a polar bulky group is substituted into the alkyl chain long-range electrostatic interactions occur as well, in some cases these interactions are energetically more important than van der Waals interactions.

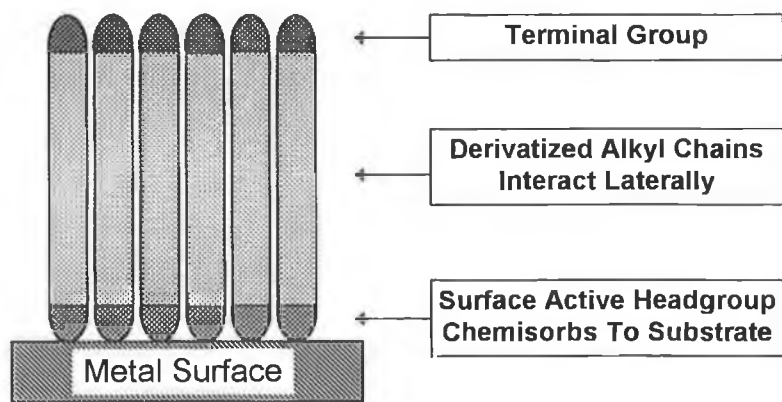


**Figure 1.5** General features of a Self-assembled monolayer.

The main disadvantage associated with self-assembly is that it is more limited when compared to the LB technique, which despite being tedious and placing significant restrictions on the molecules suitable for monolayer formation, has been applied to a broader range of systems. Self assembly relies on the specific interaction between the headgroup and the substrate, and so is limited to a certain class of compound e.g., mercaptans on gold, although with the advances in organic chemistry, the synthesis of new compounds with the required functionality is increasingly possible. Another drawback associated with self-assembly, is that precise control over the macroscopic composition of mixed monolayers is difficult, since both the kinetics of adsorption and the free energies of adsorption dictate the monolayer composition. Lastly the formation of multilayers through self-assembly is considerably more complex than the facile manner in which LB multilayers can be prepared.

## 1.3 ELECTROCHEMICAL CHARACTERIZATION

Electrochemical studies on monolayer systems deposited or self-assembled on conducting substrates can provide valuable information regarding their structure and composition. Various electrochemical techniques have been employed to probe properties such as permeability, stability and uniformity. Capacitance measurements have been used to study permeability of these layers to small ions and solvent molecules.<sup>49</sup> Techniques such as cyclic voltammetry and AC impedance have been used to determine the presence of structural defects, as well as their size and distribution.<sup>50</sup> By observing the electrochemical behaviour of suitable electroactive species in solution the microscopic integrity of the electroinactive monolayer assembly can be assessed.<sup>51</sup> In addition to the general characterization of monolayers by electrochemical methods, it is possible to monitor changes in the permeability of the layer to complexes through the study of electron and mass transfer processes. Hence, the process of molecular/drug release can be simulated at the modified electrode. Rather than looking at the diffusion of molecules through monolayers/membranes assembled on permeable supports (e.g., cellulose acetate), one can look at the diffusion of electroactive molecules through monolayers assembled at conducting supports and their subsequent oxidation or reduction. The two very different approaches yield the same information regarding the permeability of the monolayer, but electrochemistry allows one to directly determine changes in permeability by studying the shape and magnitude of the current response observed at the underlying electrode. For example, by monitoring parameters, such as the standard heterogeneous rate constant,  $k^0$  (a measure of the kinetic facility of a redox couple), and the diffusion coefficient,  $D$  (the rate of molecular diffusion to the electrode), of a solution phase species, it is possible to assess how changes in pH may affect monolayer permeability. A brief description of the electrochemical techniques used to probe the monolayers formed in this study follows.

### 1.3.1 Cyclic Voltammetry

Cyclic voltammetry is a controlled potential technique where the potential at the electrode is swept forward and backward between two fixed values. The potential is varied linearly with time and at a predetermined value of the applied potential the scan direction is reversed. The current that flows through the cell is continuously measured during the forward and reverse scans. The analysis of the resulting current-voltage response, and its dependence on scan rate, provides considerable information concerning the redox couple such as its formal potential or the standard rate constant for electron transfer.

When studying the oxidation and reduction of species in solution the scan rate,  $\nu$ , is usually in the range 0.001-100 V s<sup>-1</sup>. The lower limit is determined by the need to maintain the total time of the experiment between 10-50 seconds (the experimental timescale  $\tau = RT/F\nu$ ; where R is the Gas constant, T is temperature in Kelvin and F is Faraday's constant), which prevents mass transfer by convection. The lower limit on the timescale is determined by the double layer charging current and the uncompensated solution resistance, which distort the voltammetric wave considerably at high scan rates. Since the potential is continually changing during the course of the experiment, a charging current,  $i_{dl}$ , that is proportional to  $\nu$  continually flows. The Faradaic current,  $i_F$ , which is measured from a baseline of charging current, varies with  $\nu^{1/2}$ . Clearly, from the ratio of  $i_{dl}$  to  $i_F$ , the charging current becomes increasingly important at high values of  $\nu$ , and limits the maximum useful scan rate. The uncompensated solution resistance,  $R_U$ , is the fraction of solution resistance that exists between the reference and working electrodes. For a reference electrode placed anywhere but exactly at the electrode surface this results in an uncompensated potential drop,  $iR_U$ . If  $R_U$  is large enough that the ohmic drop ( $iFR_U$ ) is appreciable (i.e., a few mVs) then the applied potential will not be the desired value, but instead will be  $E_{app} = E + iR_U$ . This results in a flattening of the voltammetric wave and a shift in the peak potential (toward more negative potential for the cathodic peak, and more positive potential for the anodic peak). Since the Faradaic current increases with  $\nu^{1/2}$ , the larger the scan rate the larger the shift in peak potential.

The current during the first cycle is often quite different to that of subsequent cycles, both the anodic and cathodic peaks change slightly in shape and decrease until an equilibrium is established and the current traces the same line as a function of potential. Quantitative data is extracted from the first few cycles. However, since kinetic information is obtained from the scan rate dependence of the peak current and potential, care must be taken to ensure that the  $iR_U$  potential drop does not become significant.

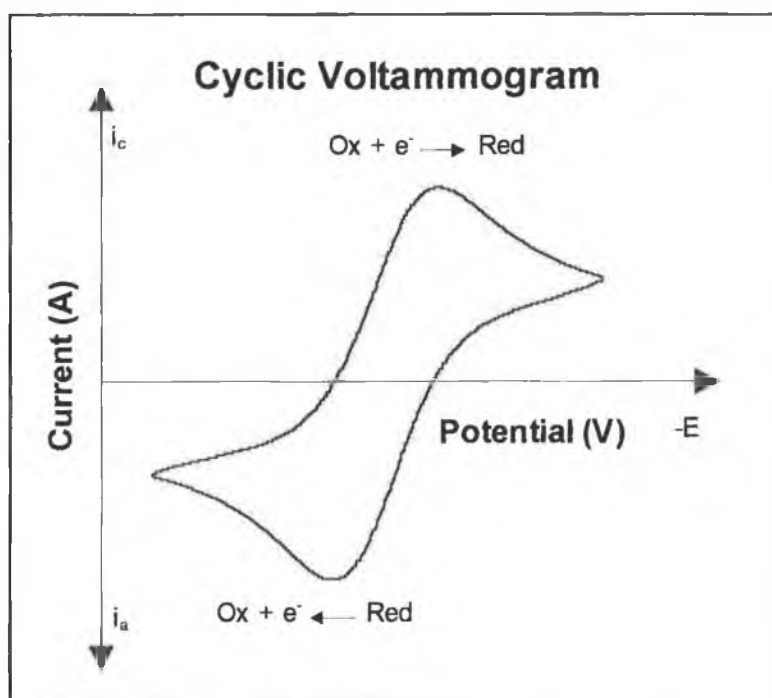


Figure 1.6 Typical cyclic voltammogram.

For rapid charge-transfer process (reversible systems), the anodic and cathodic peak potentials are separated by  $2.3 RT/nF$  V or  $59/n$  mV at 25 °C where  $n$  is the number of electrons transferred in the reaction. A quasi-reversible system shows greater separation in peak potentials and more rounded peak shapes. For irreversible systems (slow charge-transfer processes) the anodic and cathodic peak potentials are separated by several hundreds of mVs and in some cases one branch of the CV is absent.

### (i) The Estimation of Standard Rate Constants

Nicholson<sup>52</sup> used the separation in anodic and cathodic peak currents to measure rate constants for electron transfer. He found that a system which appears reversible at one scan rate may be made to exhibit kinetic behaviour at higher scan rates. As the experimental timescale decreases (i.e., on increasing the scan rate) a point is reached where the kinetics of electron transfer compete with the rate of potential change, i.e., the experimental perturbation has been made so rapid that system can no longer maintain equilibrium. The standard rate constant for electron transfer,  $k^0$ , can be determined from the observed separation in peak potential,  $\Delta E_p$ , which varies with  $\nu$ . The  $\Delta E_p$  is correlated with a function  $\psi$  given by

$$\psi = \gamma^\alpha \frac{k^0}{\pi^{1/2} D_O^{1/2} (nF/RT)^{1/2} \nu^{1/2}} \quad (1.1)$$

Where  $\gamma$  is the square root of the ratio of diffusion coefficients, i.e.,

$$\gamma = \left( \frac{D_O}{D_R} \right)^{1/2} \quad (1.2)$$

and  $\alpha$  is the transfer coefficient. Since the difference in diffusion coefficients is generally small,  $\gamma^\alpha$  is typically unity, and the relation between the peak current,  $i_p$ , and  $\psi$  is essentially independent of  $\alpha$ . The variation of  $\Delta E_p$  with  $\psi$  is given in Table 1.1 overleaf.

**Table 1.1** Variation of peak potential separation,  $\Delta E_p$ , with kinetic parameter  $\psi$  [52].

$\psi^a$	$\Delta E_p \times n, \text{ mV}^b$
20	61
7	63
6	64
5	65
4	66
3	68
2	72
1	84
0.75	92
0.50	105
0.35	121
0.25	141
0.10	212

<sup>a</sup>  $\psi$  is defined in Equation (1.1). <sup>b</sup> For  $\alpha = 0.5$ .

From variation of  $\Delta E_p$  with scan rate,  $\psi$  is determined and hence  $k^0$  can be evaluated. The Nicholson technique is useful for approximating  $k^0$  values (order of magnitude evaluation). However, care must be taken at high scan rates, since the effect of  $R_U$  on the voltage response is very similar to slow heterogeneous kinetics. If  $R_U$  is sufficiently small, then the voltage drop caused by the resistive effect is negligible compared to the  $\Delta E_p$  attributable to the kinetic effect. The effect of  $R_U$  is most important for large  $k^0$  values where the  $\Delta E_p$  induced by slow heterogeneous electron transfer differs only slightly from the reversible value (to study a system with large  $k^0$ , rapid scan rates are required, as a result the peak currents become fairly large and even a small amount of uncompensated resistance can introduce serious error). Nevertheless,  $k^0$  values of  $10^{-3} \text{ cm s}^{-1}$  can be evaluated using macroelectrodes at scan rates of between 50-100  $\text{mV s}^{-1}$  without serious problems of  $iR$  drop.

## (ii) The Estimation of Diffusion Coefficients

In theory, knowing the electrode area one can evaluate the diffusion coefficient,  $D$ , from the dependence of the peak current on the scan rate in cyclic voltammetry. The peak current for a reversible CV is given by

$$i_p = 0.4463 nF (nF / RT)^{1/2} A D_o^{1/2} v^{1/2} C_o^* \quad (1.3)$$

Therefore a plot of  $i_p$  versus  $v^{1/2}$  should be linear with zero intercept and

$$D_o = \left( \frac{\text{Slope}}{0.4463 nF (nF / RT)^{1/2} A C_o^*} \right)^2 \quad (1.4)$$

However, the diffusion coefficients obtained will only be reliable when data obtained under reversible conditions are used. Slight departures from reversibility can cause peak currents to be unreliable and the errors incurred in the value of  $i_p$  are then squared in the calculation of  $D$ .

## (iii) Double-layer Capacitance

### *Models for the Double-layer Structure*

The double-layer capacitance is a result of the charge separation in the metal solution interphase. It depends on potential, solution composition and electrode material. Helmholtz first attempted to explain the capacitive behaviour of the interphase. He viewed the electrode-solution interphase as a parallel-plate capacitor i.e., a layer of ions on the solution side and a corresponding excess charge on the surface of the metal. According to the Helmholtz model, the inner-layer capacitance is therefore given by that of a parallel plate capacitor:

$$C_H = \frac{\epsilon \epsilon_0}{d} \quad (1.5)$$

where  $d$ , the distance between the plates is equal to the distance of closest approach of the cations of the electrolyte, and  $\epsilon$ , is the dielectric constant of the solvent. It is evident, that the model assumes that the capacitance remains constant, and so does not explain the dependence of the capacitance on potential or electrolyte concentration. However, at extreme negative potentials the double-layer capacitance becomes almost independent of concentration and potential in agreement with the parallel-plate theory. The numerical value of capacitance obtained from equation 1.5 above, using  $\epsilon = 6-8$  (the dielectric constant of water at the interphase) and a typical value of 0.52 nm for  $d$  (the sum of the diameter of water and the cations hydrated radius) is in reasonable agreement with the value obtained experimentally at extreme potentials.

Gouy and Chapman used a different approach to interpret the capacitance behaviour. In their diffuse double-layer model, the excess charge on the metal side of the interphase creates an equal excess of oppositely charged ions on the solution side. The ions are attracted to the surface electrostatically, but are also subject to random thermal motion. Therefore, there is a diffuse-layer of charge in solution. The average distance of charge separation depends on potential,  $\phi_0$ , the electrolyte concentration,  $C^*$ , and charge,  $z$ , and the capacitance,  $C_{GC}$ , is given by the following relation,

$$C_{GC} = 228 z C^{*1/2} \cosh(19.5 z \phi_0) \quad (1.6)$$

As the electrode becomes more highly charged, the diffuse layer becomes more compact and the capacitance increases. In a similar fashion, the capacitance increases with electrolyte concentration. However, the agreement between their theory and experiment only holds for dilute solutions and in a limited range of potentials near the potential of zero charge (the potential where the surface charge density is zero). So like the Helmholtz model the theory fails to completely describe the capacitance behaviour in real systems.

It was Stern who realized that, while the Helmholtz and Gouy-Chapman models alone do not provide an adequate description of the experimental data, a simple combination of the two yields good agreement. As illustrated in Figure 1.7, a layer of ions on the surface constitute the Helmholtz or compact part of the double layer,

while outside this layer there is an ionic space charge which constitutes the Gouy-Chapman or diffuse double layer.

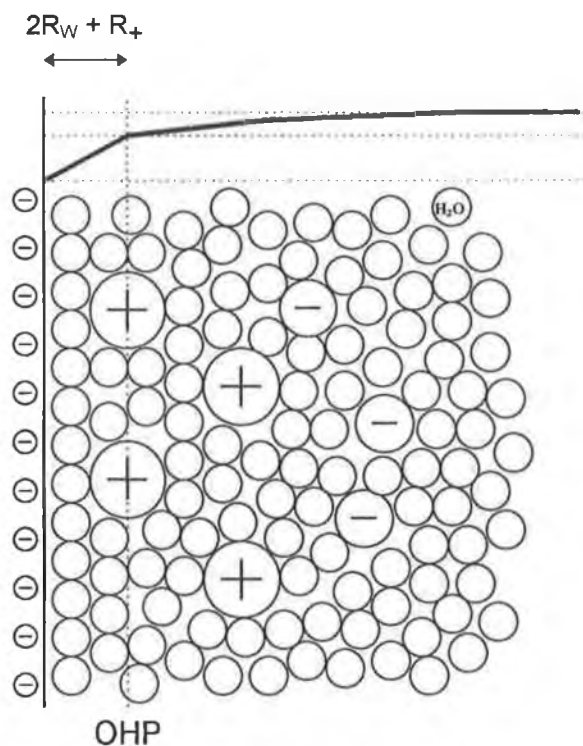


**Figure 1.7** Schematic representation of the structure of the double layer. At very negative potentials with respect to the PZC, OHP, the Outer Helmholtz Plane is shown at a distance of  $2R_W + R_+$ , where  $R_W$  and  $R_+$  represent the radii of a water molecule and solvated cation respectively. Taken from Ref. [53].

Therefore, the potential drop between the metal and the solution is divided into two segments, and the total capacitance of the interphase is given by

$$\frac{1}{C_{dl}} = \frac{1}{C_H} + \frac{1}{C_{GC}} \quad (1.7)$$

This series combination means that it is always the smallest capacitor that will dominate the overall capacitance.  $C_H$  is independent of potential while  $C_{GC}$  varies in a V-shaped fashion (see Figure 1.8). Near the PZC in systems with low electrolyte concentration, we expect to see the V-shaped function characteristics of  $C_{GC}$ . At larger electrolyte concentrations or at large polarizations, in dilute media  $C_{GC}$

becomes so large that it no longer contributes to the total capacitance and so one sees the constant capacitance  $C_H$ .

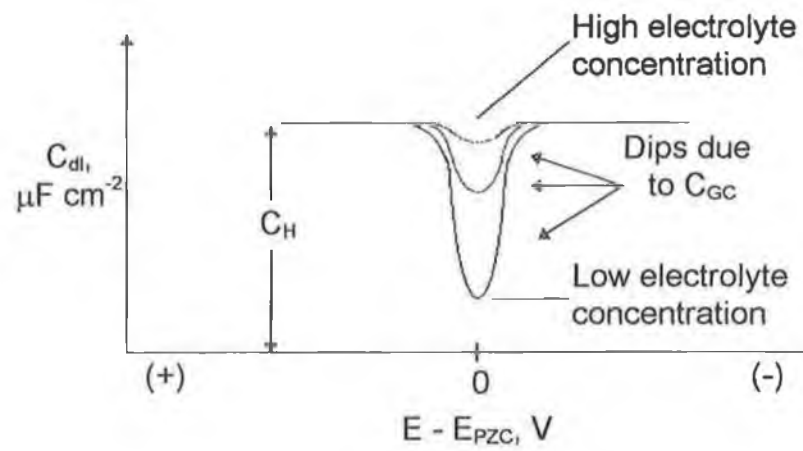


**Figure 1.8** Schematic representation of the expected behaviour of  $C_{dl}$  according to the Stern model. Taken from Ref. [54].

### Double-layer Structure of a Monolayer Modified Surface

When a monolayer is assembled on an electrode, the surface double-layer is altered. The double-layer structure may be approximated using the Stern model to a simple two capacitor system consisting of an ideal compact (Helmholtz) monolayer capacitor,  $C_M$ , and a diffuse (Gouy-Chapman) double-layer capacitor,  $C_{GC}$ , connected in series. The overall capacitance  $C_T$  is given by

$$\frac{1}{C_T} = \frac{1}{C_M} + \frac{1}{C_{GC}} \quad (1.8)$$

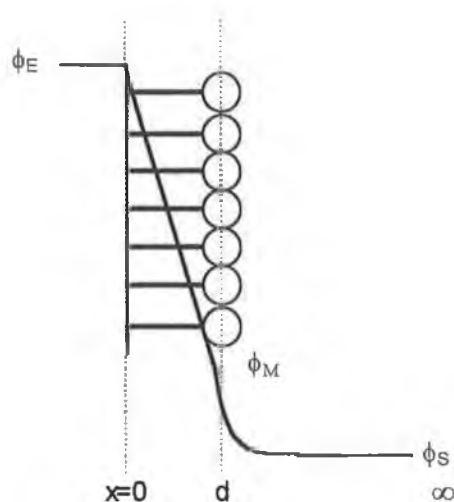


**Figure 1.9** Diagram of metal-solution and monolayer-solution interphase.  $\phi_E$ ,  $\phi_M$ ,  $\phi_S$  denote the electrostatic potential at the electrode surface, the monolayer surface, and in the bulk solution respectively.

At electrolyte concentrations of 0.1 M and higher the contribution to the total capacitance by  $C_{GC}$  is typically minimal and the measured capacitance is dominated by the monolayer capacitance. Knowing the monolayer thickness, one can evaluate the relative dielectric constant for the monolayer from the Helmholtz model.

$$C_M = \frac{\epsilon \epsilon_0}{d} \quad (1.9)$$

Given a dielectric constant of 4-10 for an organic monolayer, capacitance values greater than about  $10 \mu\text{F cm}^{-2}$  are indicative of electrolyte penetration of the monolayer. This behaviour is a direct result of the increase in the relative dielectric constant of the monolayer due to the permeation of water and ions. Capacitance measurements are therefore a valuable indication of monolayer packing quality.

### Evaluation of $C_{dl}$ by Cyclic Voltammetry

If the double-layer charging current,  $i_{dl}$ , is the only process taking place in a given potential region, then according to equation 1.10 a plot of capacitive current as a function of scan rate,  $\nu$ , yields a straight line of slope equal to the double-layer capacitance,  $C_{dl}$ .

$$i_{dl} = \nu C_{dl} \quad (1.10)$$

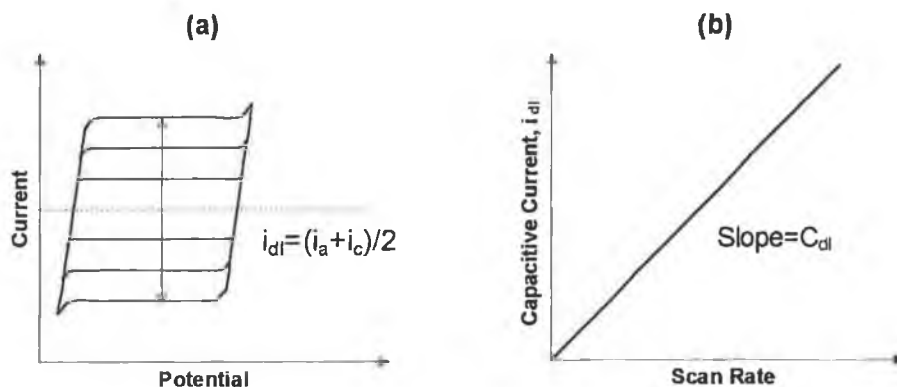


**Figure 1.10** (a) Typical double-layer charging current-potential plots at different scan rates. (b) Resulting plot of capacitive current versus scan rate.

While Faradaic current is a function of  $\nu^{1/2}$ ,  $i_{dl}$  is proportional to  $\nu$  and so double-layer charging becomes more important at higher scan rates. Also, since the capacitance depends on the microscopic area of the electrode, it increases with surface roughness, as does the capacitive current, unlike the diffusional current which remains unchanged.

### 1.3.2 Chronoamperometry

Chronoamperometry, the study of current-time transients obtained following a potential step is often used as a method to evaluate electrochemical areas, heterogeneous electron transfer rates, and diffusion coefficients. In a typical experiment, designed to determine the diffusion coefficient, a potential sufficiently anodic/cathodic of the peak potential is applied. Generally, if the reaction is well separated from any other electrode processes, an applied potential of one hundred millivolts beyond the peak potential is satisfactory. Figure 1.11 illustrates a typical current-time decay.

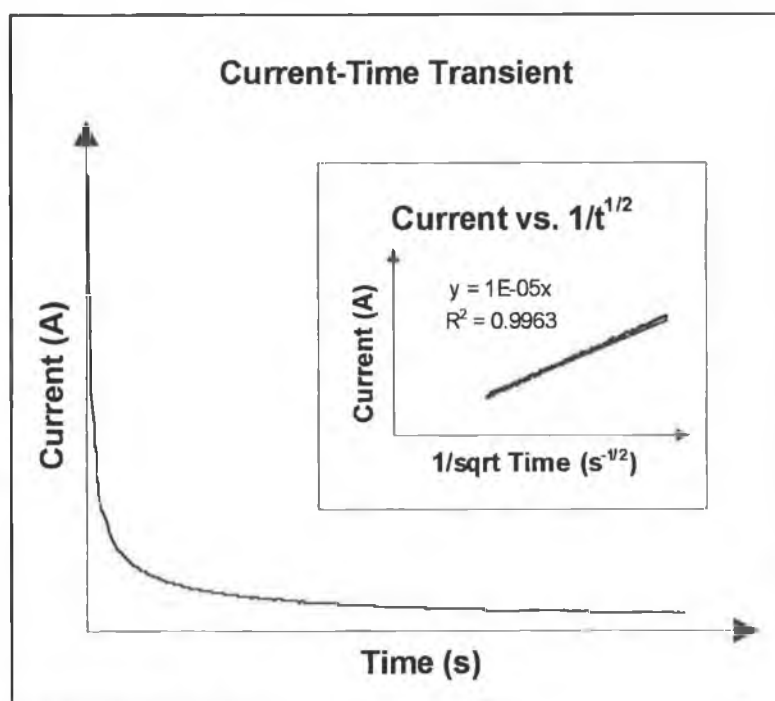


Figure 1.11 Typical current-time transient.

The insert shows that the current is inversely proportional to the square root of time in accordance with the Cottrell equation.

$$i(t) = \frac{nFA D^{1/2} C^*}{(\pi t)^{1/2}} \quad (1.11)$$

The current is directly proportional to the bulk concentration and the electrode area and inversely proportional to  $t^{1/2}$ . A non Faradaic current which also flows during the potential step, decays exponentially with a time constant  $\tau = R_U C_{dl}$ , and after a time of  $3\tau$  the current response is essentially Faradaic.

### (i) The Determination of Electrode Area

The geometric area of an electrode,  $A$ , can be evaluated from a limiting current of a substance whose diffusion coefficient,  $D$ , is precisely known. A 4 mM ferrocyanide ( $K_4FeCN_6$ ) solution containing 2 M KCl is recommended<sup>55</sup> as a reference standard for area determinations. The geometric area is calculated from the  $it^{1/2}$  curve analysis using the  $D$  value of  $0.629 \pm 0.003 \times 10^{-5} \text{ cm}^2 \text{ s}^{-1}$  obtained by von Stakelberg *et al.*<sup>56</sup> for ferrocyanide. The constancy of the product  $it^{1/2}$  at controlled potential is a measure of linear diffusion. Approximate linear diffusion conditions can be obtained with unshielded electrodes, which show  $it^{1/2}$  constancy over short periods of electrolysis. At shielded electrodes diffusion is restricted to an upward mode, peripheral contributions are eliminated, and semiinfinite linear diffusion conditions are achieved.

### (ii) The Determination of Diffusion Coefficients

A reliable method for the estimation of diffusion coefficients is via  $i(t)$  versus  $t^{1/2}$  curves. Problems associated with charging current are absent since the double-layer is charged at short times and the data is not used in the determination of the diffusion coefficient. To evaluate the diffusion coefficient,  $D$ , from a limiting current the electrode area,  $A$ , must be accurately known (see the previous section). Generally, the current-time curve is followed for about 50 seconds, and values of  $i(t)$  are plotted versus  $t^{1/2}$ . For perfect linear diffusion the plot should be that of a straight line with zero intercept, but this is rarely the case when using an unshielded electrode as the semiinfinite linear diffusion condition is only approached. The value of the slope is used to calculate  $D$  from equation 1.11 above.

### (iii) The Evaluation of $C_{dl}$

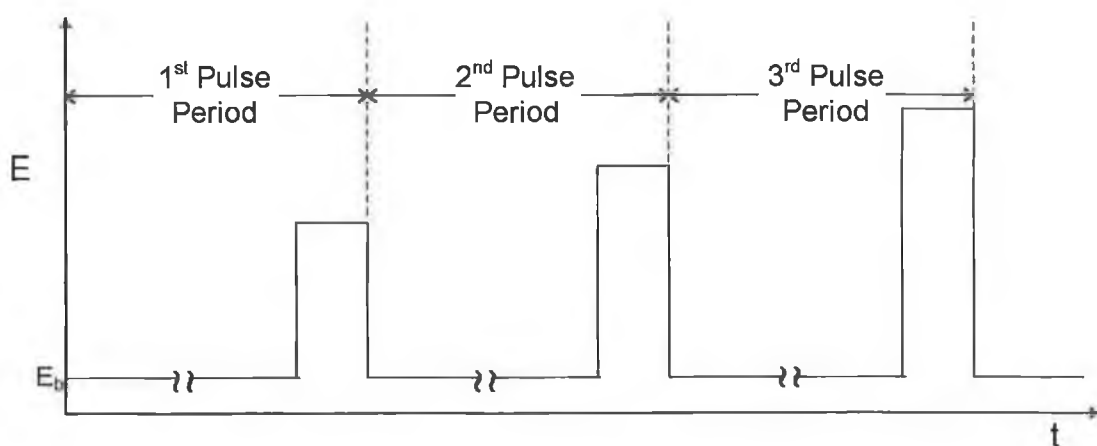
As mentioned above, a non Faradaic charging current which decays exponentially with a time constant,  $\tau$ , also flows during a potential step. In the absence of an electroactive species, or at a potential where the probe is not electroactive, the analysis of this charging current can be used to evaluate  $C_{dl}$ . Following the application of a small amplitude potential pulse,  $\Delta E$ , to the system. the double layer charging current,  $i_{dl}$ , decays according to the following relation

$$i_{dl}(t) = \frac{\Delta E}{R_U} \exp\left(\frac{-t}{R_U C_{dl}}\right) \quad (1.12)$$

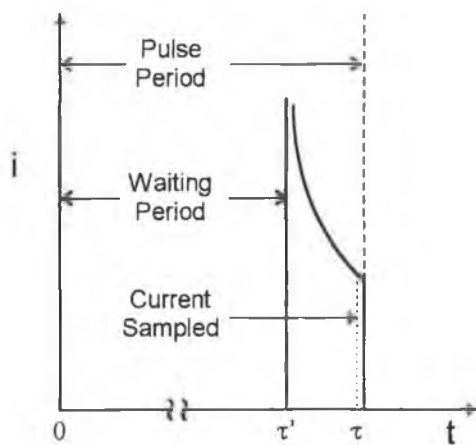
The observed current time transient is analyzed from the linear plots of  $\ln i_{dl}(t)$  vs.  $t$ . The y-intercept yields the value of solution resistance,  $R_U$ , and is used to determine the double layer capacitance from the slope.

### 1.3.3 Sampled Current Voltammetry

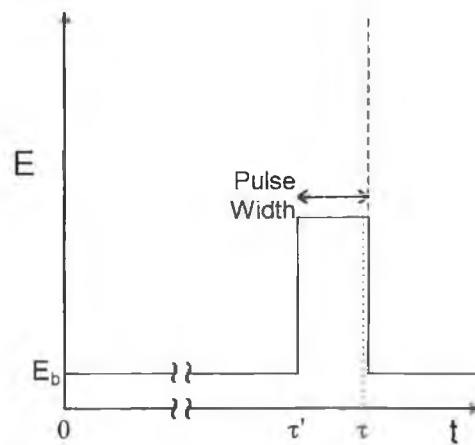
In sampled current voltammetry the electrode is held at a base potential,  $E_b$ , at which negligible electrolysis occurs. After a fixed waiting period  $\tau'$ , the potential is changed abruptly to value  $E$  for a period of about 50 milliseconds in duration. The potential pulse is ended by a return to the base potential. The current is sampled a time  $\tau$  near the end of the pulse.



(a)



(b)



(c)

**Figure 1.12** Sampling scheme for sampled current voltammetry; (a) potential program, (b) current and (c) potential during one cycle.

Since the current is measured at a time which is several times the  $R_D C_{dl}$  time constant the current measured will be totally Faradaic. The whole cycle is repeated except that

the step potential is made a few millivolts more extreme with each additional cycle. The process is continued until the potential range of interest has been investigated. As illustrated in Figure 1.13, the output is a plot of sampled current versus step potential E.

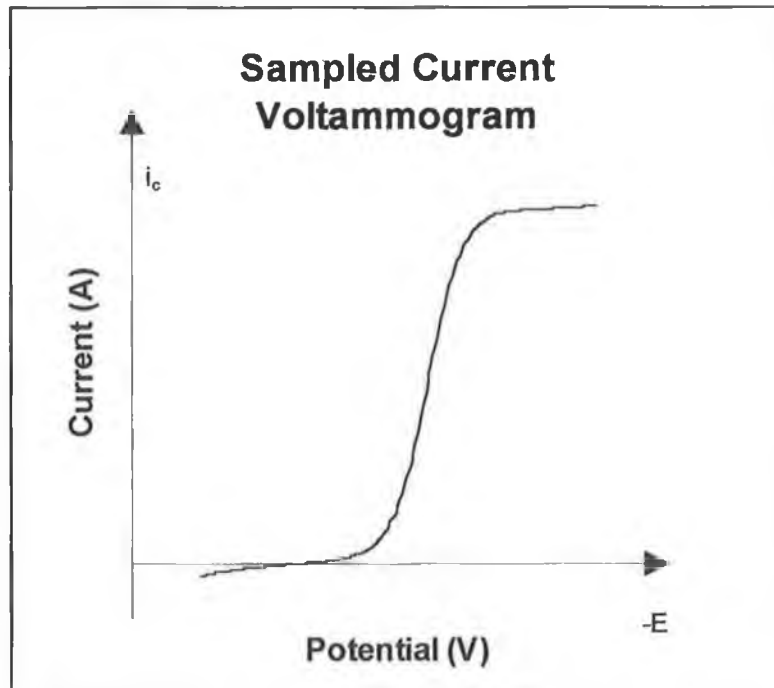


**Figure 1.13** Typical sampled current voltammogram.

The limiting current is given by the Cottrell Equation

$$i_{\text{lim}} = \frac{nFAD_0^{1/2}C_0^*}{\pi^{1/2}(\tau - \tau')^{1/2}} \quad (1.13)$$

Where  $(\tau - \tau')$  is the time measured from the pulse rise.<sup>54</sup>

### (i) The Evaluation of Standard Rate Constants

The analysis of the rising portion of the sampled current voltammogram permits the evaluation of the standard rate constant,  $k^0$ , and the transfer coefficient,  $\alpha$ , for the heterogeneous electron transfer.<sup>57, 58</sup> The current potential relation is given by

$$E = E^* \mp \frac{RT}{\alpha \mp nF} \ln \left\{ X \left[ \frac{1.75 + X^2 [1 + \exp(\pm \xi)]^2}{1 - X [1 + \exp(\pm \xi)]} \right]^{1/2} \right\} \quad (1.14)$$

where

$$E^* = E^{o'} \pm \frac{RT}{\alpha \mp nF} \ln \left\{ \frac{4}{\sqrt{3}} \frac{k^0 (\tau - \tau')^{1/2}}{D^{1/2}} \right\} \quad (1.15)$$

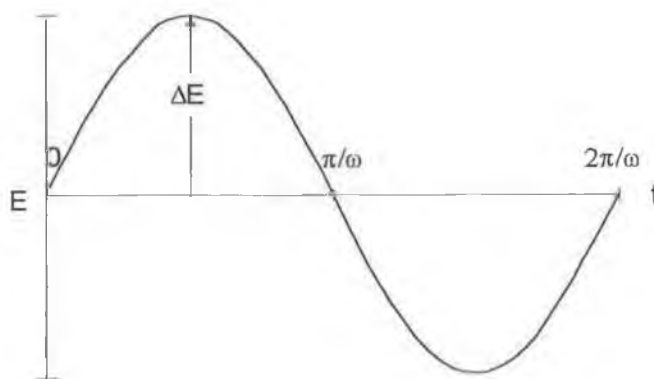
$X$  is the ratio of the current at potential  $E$  to the anodic limiting current, and  $\xi$  is a dimensionless parameter  $[(nF/RT)/(E-E^{o'})]$ . Equation 1.14 is of the form  $y = c + mx$  and when plotted yields a slope of  $RT/(\alpha \mp nF)$  and an intercept of  $E^*$  from which the two kinetic parameters  $k^0$  and  $\alpha$  can be determined.

### 1.3.4 AC Impedance

In contrast to cyclic voltammetry and chronoamperometry, AC impedance is a steady state technique used to probe the electrode-solution interphase. The technique is based on applying a sinusoidal potential modulation to the system and monitoring the amplitude and phase shift of the current response. The procedure is performed over a range of frequencies and can be quite slow as measurements have to be made one frequency at a time. Impedance experiments are usually conducted in the range of  $10^{-3}$ - $10^5$  Hz. Therefore, it is possible to distinguish between processes that have different relaxation times. Care must be taken when evaluating data acquired at extreme frequencies, as measurements at very low frequencies take a long time during which the interphase may change rendering the result meaningless, while those at high frequency are frequently unreliable due to stray capacitances and inductances.<sup>53</sup>

#### (i) The Theory of AC Impedance

During an ac impedance experiment, the dc potential is held at a constant value (e.g., the standard redox potential) while a superimposed ac oscillating potential is applied.



$$\text{Sinusoidal voltage } E = \Delta E \sin(\omega t)$$

**Figure 1.14** Alternating potential, where  $\Delta E$  is the amplitude of the sine wave and  $\omega$  is the angular frequency.

The ac current at different frequencies is the measured response. This allows us study a range of different timescales in just one experiment. In a typical ac impedance measurement, a sinusoidal voltage  $E = \Delta E \sin(\omega t)$  is applied to the cell as a perturbation where  $\omega$  is the angular frequency ( $2\pi$  times the conventional frequency in Hz) and  $\Delta E$  is the amplitude of the sine wave. The resulting ac current through a resistor  $R$  is given by

$$i = E / R = \Delta E \sin(\omega t) / R \quad (1.16)$$

while that through a capacitor  $C$  is given by

$$i = C dE / dt = \Delta E C \omega \cos(\omega t) \quad (1.17)$$

which can be expressed as a function of  $\sin(\omega t + \pi/2)$

$$i = \Delta E C \omega \sin(\omega t + \pi/2) \quad (1.18)$$

this results in a phase difference between the current and the applied potential. It is convenient to consider the resulting current as a vector which can be resolved into two components one in-phase with the applied potential and one out-of-phase, see Figure 1.15 below.

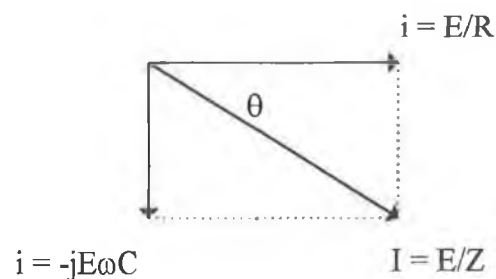


Figure 1.15 Vector diagram for ac current.

The angle between the current vector and the applied potential is called the phase angle,  $\theta$ . For a pure capacitor it is  $-\pi/2$ , for a pure resistor it is 0. For any actual interphase the value is somewhere in between depending on the nature of the interface and the frequency. Using complex notation, the in-phase and out-of-phase components are represented on the real and imaginary axes, respectively. The current for the capacitor is therefore equal to  $-jE\omega C$ , where  $j$  is the unit vector along the imaginary axis, while the current for the resistor being in-phase is equal to  $E/R$  along the real axis. The total current across both resistor and capacitor is given by the vector sum of the two potentials.

$$i = E / (R - j / \omega C) = E / Z \quad (1.19)$$

The impedance,  $Z$ , is a measure of the resistance to the ac current in the circuit. For each frequency measured it is represented by a separate point on the complex plane. The distance of the point from the origin corresponds to the magnitude of the impedance,  $|Z|$ , while the angle,  $\theta$ , formed with the real axis corresponds to the phase difference between the applied voltage and the resulting current. Both  $\theta$  and  $|Z|$  are functions of applied frequency for any given circuit. The real and imaginary impedances  $Z'$  and  $Z''$ , are plotted as a function of  $\omega$  and used to extract quantitative data for the different processes occurring in the system under study. The Nyquist plot or complex-plane impedance plot ( $-Z''$  vs.  $Z'$ ) is most commonly used when presenting impedance data. Bode plots in which  $\text{Log } |Z|$  and  $\theta$  are plotted as a function of  $\text{Log } (\omega)$  are another popular form of displaying impedance results.

## (ii) The Principle of Equivalent Circuits

The rationale for measuring impedances is that the processes that occur in an electrochemical cell can be modeled using a combination of resistors and capacitors. This is the principle of equivalent circuits. In the absence of an electroactive species the interfacial region is represented simply by a series combination of  $C_{dl}$ , the double layer capacitance of the interfacial region and  $R_U$ , the uncompensated solution resistance. When a diffusing electroactive species is present, the interfacial region is

modeled as the series combination of  $R_{CT}$ , the resistance due to the heterogeneous electron transfer (the smaller the rate of electron transfer the larger  $R_{CT}$ ) and  $Z_w$ , the Warburg impedance, (a frequency dependent reactance due to the mass transfer between the bulk solution and the electrode surface) in parallel with  $C_{dl}$ . These circuit elements are combined with  $R_U$  to give Randles Equivalent Circuit.

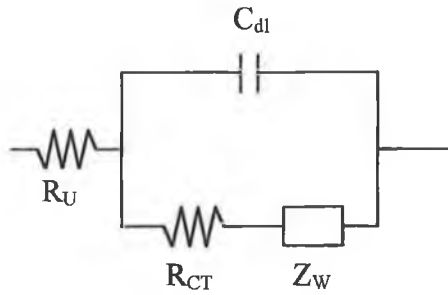


**Figure 1.16** Randles Equivalent Circuit [59].

The mathematical expressions for  $Z'$  and  $Z''$  for the above circuit are extremely complicated and it is usual to identify two limiting cases:

- In the high frequency limit,  $Z_w$  tends to zero and the relationship simplifies to

$$\left(Z' - R_U - R_{CT}/2\right)^2 + (Z'')^2 = \left(R_{CT}/2\right)^2 \quad (1.20)$$

which describes a circle centered on  $Z' = R_U + R_{CT}/2$  with radius  $R_{CT}/2$ , see Figure 1.17. The high frequency intercept is at  $Z' = R_U$  and the low frequency intercept is at  $Z' = R_U + R_{CT}$ . This is a model for slow heterogeneous electron transfer (i.e., kinetic control). Once  $R_{CT}$  has been calculated,  $C_{dl}$  can be determined from the value of  $\omega$  at the maximum value of  $Z''$ , at this value  $\omega_{max} = 1/R_{CT}C_{dl}$ .

- In the low frequency limit it simplifies to

$$Z'' = Z' - \left(R_U + R_{CT} - 2\sigma^2 C_{dl}\right) \quad (1.21)$$

which yields a straight line of unit slope, with an intercept on the real axis of  $Z' = R_U + R_{CT} - 2\sigma^2 C_{dl}$ , see Figure 1.17. This case corresponds to diffusion control, i.e. fast heterogeneous electron kinetics. The Warburg coefficient,  $\sigma$ , depends on the diffusion coefficients and concentrations.

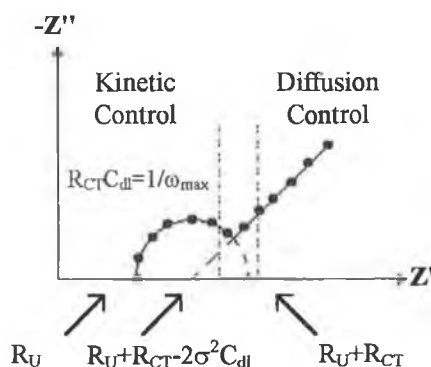


**Figure 1.17** Complex-plane impedance plot for Randles Equivalent Circuit.

In the absence of a diffusing electroactive species the equivalent circuit used to model the interfacial region simplifies considerably to a series combination of the  $R_U$  and  $C_{dl}$ , and the total impedance is given by,

$$Z = R_U - j / \omega C_{dl} \quad (1.22)$$

where the first term is the frequency independent impedance due to the resistor and the second term is the frequency dependent impedance due to the capacitor. If the interfacial region behaved ideally, then the impedance due to the solution resistance would be represented on the complex-plane impedance plot as a point a distance  $R_U$  along the real axis, while that of the double-layer capacitance would define a vertical spike coincident with the imaginary axis and displaced a distance  $R_U$  along the real axis.

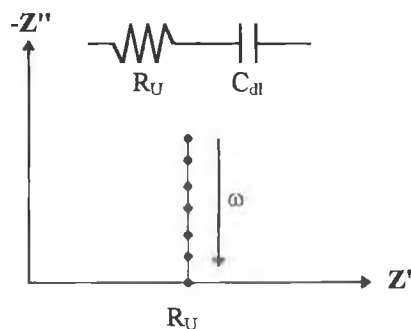


**Figure 1.18** Complex plane impedance plot for a resistor and capacitor in series.

However, it is only in the case of mercury (which forms an ideally polarizable interphase in solution) that a truly vertical spike, like that shown in Figure 1.18, is observed. For solid electrode systems (e.g., gold) that never behave ideally, the line is deviated by a constant angle  $\alpha$  which generally falls between 0 and 45°.

As mentioned previously Bode plots, in which  $\text{Log } |Z|$  and  $\theta$  are plotted as a function of  $\text{Log } (\omega)$ , are often used to present impedance data graphically. At low frequencies the circuit behaves as a capacitor and the total impedance approximates to

$$|Z| = \frac{1}{\omega C_{dl}} \quad (1.23)$$

By extrapolating the linear portion of the Bode magnitude plot ( $\text{Log } |Z|$  vs.  $\text{Log } (\omega)$ ) plot to  $\text{Log } (\omega) = 0$  the double layer capacitance can be determined. Although in practice there is rarely a region in the Bode magnitude plot where the slope is strictly equal to -1. Therefore, the phase angle can often be a more sensitive test of capacitance and a good approximation can be obtained at the maximum in Bode angle plot ( $\theta$  vs.  $\text{Log } (\omega)$ ) where equation 1.23 applies. Again in practice the phase angle never quite reaches the -90° value that is expected for a pure capacitor.

### (iii) The Interpretation of Impedance Spectra

Interpreting the results of ac impedance data relies on finding the equivalent circuit and extracting values for the individual components which are then related to the fundamental properties of the electrochemical system. Figure 1.19 below shows a

typical Nyquist plot, although in many cases the charge transfer and diffusion controlled regions on the complex plane may not be as well defined.

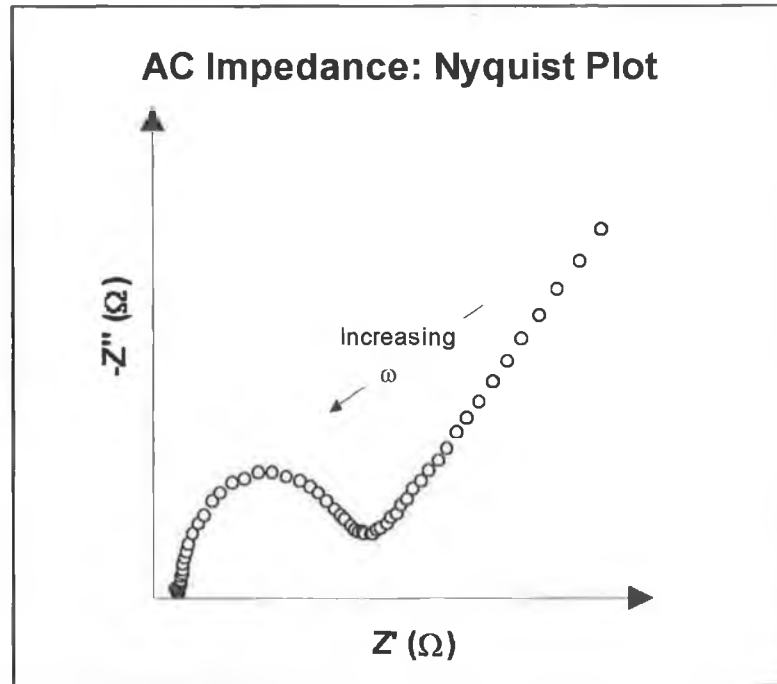


Figure 1.19 Typical Nyquist plot.

The determining feature is the charge transfer resistance,  $R_{CT}$ , and its relation to the Warburg impedance which is controlled by  $\sigma$ . If the system is kinetically slow it will show a large  $R_{CT}$  and only a very limited region where mass transfer is significant. The standard rate constant,  $k^0$ , can be determined using the following equation,

$$k^0 = \frac{2RT}{n^2 F^2 A C^* R_{CT}} \quad (1.24)$$

At the other extreme where the charge transfer is sufficiently facile so that diffusion is limiting, the semicircular region is not well defined and a straight line plot is obtained. In this case the diffusion coefficient,  $D$ , can be readily evaluated.

$$D = \left( \frac{4RT}{\sqrt{2} n^2 F^2 A \sigma C^*} \right)^2 \quad (1.25)$$

## 1.4 CONCLUDING REMARKS

In recent years there have been significant technological advances in the field of drug release. In addition to the traditional periodic formulations, more sophisticated sustained release systems are now widely available. But the future of drug release lies in state of the art self-regulating systems that are currently undergoing development. Ideally, these systems will sense when and how much drug to release, thus providing a safe and effective means of drug delivery.

The movement away from disordered polymers to more ordered structures should also improve the currently available systems in terms of reproducible release rates. Monolayer forming techniques such as Langmuir-Blodgetty and Self-Assembly will provide a means of fabricating such ordered systems. As regards characterization of monolayer systems electrochemical methods are the most versatile. As outlined in Section 1.3, both capacitance and permeation studies can be used to probe the structural integrity and the transport/release rate of solution phase analytes through monolayer systems. To monitor solution phase diffusion spectroscopically would require the use of more sophisticated materials and might be limited in terms of sensitivity.

The formation of ordered monolayers and the assessment of their permeability characteristics, with a view to developing suitable materials for the pH-modulation of drug release is the principle objective of the work discussed in the following chapters. Three different systems based on organic compounds that contain a terminal carboxylic acid functionality will be presented and the effect of pH on the structure and permeability of these monolayers reported. The suitability of the systems studied and monolayer systems in general to the design of a pH-modulated drug delivery system is the overall aim of this thesis.

## 1.5 REFERENCES

- [1] Langer, R. *Science* **1990**, *249*, 1527.  
Langer, R. *Acc. Chem. Res.* **1993**, *26*, 537.
- [2] Domb, A.; Gallardo, C.; Langer R.; *Macromolecules* **1989**, *22*, 3200.
- [3] Tamada, J. A.; Langer, R. *Proc. Natl. Acad. Sci. USA* **1993**, *90*, 552.
- [4] Widder, K.; Flouret, G.; Senyei, A.; *J. Pharm. Sci.* **1979**, *68*, 79. Hsieh, D. S. T.; Langer, R.; Folkman, J. *Proc. Natl. Acad. Sci. USA* **1981**, *78*, 1863.
- [5] Kost, J.; Leong, K.; Langer, R. *Proc. Natl. Acad. Sci. USA* **1989**, *86*, 7663.
- [6] Theeuwes, F. *J. Pharm. Sci.* **1975**, *64*, 1987.
- [7] Wood, D. A. In: Florence, A. T. (ed.) *Critical reports on Applied Chemistry*, Vol. 6: Materials Used in Pharmaceutical Formulation, Blackwell Scientific Publications, Oxford, **1984**, p. 71.
- [8] Lehr, C.-M.; Bouwstra, J. A.; De Boer, A. G.; Verhoef, J. C.; Breimer, D. D.; Junginger, H. E. In: Juginger, H. E. (ed.) *Drug Targeting and delivery: concepts in dosage form design*, Ellis Horwood Ltd., London, **1992**, p. 95.
- [9] Chambliss, W. *Pharm. Tech.* **1983**, *7*, 124.
- [10] Saffran, M.; Kumar, G. S.; Savariar, C.; Burnham, J. C.; Williams, F.; Neckers, C. D. *Science* **1986**, *233*, 1081.
- [11] Alonso, M. J.; Cohen, S.; Park, T. G.; Gupta, R. K.; Siber, G. R.; Langer, R. *Pharm. Res.* **1993**, *10*, 945.
- [12] Tamada, J. A.; Langer, R.; *J. Biomater. Sci. Polym. Ed.* **1992**, *3*, 315.
- [13] Gref, R.; Minamitake, Y.; Peracchia, M. T.; Trubetskoy, V.; Torchilin, V.; Langer, R. *Science* **1994**, *263*, 1600.
- [14] Brem, H.; Walter, K. A.; Langer, R. *Eur. J. Pharm.* **1993**, *39*, 2.
- [15] Laurencin, C.; Gerhart, T.; Witschger, P.; Satcher, R.; Domb, A.; Habff, P.; Edsberg, L.; Hayes, W.; Langer, R. *J. Orthop. Res.* **1993**, *11*, 256.
- [16] Tice, T. R.; Cowsar, D. R. *Pharm. Tech.* **1984**, *8*, 26.
- [17] Burgess, D. J. In: Pezzuto, J. M.; Johnson, M. E. (eds.) *Biotechnology and Pharmacy*, Chapman & Hall, New York, **1993**, p. 95.
- [18] Juginger, H. E. (ed) *Drug Targeting and delivery: concepts in dosage form design*, Ellis Horwood Ltd., London, **1992**.
- [19] Fendler, J. H. *Chem. Eng. News* **1984**, *62*, 31.
- [20] Hwang, K. J. In: Ostro, M. J. (ed.) *Liposomes: From Biophysics to Therapeutics*, Dekker, New York, **1987**, p. 109.
- [21] Liu, D.; Mori, A.; Huang, L. *Biochem. Biophys. Acta* **1991**, *1104*, 95. Mori, A.; Klibanov, A. L.; Torchilin, V. P.; Huang, L. *FEBS Lett.* **1991**, *284*, 263.
- [22] Allen, T. M.; Chonn, A. *FEBS Lett.* **1987**, *223*, 42.
- [23] Hupfer, B.; Ringsdorf, H.; Schupp, H. *Makromol. Chem.* **1981**, *182*, 247. Hub, H. H.; Hupfer, B.; Koch, H.; Ringsdorf, H. *J. Macromol. Sci. Chem.* **1981**, *A14*, 701. Regen, S. L.; Czech, B.; Singh, A. *J. Am. Chem. Soc.* **1980**, *102*, 6638. Johnston, D. S.; Sanghera, S.; Pons, M.; Chapman, D. *Biochem. Biophys. Acta* **1980**, *602*, 57. Juliano, R. I.; Hsu, M. J.; Regan, S. L.; Singh, M. *Biochem. Biophys. Acta* **1984**, *770*, 109.
- [24] Samuel, N. K. P.; Singh, M.; Yamaguchi, K.; Regen, S. L. *J. Am. Chem. Soc.* **1985**, *107*, 42.
- [25] Bader, H.; Dorn, K.; Hupfer, B.; Ringsdorf, H. *Adv. Polymer Sci.* **1985**, *64*, 1.

- [26] Michel, Ch.; Purmann, Th.; Mentrup, E.; Michel, G.; Kreuter, J. *Proc. Int. Symp. Control. Release Bioact. Mater.* **1991**, *18*, 485.
- [27] Weiner, N.; Williams, N.; Birch, G.; Ramachandran, C.; Shipman, C.; Flynn, G. *Antimicrob. Agents Chem. Ther.* **1989**, *33*, 1217.
- [28] Ganesan, M. G.; Weiner, N. D.; Flynn, G. L.; Ho, N. F. H. *Int. J. Pharm.* **1984**, *20*, 139.
- [29] Knepp, V. M.; Hinz, R. S.; Szoka, F. C.; Guy, R. H. *J. Control. Release* **1988**, *10*, 211.
- [30] Knepp, V. M.; Szoka, F. C.; Guy, R. H. *J. Control. Release* **1990**, *12*, 25.
- [31] Arrieta-Molero, J. F.; Aleck, K.; Sinha, M. K.; Brownschidle, C. M.; Shapiro, L. J.; Sperling, M. A. *Hormones Res.* **1982**, *16*, 249.
- [32] Soehngen, E. C.; Godin-Ostro, E.; Fielder, F. G.; Ginsberg, R. S.; Slusher, M. A.; Weiner, A. L. *Arthr. Rheum.* **1988**, *31*, 414.
- [33] Chiang, C. M.; Weiner, N. *Int. J. Pharm.* **1987**, *37*, 75.
- [34] Patel, H. M.; Tuzel, N. S.; Stevenson, R. W. *Biochem. Biophys. Acta* **1985**, *839*, 40.
- [35] Edelman, E.; Kost, J.; Bobeck, H.; Langer, R. *J. Biomed. Mat. Res.* **1985**, *19*, 67.
- [36] Nanavaty, M.; Brucks, R.; Grimes, H.; Siegel, F. P. *Proc. Int. Sym, Control. Release Bioact. Mater.* **1989**, *16*, 310.
- [37] Kwon, I. C.; Bae Y. H.; Kim, S. W. *Nature* **1991**, *354*, 291.
- [38] Alhaique, F.; Marchetti, M.; Ricciari, F.; Santucci, E. *J. Pharmacol.* **1981**, *33* 413. Brannon-Peppas, L.; Peppas, N. A. *Biomaterials* **1990**, *11*, 635.
- [39] Okano, T. *Adv. Polymer Sci.* **1993**, *110*, 179.
- [40] Stevenson, W. T. K.; Sefton, M. V. *TRIP* **1994**, *2*, 99.
- [41] Heller, J.; Trescony, P. *J. Pharm. Sci.* **1979**, *68*, 919
- [42] Kost, J.; Horbett, T. A.; Ratner, B. D.; Singh, M. *J. Biomed. Mater. Res.* **1985**, *19*, 1117.
- [43] Fischel-Ghodsian, F.; Brown, L.; Mathiowitz, E.; Brandenburg, D.; Langer, R. *Proc. Natl. Acad. Sci. USA* **1988**, *85*, 2403.
- [44] Roberts, G. *Langmuir-Blodgett Films*, Plenum Press, New York, **1990**.
- [45] Ulman, A. *An Introduction To Ultrathin Organic Films. From Langmuir-Blodgett To Self Assembly*, Academic Press Inc. San Diego, CA **1991**.
- [46] Blodgett, K. B. *J. Am. Chem. Soc.* **1935**, *57*, 1007.
- [47] Blodgett, K. B.; Langmuir, I. *Phys. Rev.* **1937**, *51*, 964.
- [48] Sagiv, J. *J. Am. Chem. Soc.* **1980**, *102*, 92.
- [49] Cheng, Q.; Brajter-Toth, A. *Anal. Chem.* **1995**, *67*, 2767.
- [50] Sabatani, E.; Rubinstein, I.; Maoz, R.; Sagiv, J. *J. Electroanal. Chem.* **1987**, *219*, 365.
- [51] Kryszynski, P.; Brzostowska-Smolka, M. *J. Electroanal. Chem.* **1997**, *424*, 61.
- [52] Nicholson, R. S. *Anal. Chem.* **1965**, *37*, 1351.
- [53] Gileadi, E. *Electrode Kinetics For Chemists, Chemical Engineers & Materials Scientists*, VCH, **1993**.
- [54] Bard, A. J.; Faulkner, L. R. *Electrochemical Methods*, Wiley, New York, **1980**.
- [55] Adams, R. N. *Electrochemistry At Solid Electrodes*, Chapter 3, Marcel Dekker, New York, **1969**.

- [56] Von Stackelberg, M.; Pilgram, M.; Toome, V. *Z. Elektrochem.* **1953**, *57*, 342.
- [57] Matsuda, H, *Bull. Chem. Soc. Jpn.* **1980**, *53*, 3439.
- [58] Forster, R. J.; Vos, J. G. *J. Electroanal. Chem.* **1991**, *314*, 135.
- [59] Randles, J. E. B. *Disc. Faraday Soc.* **1947**, *1*, 11.

---

## **CHAPTER 2**

### **Formation of Organized Polymeric Films: *Cis*-11-Eicosenoic Acid**

---

## 2.1 INTRODUCTION

The first stage in the development of triggered drug release systems was the construction of organized two-dimensional polymer films using the Langmuir-Blodgett (LB) technique. The low chemical, mechanical and thermal stability of unpolymerized LB films were major obstacles for their technological application. In order to overcome the problems in stability, the formation of polymeric monolayer films has been intensely researched.

Figure 2.1 illustrates the two basic approaches to obtaining polymeric films. These approaches use either polymerizable monomeric amphiphiles or preformed polymers containing both hydrophilic and hydrophobic side groups.<sup>1</sup>

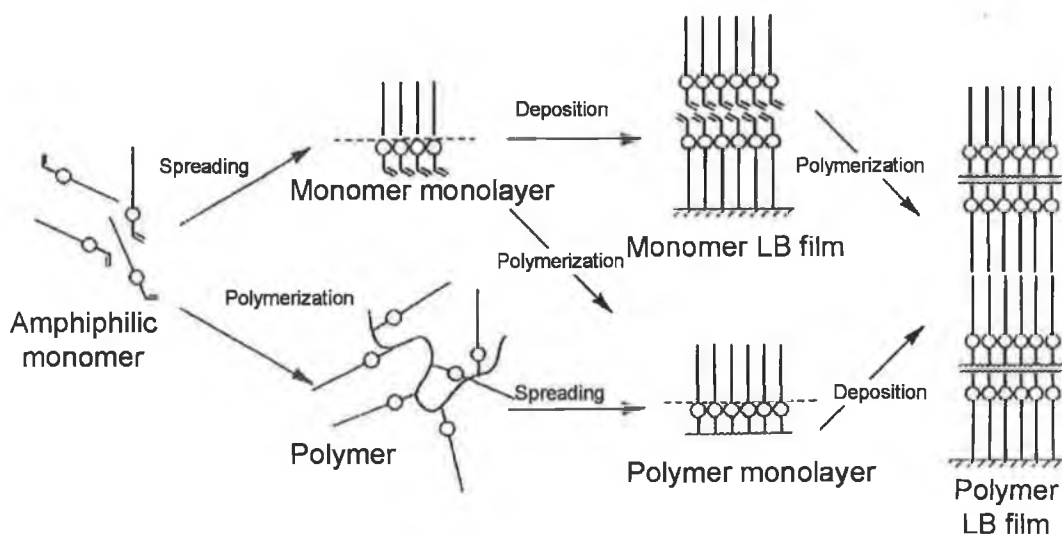


**Figure 2.1** Preparation of polymer Langmuir-Blodgett films. Adapted from Ref. [1].

Since prepolymerized amphiphiles form Langmuir films that are viscous and very difficult to transfer to a substrate, the primary focus of this work is on the formation of monolayers of monomeric amphiphiles. Only certain classes of monolayer forming materials can be polymerized without destruction of their lamellar structure. Generally, monomeric amphiphiles possess one or more unsaturated bonds as active sites. Typical polymerizable amphiphiles contain either vinylic<sup>2</sup> or diacetylenic<sup>3</sup> groups although there have been a few reports on the polymerization of dienic<sup>4</sup> and cyclic<sup>5</sup> compounds. These systems are synthetically flexible, and the polymerizable

unit can be located near the hydrophilic end-group, near the hydrophobic end or alternatively at the centre of the hydrocarbon chain.

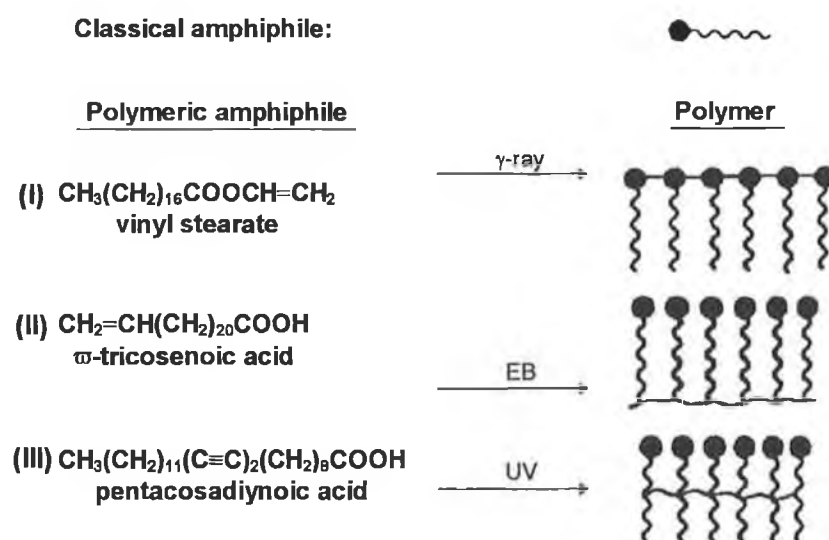


**Figure 2.2** Polymers formed from the various types of polymeric amphiphiles. Examples of monomers are (I) vinyl stearate; (II)  $\omega$ -tricosenoic acid; (III) 10,12-pentacosadiynoic acid. (I), (II) and (III) are polymerized by  $\gamma$ -ray, electron beam and UV light respectively.

Figure 2.2 above shows three typical polymeric amphiphiles. Polymerization of the monolayer structure can be initiated by irradiating with  $\gamma$ -rays, x-rays, electron-beams or UV light.<sup>6</sup> The polymerization reaction can be performed either prior to monolayer transfer at the air/water interface or after transfer of the monomeric LB film to a solid support.

It was decided to focus on acidic amphiphiles and monitor the change in monolayer permeability with increasing pH. There have only been a few limited studies concerning polar amine amphiphiles<sup>7, 8</sup> and so relatively little information exists regarding their incorporation into Langmuir-Blodgett films. The vast majority of molecular systems studied include a carboxylic acid functionality to obtain the required hydrophilicity. The polymerization of Langmuir monolayers of unsaturated fatty acids with non-conjugated double bonds in the middle of the hydrocarbon chain has been previously reported.<sup>9</sup> This chapter details the preliminary investigations carried out on monolayers of a *cis*-type fatty acid, eicosenoic acid.

## 2.2 EXPERIMENTAL

### 2.2.1 Materials/Reagents

*cis*-11-Eicosenoic acid (98%) was purchased from Aldrich (Gillingham, UK) and used without further purification. Arachidic acid (>99%) obtained from Fluka (Gillingham, UK) was used as a reference standard to calibrate the LB trough. Chloroform ( $\geq 99.8\%$ ), supplied by Fluka was used as the spreading solvent for the monolayer preparation. Ultra-pure water (resistivity  $\geq 18 \text{ M}\Omega \text{ cm}$ ), obtained from a Millipore Milli-Q filtering system was used as the pure water subphase in equilibrium with atmospheric  $\text{CO}_2$ . Inorganic salts and buffers, used to alter the subphase composition and pH, were reagent grade quality.

### 2.2.2 Monolayer Formation

Surface pressure-Area ( $\pi$ -A) isotherms of the Langmuir films were studied using a Nima Technology (Coventry, UK) Model 2022 circular, alternate layer, Langmuir-Blodgett trough. The surface pressures were measured to 0.1 mN/m using a Wilhelmy plate pressure sensor, which was calibrated prior to use. Monolayers were spread from dilute chloroform solutions ( $\sim 1 \text{ mg/ml}$ ) of the amphiphile on the aqueous subphase surface by means of a Hamilton microsyringe. Each drop of solution was allowed to spread out and evaporate before the next was applied. Complete solvent evaporation was achieved within 10 minutes. The initial molecular area after spreading was typically between 70-80  $\text{\AA}^2/\text{molecule}$ . A constant barrier speed of 50  $\text{cm}^2/\text{min}$  was applied during each compression. Reproducible  $\pi$ -A isotherms were obtained at room temperature, on each of the subphases studied.

### 2.2.3 LB Film Deposition

LB films were deposited onto standard microscope slides (7.6 cm  $\times$  2.6 cm). The slides were cleaned by sonicating in detergent, rinsing in Milli-Q deionized water,

sonicating in isopropanol and finally rinsing in deionized water. Hydrophilic slides were prepared by soaking overnight in NaOH ( $2 \text{ g/dm}^3$ ), and rinsing well in deionized water prior to use. Oven dried slides were rendered hydrophobic by immersing them in a 5% chloroform solution of  $(\text{CH}_3)_2\text{SiCl}_2$  ( $>99.5 \%$ , Fluka) for 10-15 minutes, rinsing in methanol and storing in distilled water. A deposition pressure, within the 20-25 mN/m range was chosen, and maintained at the chosen value  $\pm 0.5 \text{ mN/m}$ , while the monolayer was transferred onto the hydrophilic/silanized glass substrate at dipping speeds typically in the region of 30-50 mm/min. Deposition was started after a stabilization period of 5 minutes at the selected deposition pressure. A substrate area of approximately  $12.5 \text{ cm}^2$  ( $4.8 \text{ cm} \times 2.6 \text{ cm}$ ) was immersed through the compressed monolayer. The quality of the LB film obtained was estimated through the transfer ratio (i.e., the ratio of the removed film area to the theoretical substrate area) calculated after each down and upstroke. In order to give a good indication of the monolayer transferability from the subphase studied, the substrate was passed through the compressed monolayer several times.

## 2.3 RESULTS & DISCUSSION

### 2.3.1 Calibration with Arachidic Acid

Arachidic acid ( $C_{19}H_{39}COOH$ ), is a linear molecule composed of a saturated alkyl chain and a terminal carboxylic acid group and is often used as a reference standard in LB systems. Like Stearic acid ( $C_{17}H_{35}COOH$ ), the other most common standard used, the arachidic acid molecule possesses a good hydrophobic/hydrophilic balance and forms very stable monolayers at the air-water interface. Both standards show a loss of less than  $0.001\% \text{ min}^{-1}$  in the surface area of a monolayer at  $20\text{ }^\circ\text{C}$  and a surface pressure of  $10 \text{ mN/m}$ .<sup>10</sup> The reproducibility and accuracy of surface pressure isotherms can be verified by recording the surface pressure-area isotherms of these standards.

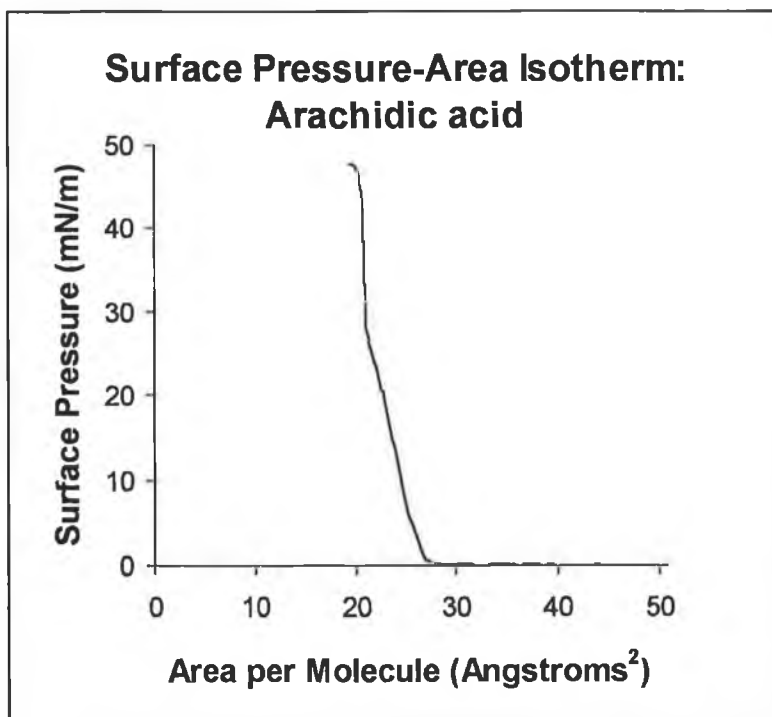
#### (i) Surface Pressure-Area Isotherms

Figure 2.3 shows a typical compression isotherm for arachidic acid on a pure water subphase. A surface tension of  $72.8 \text{ mN/m}$  recorded for the subphase prior to floating of the monolayer confirmed the cleanliness of the water used. The two phase transitions, from gas to liquid and liquid to solid, described in Section 1.2.1(ii) are clearly evident. By extrapolating the second linear portion to zero surface pressure, the intercept gives the area per arachidic acid molecule that would be expected for the hypothetical state of an uncompressed closely packed monolayer. The value of  $22 \text{ \AA}^2/\text{molec}$  compares well with the area occupied by arachidic acid molecules in a single crystal and is consistent with the concept that a compact monolayer is like a two-dimensional solid.

#### (ii) Deposition

It was found that good quality LB films of cadmium arachidate could be deposited easily from  $0.1 \text{ mM CdCl}_2$  subphases at an acceptable dipping speed of  $50 \text{ mm/min}$ , as shown in Figure 2.4. The uniformity of the transfer ratios obtained,

although slightly higher than unity, is indicative of good film transfer to the glass substrate.



**Figure 2.3** The monolayer was spread from 100  $\mu$ l of 1.02 mg/ml chloroform solution on a subphase of Milli-Q deionized water (pH 5.5).

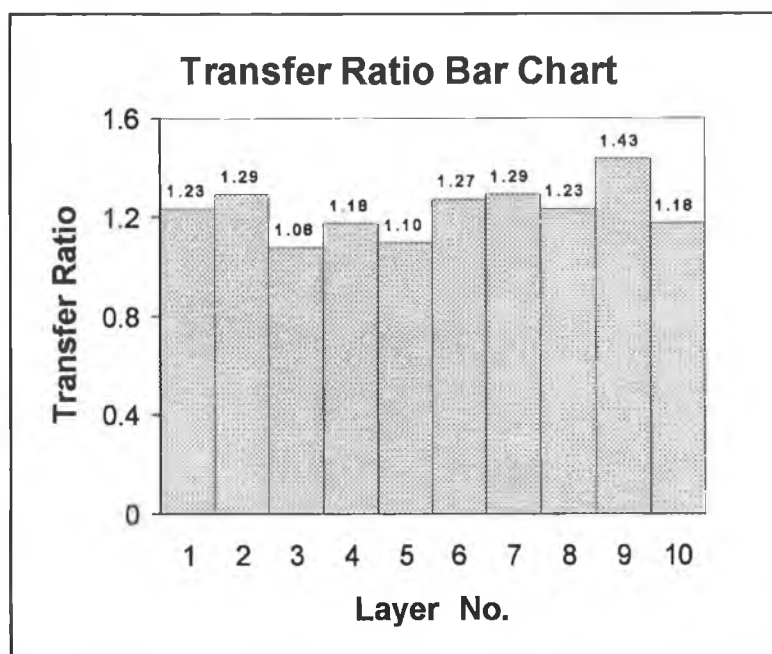


**Figure 2.4** Molecule: Arachidic Acid. Subphase: 0.1mM CdCl<sub>2</sub>. Surface Pressure: 25mN/m. Dipper Speed: 50 mm/min. Substrate: Silanized Glass. Compartment: A.

## 2.3.2 Langmuir Films of Eicosenoic acid

### (i) Surface Pressure-Area Isotherms

The properties of Langmuir films of eicosenoic acid on various subphases were studied by measuring the changes in surface pressure upon monolayer compression. The minimum equilibration period required prior to compression was established by comparing isotherms obtained as a function of time. As there was no visible change in  $\pi$ -A isotherms recorded at 10, 20 and 30 minutes after spreading, subsequent compressions were started 10 minutes after spreading.

#### *Pure Water Subphase (pH 5.5)*

In Figure 2.5 the characteristic compression isotherm for *cis*-11-Eicosenoic acid,  $(\text{CH}_3(\text{CH}_2)_7\text{CH}=\text{CH}(\text{CH}_2)_9\text{COOH})$ , on a pure water subphase is shown. Due to dissolved atmospheric carbon dioxide the pure water subphase attains a slightly acidic pH (5.5). The  $\text{p}K_a$  of eicosenoic acid in solution is expected to be similar to that of other long chain fatty acids, which typically have a  $\text{p}K_a \sim 4.8$  (weak acids),<sup>11</sup> although there have been reports of a positive shift in this value to a  $\text{p}K_a$  of 5.6 at the air-water interface.<sup>12</sup> Therefore, on a pure water subphase the monolayer is expected to be at least partially dissociated. The  $\pi$ -A isotherm recorded was quite expanded, with a mean molecular area corresponding to the initial increase in surface pressure,  $A_i$ , of approximately  $53 \text{ \AA}^2/\text{molec}$ . Throughout the compression the surface pressure increased uniformly indicating that the monolayer remained in the liquid-expanded state. The monolayer could be compressed to a zero pressure molecular area,  $A_0$ , of  $38 \text{ \AA}^2/\text{molec}$ . There was no visible phase transition to a liquid-condensed state and monolayer collapse occurred in the liquid-expanded state, at a collapse pressure,  $\pi_c$ , of  $32.5 \text{ mN/m}$ . This is consistent with the fact that eicosenoic acid (EA) is liquid in the bulk at temperatures (23-24 °C), just above room temperature. The *cis*-type double bond has quite an effect on the structure of the EA molecule and the manner in which it packs at the air-water interface when compressed. As is evident from the large value  $A_0$ , its molecular configuration prevents the formation of a tightly and homogeneously packed monolayer. For the production of high quality LB films it is

essential that the spread monolayer is in a condensed state during deposition. In order to achieve a condensed state the molecular arrangement of the Langmuir film has to be altered, this can be accomplished by varying the subphase pH and/or composition.

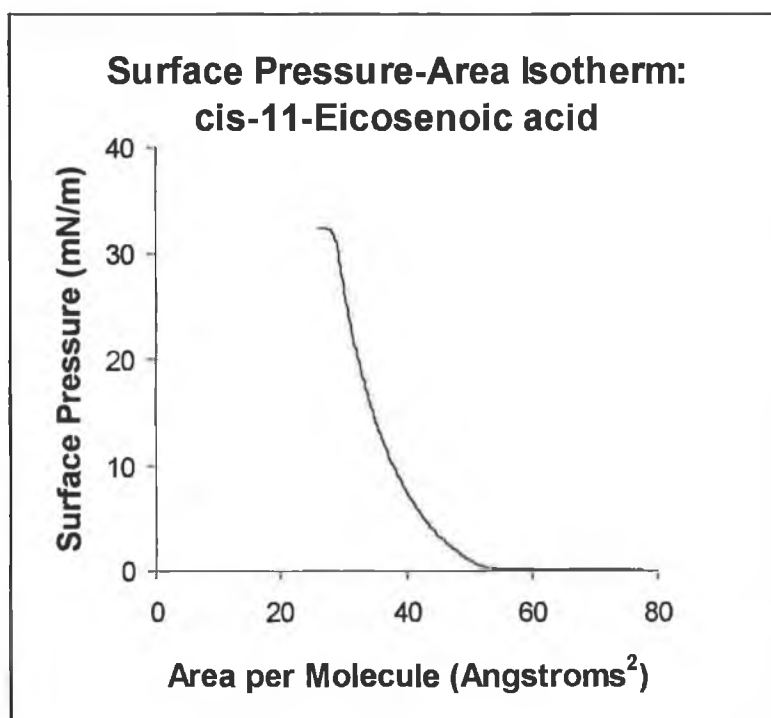


**Figure 2.5** The monolayer was spread from a dilute chloroform solution of Eicosenoic acid (~1mg/ml) on a subphase of Milli-Q deionized water (pH 5.5).

#### *The Effect of Subphase pH on the $\pi$ -A Isotherms*

Compression isotherms of EA were studied on subphases buffered at various pH. Figure 2.6 shows  $\pi$ -A isotherms recorded on citrate/phosphate subphases at pH values of 2.30, 3.95, 6.00 and 7.85. At low pH (2.30) the isotherm recorded corresponds to that of the free acid (i.e., all the EA molecules are in the undissociated form) and monolayer collapse occurs at a surface pressure equal to the Equilibrium Spreading Pressure, ESP, of the pure acid monolayer. The ESP of EA was found to be 30.6 mN/m, a value slightly lower than the collapse pressure for the monolayer on a pure water subphase. The observed value of  $A_i$  was 57 Å<sup>2</sup>/molec. As the pH is increased, there is a concurrent increase in the collapse pressure of the monolayer. At pH 3.95 ionization of the EA occurs, and carboxylate ions are present in the

monolayer while hydrogen ions are located in the subphase. There is a noticeable decrease in the value of  $A_i$  as the pH is increased. The observed condensation appears to arise from the known attraction between unionized and ionized fatty acid molecules.<sup>13</sup> At basic pH (7.85) the collapse pressure of the monolayer rises to 49.5 mN/m while  $A_i$  increases to values in excess of 100 Å<sup>2</sup>/molec.

Figure 2.7 shows  $\pi$ - $A$  isotherms recorded on phosphate subphases at pH 4.40 and 9.18. The observed collapse pressure at pH 9.18 is almost identical in value to that observed at pH 7.85, suggesting that there is a limiting collapse pressure for the completely dissociated monolayer, which is independent of pH once complete dissociation of the monolayer has occurred. Therefore, at any fixed surface pressure the monolayer contracts on going from a fully associated to a partially dissociated film. However, on increasing the pH further, the monolayer becomes increasingly dissociated, resulting in expansion of the monolayer due to the electrostatic repulsion of the adjacent carboxylate head groups.

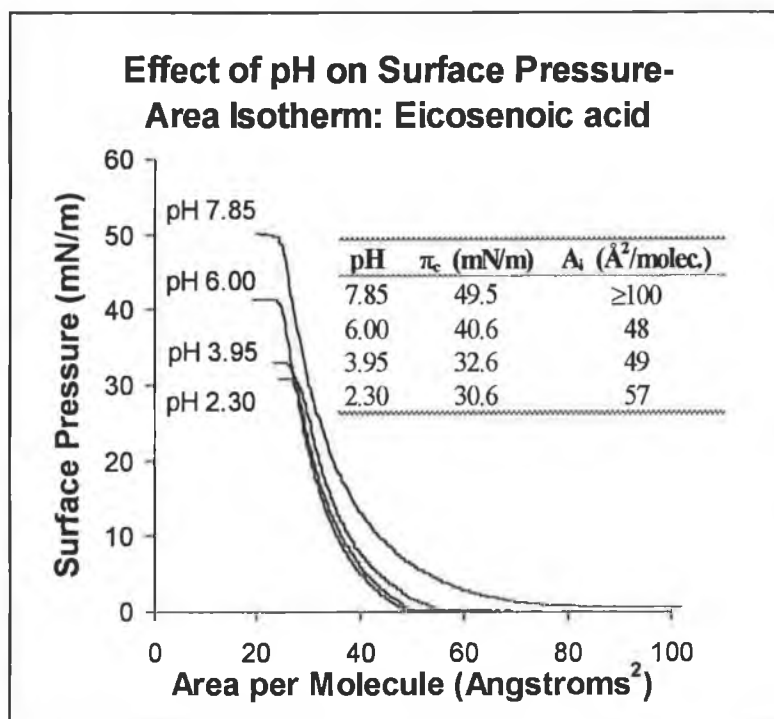


**Figure 2.6** Monolayers were spread from a dilute chloroform solution of Eicosenoic acid on citrate/phosphate subphases of varying pH.

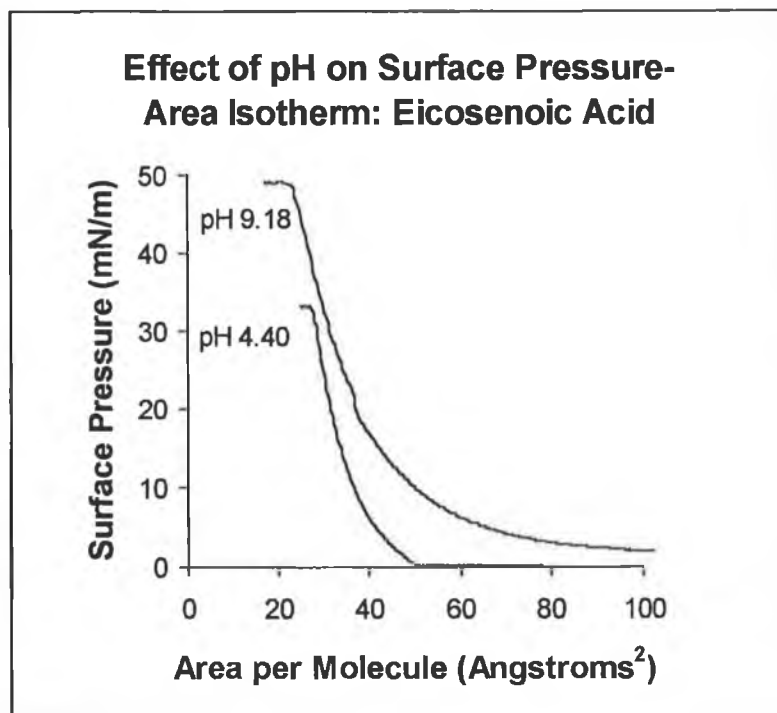


**Figure 2.7** Monolayers were spread from dilute chloroform solutions of Eicosenoic acid on phosphate subphases: (a) 0.1 M  $\text{NaH}_2\text{PO}_4$  (pH 4.40), (b) 0.1 M  $\text{Na}_2\text{HPO}_4$  (pH 9.18).

#### *The Effect of Subphase Composition on the $\pi$ -A Isotherms*

It is evident from the  $\pi$ -A isotherms presented above, that while EA monolayers have some desirable properties for triggered drug release, varying the subphase pH alone does not improve the processability of the EA monolayer. The monolayers formed at the air/water interface remained in the liquid-expanded state at room temperature during the course of the compression. In order to apply the LB technique in a reproducible manner the monolayer must be sufficiently condensed. One approach to achieving this objective is to associate several carboxylate units by complexing them with a metal cation. Multivalent cations have a marked effect on the carboxylate anions and influence monolayer properties considerably. Metal salts form stronger intermolecular interactions than pure acids and so enable the formation of more condensed monolayers, with increased stability and transferability. It is also essential that the monolayer is in a solid-expanded state to allow the resultant LB film to be polymerized. The EA molecules must lie parallel to each other in a solid state, yet still have enough freedom to reorientate themselves during the polymerization process. It is clear that EA is sterically difficult to compress to an area suitable for

polymerization of the monolayer. However, by varying the subphase composition, the ionizable carboxylic acid head groups may be used to control the intermolecular distance of the monolayer and possibly improve interchain alignment, thereby enhancing the reactivity of the initially expanded monolayer. The extent to which metal ions present in the subphase are incorporated into the monolayer depends on the degree of dissociation of the monolayer which increases with both pH and metal ion concentration. The subphase pH can also affect the form in which the ion exists as some metal ions, for example  $\text{Al}^{3+}$  hydrolyzes readily (i.e., they tend to form soluble complexes with hydroxide ions).<sup>13</sup> To compare the monolayer condensing effect of divalent and trivalent metal ions,  $\pi$ -A isotherms were recorded on subphases containing  $\text{ZnCl}_2$  and  $\text{AlCl}_3 \cdot 6\text{H}_2\text{O}$ .

### Divalent Ions

The effect of divalent ions on the  $\pi$ -A isotherms of EA was studied by recording compression isotherms on subphases containing  $\text{Zn}^{2+}$  at 0.1, 1.0 and 10 mM concentrations. The pH of each subphase was typically 5.6. Figure 2.8 shows that at a concentration of 0.1 mM the value of  $A_i$  was similar to that observed for  $\pi$ -A isotherms recorded on a pure water subphase, indicating that at this concentration the metal ion had very little effect on the  $\pi$ -A isotherm. There was also a slight increase in the collapse pressure of the monolayer, 34.4 mN/m compared to 32.5 mN/m on pure water. At 1.0 mM  $\text{Zn}^{2+}$  there was a definite condensation of the monolayer with  $A_i$  shifting to lower molecular areas, and the collapse pressure increasing to 35.7 mN/m. The induced condensation is a result of the covalent 2:1 complex formed between the EA and the divalent cation.<sup>13</sup> At 10 mM  $\text{Zn}^{2+}$  a substantial monolayer condensation was achieved although it is questionable that the limiting area obtained ( $31 \text{ \AA}^2/\text{molec.}$ ) will be sufficient to permit polymerization of the resultant LB film.

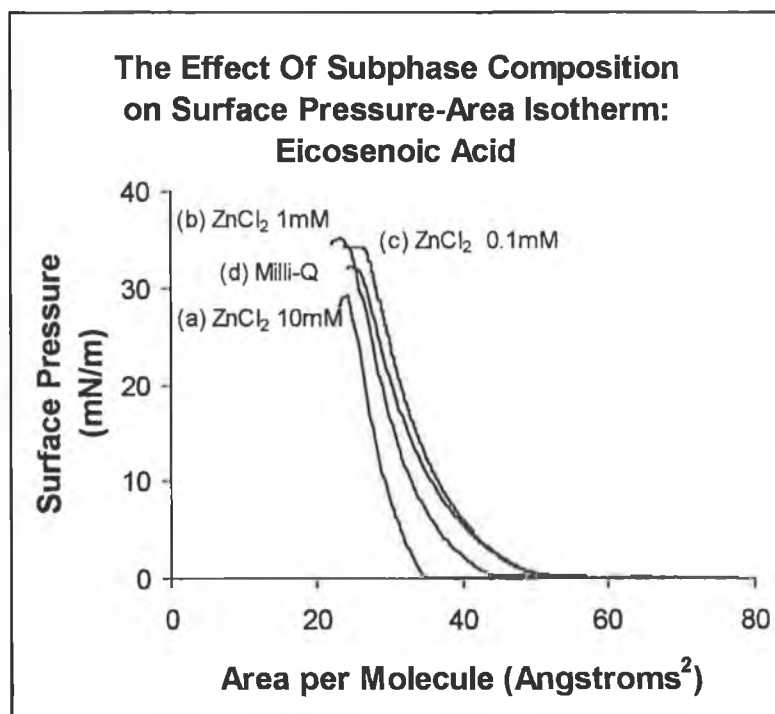


**Figure 2.8** The effect of divalent ion concentration on the Surface Pressure-Area isotherm: (a) 10 mM ZnCl<sub>2</sub>, (b) 1.0 mM ZnCl<sub>2</sub>, (c) 0.1 mM ZnCl<sub>2</sub>, (d) Milli-Q deionized water.

### Trivalent Ions

The possibility of inducing monolayer condensation on subphases containing trivalent cations was investigated by studying  $\pi$ -A isotherms of EA in the presence of Al<sup>3+</sup>. The monolayer condensing effect of the trivalent aluminium ion was found to be far superior to that of the divalent zinc ion, as shown in Figure 2.9. A concentration of 0.1 mM Al<sup>3+</sup> was sufficient to condense the monolayer considerably, to limiting areas of 30 Å<sup>2</sup>/molec. In the case of the divalent zinc ion a 10mM concentration was required to achieved the same level of condensation. Aluminium forms soluble Al(OH)<sup>2+</sup> monohydroxy complexes at low pH, and far superior condensation (~100 times more powerful) of the monolayer is achieved via hydrogen bonding interactions between the larger hydrolyzed ion and the ionized EA molecules. A solid-like phase has been observed in  $\pi$ -A isotherms of oleic acid monolayers (C<sub>17</sub>H<sub>34</sub>COOH), this molecule also contains a *cis*-type double bond and difficulties in monolayer condensation were previously reported.<sup>13</sup> It may be that the geometry of the *cis*-unsaturation in the hydrocarbon chain prevents further condensation of the EA monolayer.

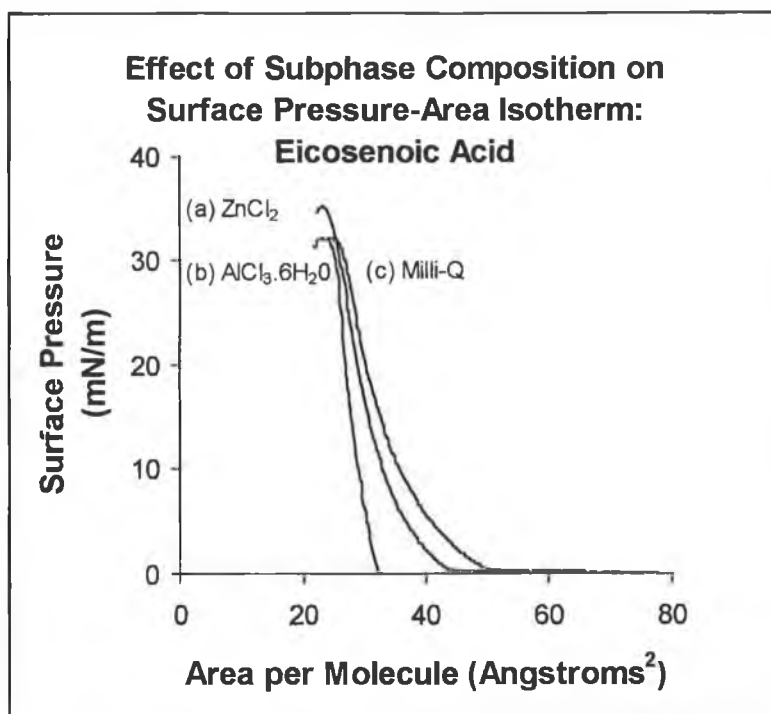


**Figure 2.9** The effect of multivalent ions on the Surface Pressure-Area isotherm: (a) 0.1 mM  $\text{AlCl}_3 \cdot 6\text{H}_2\text{O}$ , (b) 1.0 mM  $\text{ZnCl}_2$ , (c) Milli-Q deionized water.

## (ii) Deposition

The efficiency of monolayer transfer to a solid substrate is given by its transfer ratio (i.e., the ratio of the removed film area to the theoretical substrate area), which is measured for each substrate pass through the air-water interface. The measured transfer ratio is an averaged value over the entire immersed surface. Irregular transfer ratios outside the  $1.00 \pm 0.05$  range are generally indicative of poor film quality. However, if the substrate is not smooth, then the actual area is greater than the geometric area and higher transfer values higher than unity are observed. Therefore, transfer ratios  $\pm 5\%$  are acceptable. Poor transfer ratios are a result of patchy film adhesion, caused by undefined regions where the film has been deposited and peeled off. A number of experimental conditions affect the transfer ratio, in particular the nature and concentration of ionic components in the aqueous subphase, the deposition pressure of the monolayer, the nature of the solid substrate and the dipping speed of the substrate through the monolayer.

The LB deposition of EA monolayer from multivalent subphase solutions to hydrophilic/silanized glass substrates was investigated. Since the optimum deposition

pressure and substrate velocity have to be determined experimentally, these two parameters were varied systematically. The transferability of monolayers from subphases containing divalent cations at 1 mM concentrations (pH 5.6) was very poor. Increasing the pH to 7.3 with 0.1 mM NaHCO<sub>3</sub> resulted in no improvement in the monolayer transfer. The observed transfer ratios, which were irreproducible and greater than three in some cases, are abnormally high. Surface pressures were found to increase on every alternate passage through the interface, indicating that each time a monolayer was coated onto the slide it peeled off and respread on the subphase surface with subsequent immersion/emersion. Stripping off occurred irrespective of the substrate nature (hydrophilic/hydrophobic). Increasing the deposition pressure had the effect of increasing the transfer values further. Varying the dipping speed between 5 and 65 mm/min did not significantly improve the transfer ratios at any deposition pressure. In fact, at the very slow speeds very high ratios (>3) were observed confirming that the monolayer was unstable and collapsed continuously as the deposition proceeded. When LB films were deposited onto hydrophilic and silanized glass substrates from subphases containing aluminium ions at a concentration of 0.1 mM (see Figure 2.10 & 2.11), the transfer ratios improved considerably, owing to the more condensed nature of the monolayer. An optimum dipping speed of 40 mm/min was used. More reasonable values (0.9 to 1.3) were obtained indicating that the stability of the monolayer had increased substantially. However, it was still not possible to form multilayers on the hydrophilic glass surface as the monolayer repeatedly peeled off on the second immersion as indicated by the negative transfer ratios.

LB films of the saturated Arachidic acid were prepared to eliminate substrate preparation and deposition conditions as possible contributing factors to the poor transfer ratios obtained in the case of the EA monolayers. Since multilayers of arachidic acid could be formed without the complications associated with of EA system, one can only conclude that problem lies in the processability of the EA monolayer. It appears that monolayers of eicosenoic acid, due to their instability are not suitable for deposition onto solid substrates using the LB technique, and prefer to remain at the air-water interface.

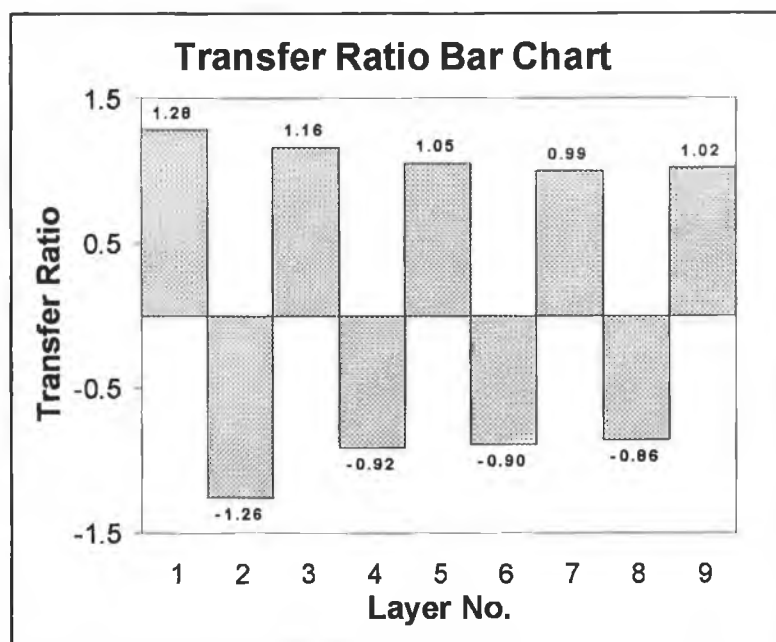


**Figure 2.10** Molecule: Eicosenoic acid. Subphase: 0.1 mM  $\text{AlCl}_3 \cdot 6\text{H}_2\text{O}$ . Surface pressure: 22 mN/m. Dipper speed: 40 mm/min. Substrate: Hydrophilic glass. Compartment: A.

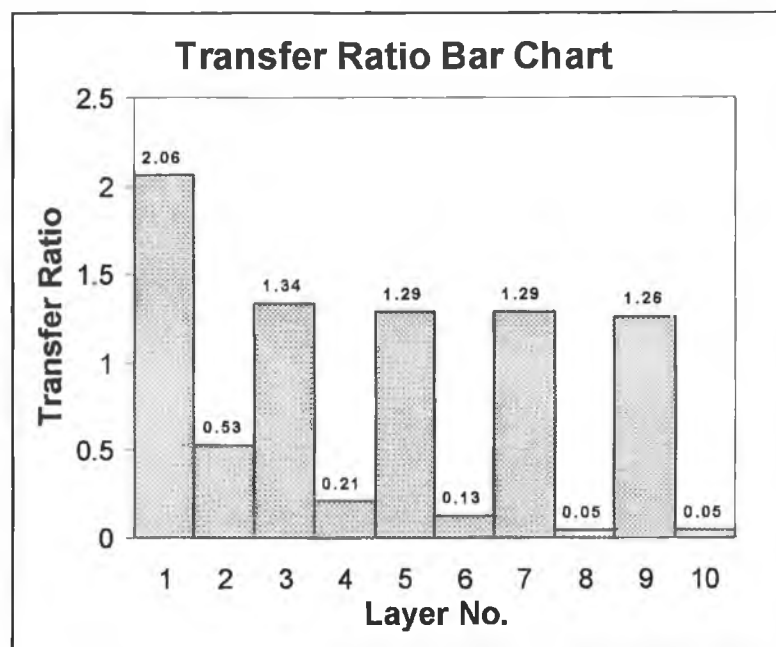


**Figure 2.11** Molecule: Eicosenoic acid. Subphase: 0.1 mM  $\text{AlCl}_3 \cdot 6\text{H}_2\text{O}$ . Surface pressure: 25 mN/m. Dipper speed: 30 mm/min. Substrate: Silanized glass. Compartment: A.

## 2.4 CONCLUSIONS

Due to difficulties in condensing the eicosenoic acid molecules to a solid-expanded state at the air/subphase interface, poor adhesion of the monolayer to the substrate was frequently encountered and as a result good deposition of EA was not feasible. However, it is evident from the  $\pi$ -A isotherms recorded as a function of subphase pH, that deprotonation of the acid groups within the monolayer at basic pH creates electrostatic repulsion within the film, causing it to expand. The fact that additional expansion of an intrinsically quite expanded layer (manifested by the large observed  $A_s$  of  $\sim 50 \text{ \AA}^2/\text{molec}$ ), occurred on increasing the subphase pH, emphasizes the magnitude of the electrostatic repulsion that exists between the ionized carboxylic acid group within the monolayer. Consequently, pH induced structural changes can potentially control the monolayer permeability. This is promising, since other unsaturated fatty acid molecules, which form high density Langmuir films and undergo facile UV-polymerization can be used as monomers for the manufacture of organized pH responsive polymers. The solid state polymerization of LB films of diacetylenic acids has been reported in the literature,<sup>14, 15</sup> and these amphiphilic monomers appear to be potential candidates for controlled release systems. Investigations into the structural characteristics of these diynoic acid films, in different physical/chemical environments were carried out, the details of which are discussed in the following chapter.

## 2.5 REFERENCES

- [1] Miyashita, T. *Prog. Polym. Sci.* **1993**, *18*, 263.
- [2] Cemel, A.; Fort, Jr., T.; Lando, J. B. *J. Polym. Sci.* **1972**, *10*, 2061.  
Laschewsky, A.; Ringsdorf, H.; Schmidt, G. *Polymer* **1988**, *29*, 448.
- [3] Tieke, B.; Graf, H.-J.; Wegner, G.; Naegele, B.; Ringsdorf, H.; Banerjee, A.; Day, D.; Lando, J. B. *Colloid Polym. Sci.* **1977**, *255*, 521.
- [4] Ringsdorf, H.; Schupp, H. *J. Macromol. Sci. Chem.* **1981**, *A15*, 1015.  
Laschewsky, A.; Ringsdorf, H. *Macromolecules* **1988**, *21*, 1936.
- [5] Nakanishi, F. *Thin Solid Films* **1989**, *179*, 71.
- [6] Sugi, M. *J. Mol. Electron.* **1985**, *1*, 3.
- [7] Gaines, G. L. Jr. *Nature* **1982**, *298*, 544.
- [8] Walsh, S. P.; Lando, J. B. *Langmuir* **1994**, *10*, 252.
- [9] Peltonen, J. P. K.; He, P.; Lindén, M.; Rosenholm, J. B. *Thin solid films* **1992**, *210/211*, 372.
- [10] Gaines, G. L. Jr. *Insoluble Monolayers at Liquid-Gas Interfaces*, Wiley-Interscience, New York, London, Sydney **1966**.
- [11] Roberts, G. *Langmuir-Blodgett Films*, Plenum Press, New York, **1990**.
- [12] Betts, J. J.; Pethica, B. A.; *Trans. Faraday Soc.* **1956**, *52*, 1581.  
Joos, P. *Bull. Soc. Chim. Belg.* **1971**, *80*, 277.
- [13] Lindén, M.; Rosenholm, J. B. *Langmuir* **1995**, *11*, 4499.  
Peltonen, J. P. K.; He, P.; Lindén, M.; Rosenholm, J. B. *J. Phys. Chem.* **1994**, *98*, 12403.
- [14] Ogawa, K. *J. Phys. Chem.* **1991**, *95*, 7109.
- [15] Deckert, A. A.; Horne, J. C.; Valentine, B.; Kiernan, L.; Fallon, L. *Langmuir* **1995**, *11*, 643.

---

## **CHAPTER 3**

# **Formation, Polymerization and Characterization of Tricosadiynoic Acid Monolayers**

---

### 3.1 INTRODUCTION

The studies detailed in the previous chapter on the eicosenoic acid system, showed that at basic pH, deprotonation of the carboxylic acid functionalities within the monolayer, created electrostatic repulsion between neighbouring ionized groups and ultimately resulted in monolayer expansion. Having demonstrated that a change in the pH of the monolayer microenvironment can induce structural changes within the monolayer, further investigations into monolayer systems of polymerizable amphiphiles are justified.

In order to circumvent the problems encountered with the EA films, two factors were considered carefully when choosing the second compound, namely the molecular structure and the polymerization process. The formation and polymerization of EA monolayers was hindered by the unfavourable manner in which the EA molecules associate. Therefore, a molecules structure, which dictates the way in which it packs in two dimensions, is crucial to the formation of a polymerized monolayer. It is only through favourable intermolecular interactions that monolayer stability and structural order are maintained during the LB transfer and polymerization processes. The polymerization process itself is also of great important, since it must proceed with complete retention of the ordered monolayer structure. Consequently, it is necessary to utilize compounds containing a functional group which undergoes topochemical polymerization (i.e., the transition from monomer to polymer takes place without destruction of the crystal lattice).

Tricosadiynoic acid, an amphiphilic diacetylene meets the above requirements since is packs well at the air water interface, contains two conjugated triple bonds (which undergo topochemical polymerization) and possesses a terminal carboxylic acid functionality. The compound appears to be a potential candidate for the manufacture of organized pH responsive polymers, and it is hoped that the high density ordered polymer LB films formed may be used in controlled release systems.

### 3.1.1 Polymerization of Diacetylenes

Diacetylenes are known to form highly ordered polymers by topochemical polymerization in the solid state. The topochemical reaction retains the molecular packing in the crystal lattice and leads to chains of conjugated double and triple bonds<sup>1</sup> which absorb strongly in the visible region. The mechanism has been extensively studied and proceeds as radical stepwise 1, 4-addition to the conjugated triple bond as shown in Figure 3.1. The intermediate is a carbene, with two non bonded electrons on the carbon atom, and the reaction proceeds so rapidly that oxygen quenching is not a problem unlike double bond additions that are rapidly quenched by oxygen and must be conducted under an inert atmosphere.

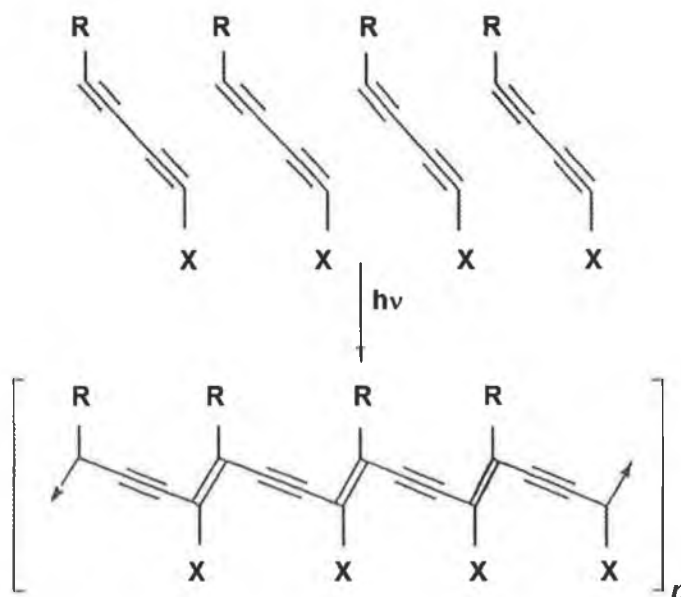
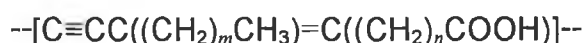


Figure 3.1 Polymerization of Diacetylenes.

Diacetylenes only polymerize in situations where the molecules are in a 2D or 3D regular arrangement and polymerization occurs when the van der Waals distance is close to the chemical bond length and when the diacetylene rod is at  $45^\circ$  angle to the plane of polymerization. In solution or in a disordered solid state they are completely inactive to polymerization.<sup>2,3</sup>

### 3.1.2 LB Films of Diacetylenic Acids

Several publications<sup>4-7</sup> have shown that the use of diacetylenic monocarboxylic acids,  $\text{CH}_3(\text{CH}_2)_m\text{C}\equiv\text{CC}\equiv\text{C}(\text{CH}_2)_n\text{COOH}$ , in LB monolayers, leads to the formation of highly oriented, extremely thin, colored polymer films of exactly defined thickness. The polymerization reaction is brought about by UV irradiation of the monomer molecules, which induces the 1, 4-addition of adjacent diacetylene groups and results in the formation of a conjugated polymer backbone of the general structure



where  $m$  and  $n$  are the number of methylene units between the polyacetylene backbone and the terminal methyl and carboxylic acid groups of the polymer sidechains. The conjugated backbone has two resonance forms, namely the acetylenic and butatrienic isomers. The chain growth is one-dimensional and is restricted to areas where the molecules are in a perfectly crystalline arrangement.

Wegner *et al.*<sup>4, 5</sup> were the first to report on the polymerization of LB monolayers of amphiphilic diacetylenes by UV irradiation. The visible absorption spectrum of the pure polymer films contained maxima at 537 and 498 nm. X-ray diffraction data showed that the arrangement of the layers before and after polymerization were essentially identical. They suggested that the long hydrophobic chain which allows for spreading at the air-water interface helps retain order throughout the reaction because of side chain association.

Since the discovery that amphiphilic molecules containing a diacetylene group could be polymerized in monolayer form, there has been extensive interest in these systems. Early work focused primarily on optimizing experimental conditions such as subphase composition, pH, temperature and UV irradiation time. Tieke *et al.*<sup>6, 7</sup> investigated the influences of the aliphatic chain length, molecular structure and cadmium salt formation on the solid state reactivity of diacetylene monolayers. They found that the positioning of the diacetylene unit in the middle of the aliphatic chain reduced the monolayer stability. Fatty Acids with the diacetylene group positioned near the polar headgroup formed more stable monolayers, but the packing was less favourable for polymerization. They reported that a variation in the number of

methylene units between the diacetylene unit and the acid headgroup influenced the packing more than a change in the number of methylene units at the hydrophobic chain end. The presence of divalent metal ions was found to increase the stability of acids with less than sixteen methylene units in the hydrophobic chain. They concluded that polymerization behaviour is determined by the paraffin chain packing and that diacetylenic acids with the diacetylene group amidst the hydrocarbon chain provided the correct topology and degree of flexibility needed for the polymerization reaction.

The observed UV polymerization of Langmuir films in the so-called expanded state by Day *et al.*<sup>8</sup> suggested that diacetylene molecules aggregate and form domains in which all molecules are aligned immediately after spreading. Studies carried out using polarizing microscopy confirmed that diacetylene monolayers exhibited a domain structure.<sup>9</sup> Since topochemical polymerization proceeds as a lattice-controlled one-dimensional chain growth, the polymer chains are aligned parallel to each other within each domain. No epitaxy was found in diacetylene multilayers, i.e., the bottom layer does not dictate a packing pattern for all the subsequent layers built on top of it. A number of factors were found to influence the morphology of these multilayers including spreading solvent, subphase temperature and surface pressure.

Day and Ringsdorf<sup>10</sup> found that upon further UV irradiation the blue polymer converted irreversibly to a red form. Many groups have since reported similar color changes on exposure to solvents or elevated temperatures, and attempts to elucidate the mechanism of the chromism have preoccupied researchers for decades.<sup>10-12, 15</sup> Although the exact mechanism remains uncertain, it is generally accepted that the electronic properties of the backbone are strongly coupled to the side chains and that the  $\pi$ -electron conjugation in the red form is reduced. The absorption maximum of the polymer formed is closely related to the conjugation length, i.e., the length over which the backbone planarity is maintained without interruption. Therefore, the longer the conjugation length the longer the wavelength of maximum absorption.<sup>11</sup> The structure of the red form ( $\lambda_{\text{max}}$  ca. 530 nm) differs significantly from the blue form ( $\lambda_{\text{max}}$  ca. 640 nm), which, due to better organization, shows greater electron conjugation within the polymer chain. Hence, the nature of the absorption blue shift is considered to be a disruption in the extended conjugation of the  $\pi$ -system.

Resonance Raman studies have revealed that the color phase transition can be correlated with the ratio of the Raman peaks due to the C≡C and C=C stretching modes, which suggests that the blue and red forms of the polymer LB film are structurally different.<sup>12</sup> X-ray crystallographic and electron microscopy data indicate that the transformation from blue to red involves a rearrangement of the side groups and a small translation of the polymer chains.<sup>13</sup> It has been reported that the conformation of the side group changes by rod-coil transition of the backbone chain.<sup>14</sup> Charych *et al.*<sup>15</sup> used resonance Raman and visible absorption spectroscopy to probe the polydiacetylene backbone and <sup>13</sup>C NMR and FTIR to probe the side chains. Their studies suggest that the electronic properties of the polymer backbone are strongly coupled to the side chains conformation, although the exact mechanism of interconversion is unknown. There is some disagreement in the literature over the degree of order in the side chain groups within the blue and red forms of the polymer. While some studies reveal that the color change is due to the onset of a fluctuation and/or a structural disorder of the side chain groups linked to the polymer backbone<sup>16</sup>, others have found that thermochromic transition are induced by a reorganization of the side chains, from a partially disordered configuration in the blue phase, to a completely ordered one in the red phase.<sup>15</sup> In certain cases reversible color changes have been observed; for example Kaneko *et al.*<sup>12</sup> investigated the influence of annealing temperature on the absorption spectrum of polydiacetylene LB films and found that in the case of heptacosadiynoic acid, a reversible color change was observed for short annealing times at temperatures below 70 °C. However, in contrast to this they found that an irreversible color change was observed for an identically prepared polymer LB film of tricosadiynoic acid. X-ray diffraction patterns of the LB films revealed that the reversible phase transition is retained as long as the ordered layer structure of the polymer film is preserved.

Although a considerable amount of the early research in the area of diacetylenic amphiphiles focused primarily on LB films of carboxylic acids, a number of studies have investigated the possibility of forming polymerizable liposomes from phospholipid derivatives of the 10, 12-diynoic acids.<sup>17, 18</sup> Hub *et al.* synthesized polymerizable phospholipid-like monomers containing a diacetylene moiety. They found that sonication of aqueous suspensions of these phospholipid analogs yielded

liposomes which could be polymerized by UV light with complete retention of structure.<sup>18</sup> This suggests that topochemical polymerization can occur in the spherical double layer orientation of the monomers. O' Brien *et al.*<sup>17</sup> studied polymerization of lipid diacetylenes and found that polymerization of bilayer membranes containing symmetrical lipids was dramatically more efficient and resulted in the formation of a blue polymer ( $\lambda_{\text{max}} = 644 \text{ nm}$ ) suggesting that these polymerized bilayers have longer average conjugation lengths and/or a more ordered structure. This was thought to be due to the proper stereochemical arrangement of the diacetylenic groups in the  $\alpha$  and  $\beta$  chains of the symmetrical molecule. The possibility of forming stable spherical polymer membranes from lipid diacetylenes could prove very advantageous if analogous monolayer membranes of these lipid systems display pH dependent permeability characteristics.

Another factor which can influence the color of the polymer formed is the molecular density within the LB film. Tomioka *et al.*<sup>19</sup> found that as the surface pressure increased, the color changed from blue to red and concluded that there was a correlation between the degree of packing and the color of the polymer. The high density films appeared red due to the compression induced distortion of the polymer chain which reduces the delocalization of the  $\pi$ -electrons. Ogawa<sup>20</sup> studied the effect of molecular density on polymerization of diacetylene films and discovered that the type of polymer formed depended on the molecular density. Low-density type monolayers resulted in the formation of polydiacetylene which decomposed upon excessive irradiation, while the high-density type monolayers formed a polyacetylene polymer which did not decompose on continued irradiation. Further studies<sup>21</sup> on the effect of molecular density on the electron beam polymerization of diacetylenic acids, using X-ray diffraction analysis and IR spectroscopy supported these conclusions. Deckert *et al.*<sup>22</sup> studied the polymerization and thermochromism of high and low-density LB films of cadmium salts of 5, 7-diynoic acids. In agreement with previous studies on the influence of molecular densities, they found that the red monoclinic form of the polymer is obtained when polymerization is carried out at higher densities and higher temperatures.

Molecular modeling has been used to study molecular orientations in films of different molecular densities. Higashino *et al.*<sup>23</sup> simulated the molecular arrangement

of diacetylene LB films revealing that in the low-density type films, the molecules which form a polydiacetylene had a gauche-trans conformation, while in the high-density film the molecules were in the trans-trans conformation necessary for the formation of a polyacetylene.

10, 12-Tricosadiynoic acid is a longchain monocarboxylic acid with a diacetylenic functionality situated at the middle of the hydrocarbon chain. This research focused on the formation of LB monolayers from this compound and their subsequent polymerization, with the aim of carrying out electrochemical permeation studies on the resultant polymerized monolayers. The barrier properties of polymerized monolayers have not been previously reported in detail. The intention is that by investigating the permeability of these monolayers to simple ions and larger inorganic complexes, valuable information concerning the possible use of these structures as components for drug release systems would be obtained.

## 3.2 EXPERIMENTAL

### 3.2.1 Materials/Reagents

10, 12-Tricosadiynoic acid (98 %) was purchased from Lancaster Synthesis (Morecambe, UK). Chloroform ( $\geq 99.8$  %), supplied by Fluka (Gillingham, UK) was used as the spreading solvent for the monolayer preparation. Ultra-pure water (resistivity  $\geq 18$  M $\Omega$  cm), obtained from a Milli-Q filtering system (Millipore Corp., USA) was used as the pure water subphase in equilibrium with atmospheric CO<sub>2</sub>. In order to remove polymer formed during storage, the tricosadiynoic acid (TDA) was recrystallized from boiling light petroleum ether (40-60 °C) immediately prior to volumetric preparation of a  $\sim 1$  mg/ml CHCl<sub>3</sub> solution. This is essential as the presence of trace amount of polymer decreases the stability of the Langmuir film and can induce the premature collapse of a fresh film at constant surface pressure. Inorganic salts and buffers, used to alter the subphase composition and pH respectively, were reagent grade quality.

For the permeation studies lithium perchlorate (95+ %) obtained from Aldrich (Gillingham, UK) was used to make up electrolyte solutions. Potassium ferricyanide (99+ %) was also obtained from Aldrich. The ITO coated glass substrates (Resistance 400  $\Omega$  cm<sup>-2</sup>) were purchased from Applied Films Corp. (Boulder, USA). Aqueous solutions were freshly prepared from ultra-pure water and degassed with nitrogen prior to use.

### 3.2.2 Preparation of TDA Monolayers

Surface pressure-Area ( $\pi$ -A) isotherms of Langmuir films of TDA were recorded using a Nima Technology (Coventry, UK) Model 2022 circular, alternate layer, Langmuir-Blodgett trough. The surface pressures were measured to an accuracy of 0.1 mN/m using a Wilhelmy plate pressure sensor. Monolayers were spread from dilute chloroform solutions ( $\sim 1$  mg/ml) of TDA on the aqueous subphase surface by means of a Hamilton microsyringe. Complete solvent evaporation was

achieved within 10 minutes. A constant barrier speed of 50 cm<sup>2</sup>/min was applied during each compression. Reproducible  $\pi$ -A isotherms were obtained at room temperature on the subphases studied.

LB films were deposited onto standard microscope slides and ITO coated glass slides (7.6 cm × 2.6 cm). Both the glass and ITO/glass substrates were cleaned by sonicating in detergent, rinsing in Milli-Q deionized water, sonicating in isopropanol and finally rinsing in deionized water. The ITO/glass slides were then rinsed in acetone. Hydrophilic glass slides were prepared by soaking overnight in NaOH (2 g/dm<sup>3</sup>), and rinsing well in deionized water prior to use. Oven dried glass slides were rendered hydrophobic by immersing them in a 5 % chloroform solution of (CH<sub>3</sub>)<sub>2</sub>SiCl<sub>2</sub> (>99.5 %, Fluka), for 10-15 minutes, rinsing in methanol and storing in deionized water. A deposition pressure, within the 20-25 mN/m range was chosen, and maintained at the chosen value  $\pm 0.5$  mN/m, while the monolayer was transferred onto the substrate at dipping speeds typically in the region of 30-50 mm/min. A substrate area of approximately 12.5 cm<sup>2</sup> (4.8 cm × 2.6 cm) was immersed through the compressed monolayer. The quality of the LB film obtained was estimated through the transfer ratio (i.e., ratio of the removed film area to the geometric substrate area) calculated after each immersion/emersion.

Polymeric TDA films (PTDA) were formed in two ways. Monomeric TDA monolayers were either polymerized after LB deposition, or alternatively they were polymerized at the air-water interface prior to deposition. In the second case a polymeric PTDA monolayer is deposited. Polymerization of the TDA molecules was achieved by irradiating with UV light (Model UVGL-58 lamp, UVP inc., USA) at 254 nm. Transmission visible spectra of TDA and PTDA modified substrates were obtained using a UV-3100 UV-Vis NIR Spectrophotometer (Shimadzu) using the unmodified glass or ITO/glass substrate as the reference.

### 3.2.3 Permeation Studies

Electrochemical measurements were performed using a CH Instruments Model 660 Electrochemical Workstation (CH Instruments Inc., Cordova, USA) in a specially constructed three-electrode, teflon electrochemical cell which is depicted in Figure 3.2 below. The unmodified/modified ITO-coated glass slide acted as the working electrode, the geometrical area sampled was approximately  $0.16 \text{ cm}^2$ . Each slide could be sampled at three different locations by simply placing the platinum counter electrode and Ag/AgCl reference electrode (BAS, Stockport, UK) in the relevant compartment. All potentials are reported with respect to the Ag/AgCl reference electrode whose potential is 44.2 mV more positive than SCE.<sup>24</sup>

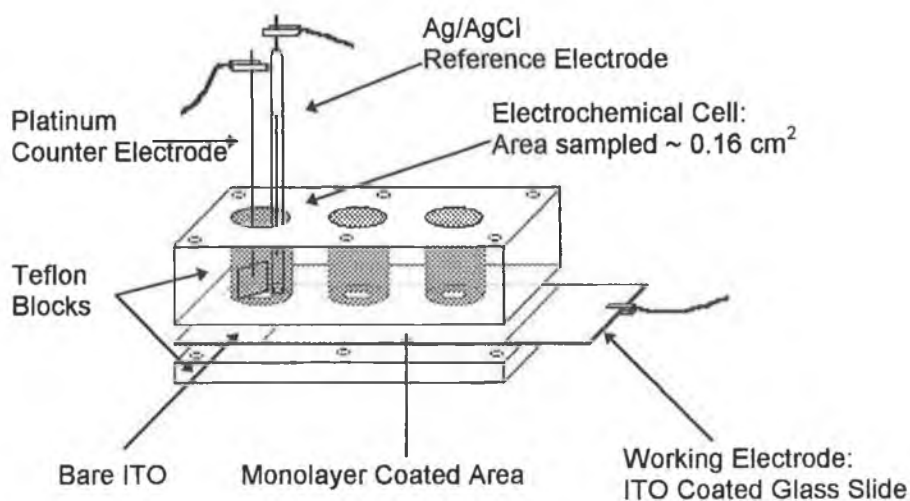


**Figure 3.2** Electrochemical cell used for capacitance/permeation studies.

## 3.3 RESULTS & DISCUSSION

### 3.3.1 Surface Pressure-Area Isotherms

#### (i) TDA Monolayers

Figure 3.3 shows characteristic compression isotherms obtained for 10, 12-Tricosadiynoic acid (TDA). The isotherms recorded were very reproducible, and neither the solution concentration nor the initial area had any measurable effect on the zero pressure molecular area,  $A_0$ , or the collapse pressure,  $\pi_c$ , for the TDA monolayers.

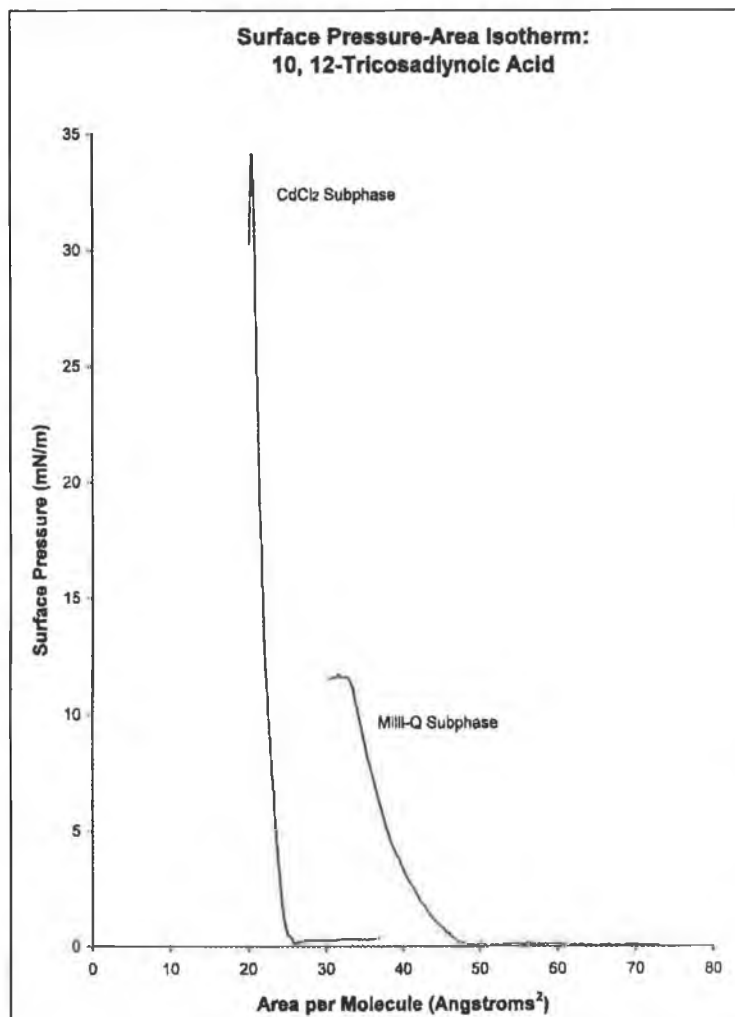
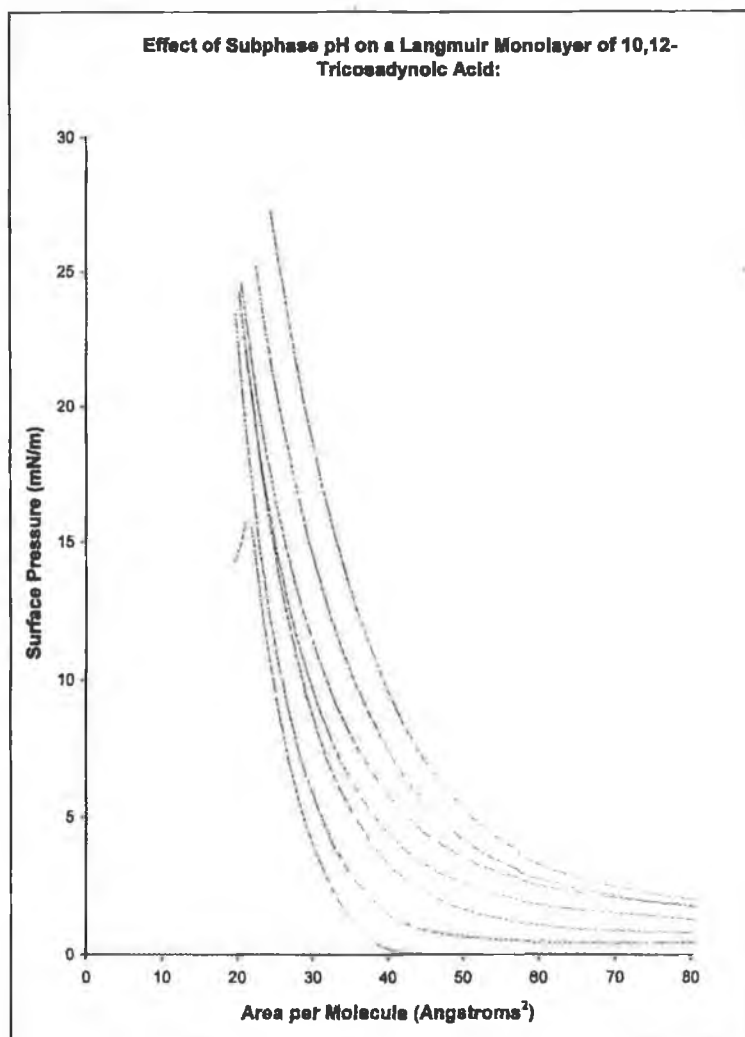


Figure 3.3 Surface pressure-area isotherms for TDA. Curve (a): Milli-Q pure water subphase. Curve (b) Subphase containing  $3 \times 10^{-4}$  M CdCl<sub>2</sub> and  $5 \times 10^{-5}$  M NaHCO<sub>3</sub>.

On a pure water subphase the monolayer is quite expanded, the average molecular area on the initial increase of surface pressure,  $A_i$ , was approximately  $48 \text{ \AA}^2/\text{molec}$ . The  $\pi$ -A isotherm is essentially featureless and the surface pressure increased monotonically with compression. The stability of the monolayer on pure water was quite low and monolayer collapse occurred at a surface pressure of  $12.3 \text{ mN/m}$ . By adding  $\text{Cd}^{2+}$  ions to the subphase at a concentration of  $3 \times 10^{-4} \text{ M}$  the monolayer stability was greatly enhanced, and it could withstand pressures in excess of  $20 \text{ mN/m}$ . A steep increase in surface pressure occurred at an  $A_i$  of  $25 \text{ \AA}^2/\text{molec}$  and the monolayer collapsed at a surface pressure of  $35 \text{ mN/m}$ . The zero pressure area for a TDA molecule within the monolayer was  $23 \text{ \AA}^2/\text{molec}$  indicating that the monolayers formed are in a sufficiently condensed state to undergo LB deposition.

## (ii) Effect of pH on TDA Monolayers

The effect of subphase pH on the  $\pi$ -A isotherm of a Langmuir film of TDA was investigated. The monolayer was spread on a subphase of  $10 \text{ mM Na}_2\text{HPO}_4$ , pH 9. At this pH the TDA molecules are expected to be fully ionized.<sup>25</sup> Figure 3.4 shows the first compression recorded for the monolayer which reveals that at an initial spreading area of  $80 \text{ \AA}^2/\text{molec}$ , the monolayer registers a surface pressure of  $2 \text{ mN/m}$ . Clearly, electrostatic repulsion exists between the ionized carboxylic acid groups of the molecules at the interface. Prior to monolayer collapse, the monolayer was expanded to the initial area and  $\text{H}_2\text{SO}_4$  was added to the subphase. The monolayer was allowed to equilibrate for 2 minutes before recompression. Again the  $\pi$ -A isotherm was recorded, but stopped prior to monolayer collapse. The process was repeated, adding acid each time to decrease the pH, until finally the monolayer collapsed. A sample of the subphase was removed and the pH was found to be 5.3. It was found that as the subphase pH decreased the surface pressure of the monolayer recorded at a given area per molecule decreased, due to the reduction in monolayer surface charge density.



**Figure 3.4** Effect of decreasing subphase pH on monolayer compression isotherm. Subphase composition: 10 mM Na<sub>2</sub>HPO<sub>4</sub> (pH 9.05), H<sub>2</sub>SO<sub>4</sub> added to decrease pH.

Based on the results of the preliminary experiments described above, it was decided to carry out a more in depth study on the effect of pH on the  $\pi$ -A isotherm and collapse pressure of the TDA monolayer. Subphases of different pH were made up and the isotherms recorded are shown in Figure 3.5 overleaf. Interestingly, the area at which monolayer collapse occurs decreases with increasing subphase pH. This apparent increase in the stability of the ionized monolayer appears to arise because of the greater hydrophilicity of the deprotonated monolayer. The variation in  $\pi_c$  with subphase pH is plotted in Figure 3.6. For comparison, the data obtained for the Eicosenoic acid system studied in Chapter 2 is included.

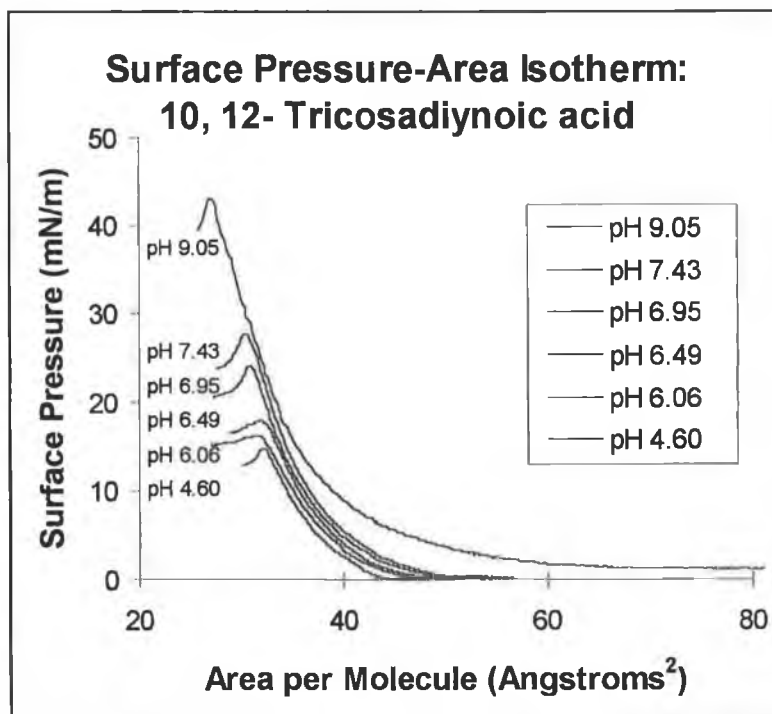


Figure 3.5 TDA monolayers recorded as a function of subphase pH. Subphase composition:  $\text{NaH}_2\text{PO}_4/\text{Na}_2\text{HPO}_4$  (total 10 mM  $\text{PO}_4^-$ ).

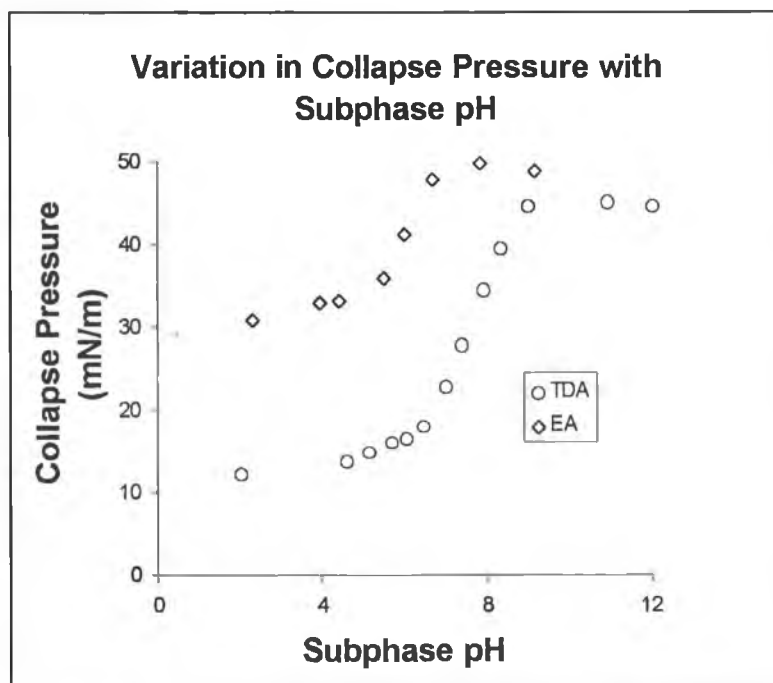


Figure 3.6 Plots of  $\pi_c$  versus subphase pH for both EA and TDA monolayers.

The  $\pi_c$  vs. pH curve follows an S-shaped trend, strikingly similar to the dissociation curves of weak acids. The collapse pressure for these layers was found to be directly related to the degree of monolayer ionization. From the point of inflection it is estimated that the monolayer  $pK_a$  is roughly 8 in the case of TDA and 6 in the case of EA. It is interesting to note that for the TDA system, the shift in  $pK_a$  is larger than that of EA. Since both compounds are long chain fatty acids, one would expect them both to have a similar solution phase  $pK_a$  value of approximately 4.8.<sup>26</sup> Several groups<sup>27</sup> have reported that in monolayer systems, the  $pK_a$  of terminal carboxylic acid groups shifts positively relative to the bulk  $pK_a$  of the compound. This shift in  $pK_a$  has been attributed to hydrogen bonding stabilization and a lower dielectric constant within the monolayer.<sup>28</sup> The higher surface  $pK_a$  value observed for the TDA system relative to the EA system confirms, that the degree of molecular association and structural order within the TDA monolayer is greater.

### 3.3.2 Formation of PTDA Films

As mentioned in the introduction, diacetylenes polymerize under topochemical control via a 1, 4-addition reaction to yield deeply colored polymers. The TDA polymer backbone consists of conjugated double and triple bonds,



which absorb strongly in the visible region (R and R' are the hydrophobic and hydrophilic substituents  $CH_3(CH_2)_9-$  and  $-(CH_2)_8COOH$ , respectively). The absorption of visible light by the polymer is extremely useful in characterizing the material. An indication of the extent of polymerization and the macroscopic homogeneity/inhomogeneity of the deposited layers can be simply obtained by recording the visible absorption spectrum of the polymer film. Figure 3.7 below shows a crystalline configuration of the TDA molecules within the monolayer.<sup>23</sup> However, this configuration is probably more representative of a single domain, as fatty acid diacetylenes are known to aggregate, forming domains of uniquely oriented molecules.<sup>9</sup>

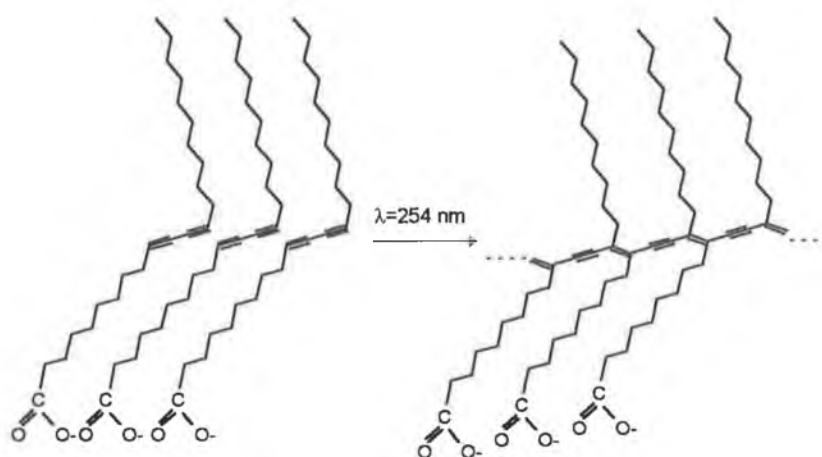


**Figure 3.7** Illustration of the gauche-trans conformation of the TDA  $[CH_3(CH_2)_9C\equiv CC\equiv C(CH_2)_8COOH]$  molecules within monolayer. On irradiation with UV light 1, 4-polymerization occurs with retention of molecular arrangement.<sup>23</sup>

The formation of polymer LB films from amphiphilic monomers can be achieved by two approaches (see Figure 2.1). The first involves the transfer of a monomeric film to a solid substrate, followed by polymerization of the molecules within the LB film form. The second involves polymerization of the floating monolayer at the air-water interface, followed by deposition of the polymer monolayer. Both approaches were used to form polymer TDA (PTDA) films.

### (i) Deposition of TDA Monolayer Followed by Polymerization

#### *Deposition of TDA Monolayers*

Since a close packed monolayer, with an interfacial area per TDA molecule of  $23 \text{ \AA}^2$  could be formed on a subphase of  $3 \times 10^{-4} \text{ M CdCl}_2$  and  $5 \times 10^{-5} \text{ M NaHCO}_3$ , the deposition of TDA monolayers was investigated. It was found that monolayers could be easily transferred to both hydrophilic and hydrophobic glass substrates at a surface pressure of  $20 \text{ mN/m}$  and a rate of  $30 \text{ mm/min}$ . As indicated in Figure 3.8, the transfer ratios observed were close to unity indicating good monolayer transfer.

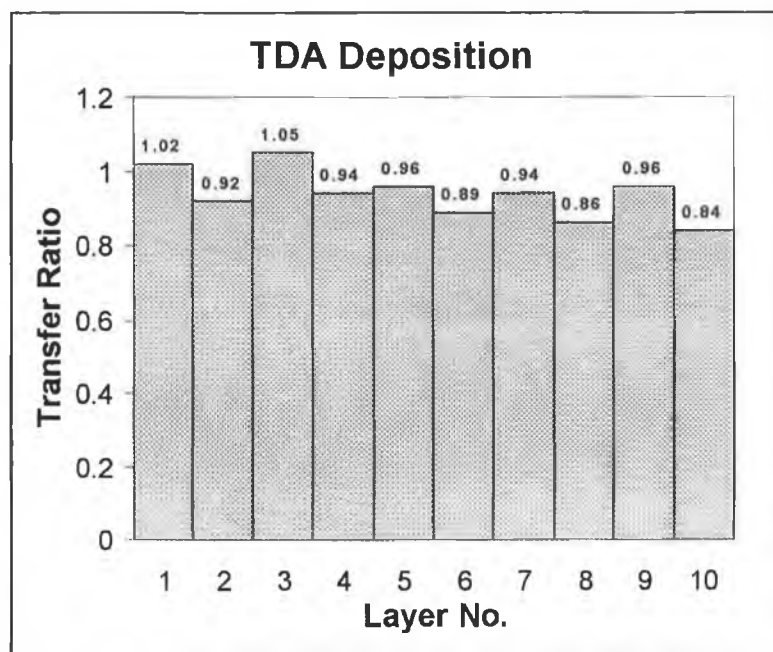


**Figure 3.8** Transfer ratios obtained for the transfer of 10 TDA monolayers to a hydrophobic glass substrate. Conditions as described in text.

### UV Polymerization of TDA LB Film

Following deposition, the LB film was irradiated with UV light and polymerization of the film was monitored as a function of irradiation time. Figure 3.9 shows the resultant polymerization profile. There are two interesting points to note; the first is that polymerization initially proceeds very rapidly before the rate decreases. The increase in the intensity of the absorption bands observed at 629 and 580 nm after 15 minutes is only very slight. The second interesting point is that in contrast to previous reports,<sup>10, 20</sup> continued irradiation does not yield the red form of the polymer.

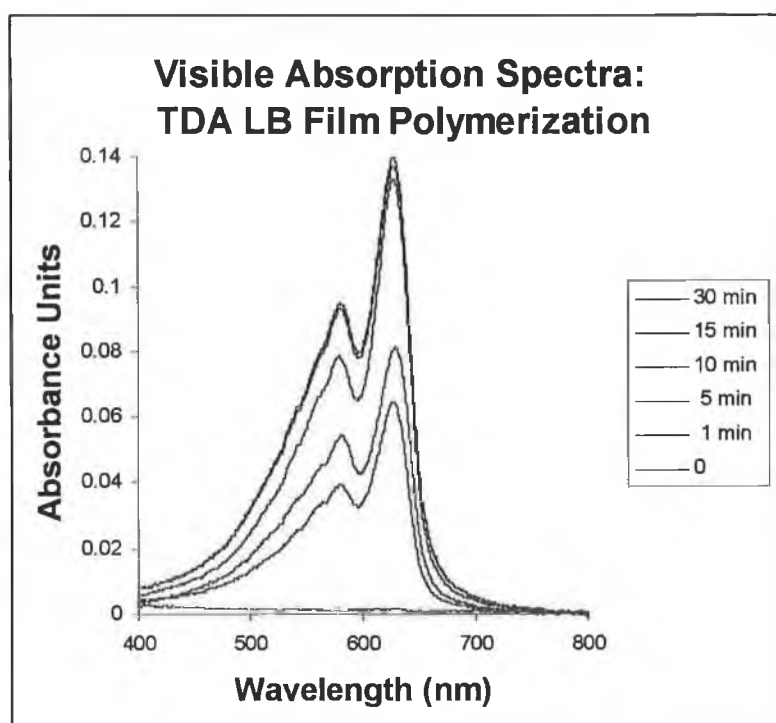


**Figure 3.9** Polymerization profile of a ten layer LB film deposited to a hydrophobic glass slide from a subphase of  $3 \times 10^{-4}$  M  $\text{CdCl}_2$  and  $5 \times 10^{-5}$  M  $\text{NaHCO}_3$ . Surface pressure: 20 mN/m. Dipping speed: 30 mm/min. From bottom to top the traces were recorded at UV irradiation time: 0, 1, 5, 10, 15, 30 minutes.

As shown in Figure 3.10, heating the sample above 80 °C resulted in the irreversible conversion of the blue polymer film to the red form ( $\lambda = 547$  and 504 nm). It is possible that the conversion reported in previous studies was in fact due to local heating within the film, as a result of prolonged irradiation or a more intense UV source. However, exposure to ethanol also results in conversion from the blue to a red form with absorption bands at the same wavelength. Therefore, heat treatment is

not the sole mechanism by which the structure of PTDA films can be changed. The mechanism by which the observed chromism occurs was not investigated here.

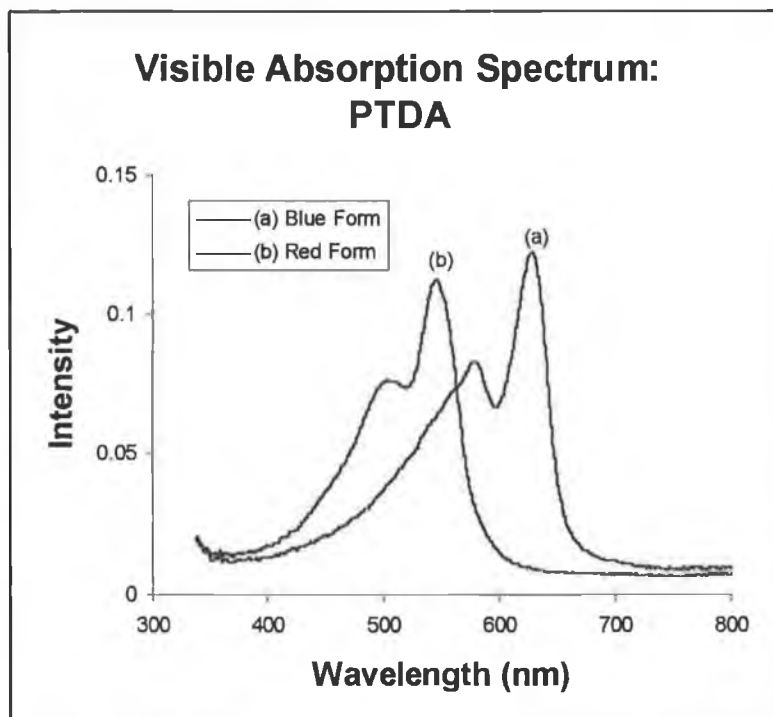


**Figure 3.10** Curve (a) Visible absorption spectrum of polymerized LB film of TDA. Absorption maxima are at  $\lambda = 629$  and  $579$  nm. Curve (b) Visible absorption spectrum of solvent/heat treated polymerized LB film of TDA. Absorption maxima are at  $\lambda = 547$  and  $504$  nm.

Figure 3.11 shows the absorption spectrum of a single monolayer deposited with a transfer ratio of 1.09, as a monomer film under the conditions described previously. Although the signal to noise ratio is poor, the relevant bands at 630 and 580 nm are evident. When the sample was heated, the expected shift in the wavelength of maximum absorption was observed. The absorbance maximum was 0.0134 absorbance units at  $\lambda_{\text{max}} = 627$  nm for the blue form and 0.0135 absorbance units at  $\lambda_{\text{max}} = 580$  nm for the red form. The molar extinction coefficients for the blue and red forms of the monolayer,  $\epsilon_B$  and  $\epsilon_R$  respectively, were estimated from the absorbance maxima using the Beer-Lambert Law. Given that the area occupied per TDA unit within the monolayer was  $23 \text{ \AA}^2$  and that the monolayer thickness is estimated<sup>23</sup> at  $21 \text{ \AA}$ , the concentration of TDA was determined to be 3.43 M. The magnitudes of  $\epsilon_B$  and  $\epsilon_R$  were calculated and found to be 18,603 and 18,742  $\text{mol}^{-1} \text{ l cm}^{-1}$  respectively.

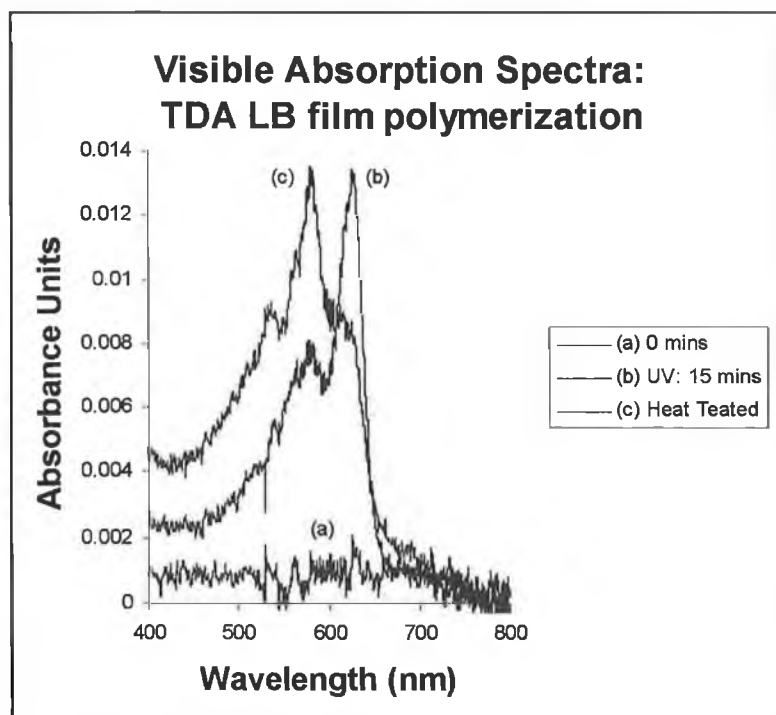


**Figure 3.11** The sample was irradiated with UV light for 15 minutes and then heated to 80 °C.

## (ii) Polymerization of TDA Monolayer Followed by Deposition

### *Polymerization Studies at the Air-Water Interface*

The polymerization of a floating TDA monolayer under constant surface pressure could be quantitatively followed by monitoring changes in the surface area per molecule. An analogous experiment in which the molecular area is maintained at a fixed value, results in an observed increase in the surface pressure. Since polymerization under constant surface pressure allows the molecules a certain degree of freedom, the effect of the polymerization pressure on the rate of polymerization was investigated here. Figure 3.12 shows the compression isotherms obtained for the polymerized TDA monolayer formed on a subphase of pure water. It is interesting to note that polymerization proceeds despite the expanded nature of the monolayer, confirming the existence of aggregates (i.e., islands of associated TDA molecules). Also, the polymerization rate seems to be greater at the lower polymerization pressure of 5 mN/m. After 15 minutes irradiation the monolayer was compressed until collapse. The collapse pressure for both polymers was approximately 29 mN/m

and the area per molecule (or more correctly per repeating unit) was almost identical. The isotherm obtained for the unpolymerized film is also shown for comparison. Note how the stability of the monolayer has substantially increased on polymerization. As the collapsed monolayer was further compressed, red bulk crystallites of polymer were observed on the water surface, indicating that the red form is obtained. This result differs from a report by Olmsted<sup>29</sup> on the formation of a blue polymer ( $\lambda = 640$  and  $580$  nm) at the air-water interface demonstrating that both experimental conditions (polymerized under nitrogen) and the monomer ( $C_{27}$  diacetylene) significantly affect the structure of the polymer film formed.

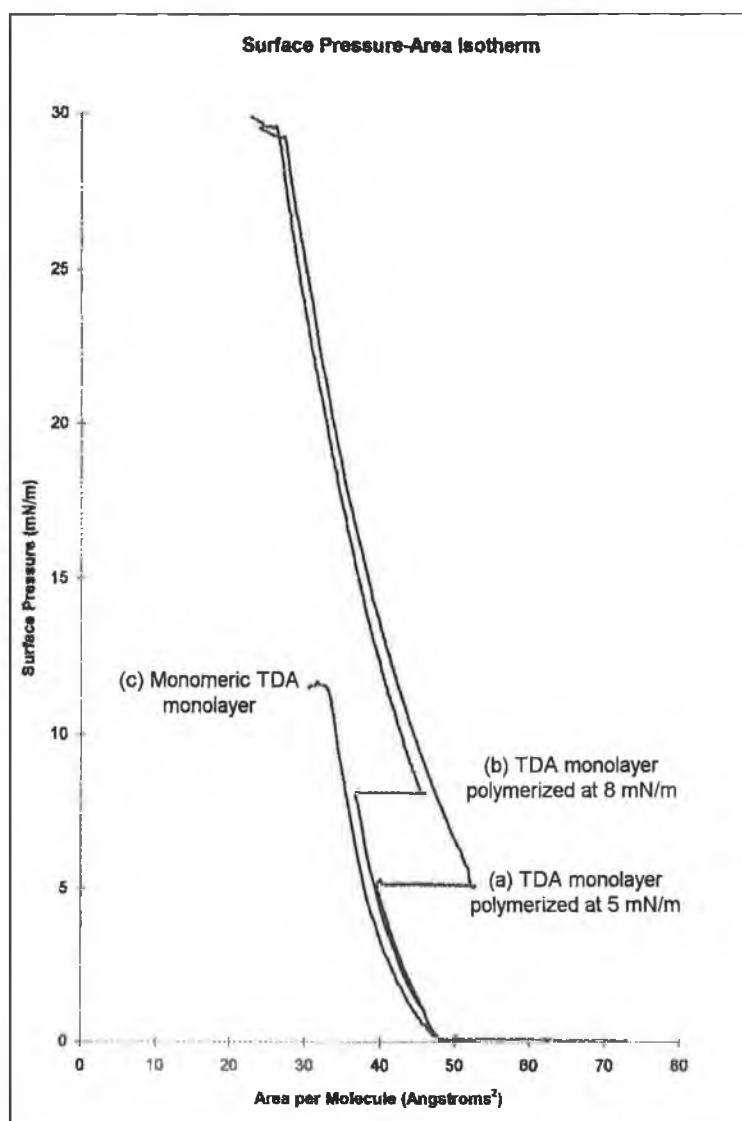


**Figure 3.12** Compression of TDA monolayers polymerized on a subphase of Milli-Q deionized water at surface pressures of (a) 5 mN/m and (b) 8 mN/m. The surface pressure-area isotherm for the monomeric TDA monolayer (c) is shown for comparison.

The fact that polymerization at the air-water interface occurs in ordered domains is not entirely unexpected. What is most surprising is that polymerization is accompanied by expansion of the monolayer (~25 %). Given that the polymerization process may be exothermic, it could be argued that local heating results in this expansion. However, since the polymerization is carried out on the water surface, one would expect that any heat generated would be quickly dissipated. It is perhaps significant to note that the polymer could be recompressed almost to its original area without destruction of monolayer structure. Had the monolayer structure ruptured at any stage during recompression, then the dramatic decrease in surface pressure typically associated with monolayer collapse would have been observed. The smooth increase in surface pressure on recompression suggests that this was not the case, and implies that there is a certain degree of flexibility within the polymerized monolayer. It is possible that on polymerization, a quite expanded polymer is formed due to the domain-like structure of the assembly, and that during recompression the polymer chains at the interface are annealed to form a more compacted polymer monolayer.

Polymerization as a function of surface pressure was also carried out on Cd<sup>2+</sup> subphases. It is evident from the Area-Time isobar displayed in Figure 3.13, that the polymerization reaction is considerably enhanced at lower surface pressures where monolayer expansion is greatest. Monolayers polymerized at 5 mN/m could withstand irradiation for up to 60 minutes, after which time the surface pressure decreases suggesting that the monolayer degrades. By comparison, monolayers polymerized at 25 mN/m degraded after 38 minutes of UV irradiation. Although, the initial difference in the average area per TDA molecule at the high and low surface pressures is quite small, typically 1-2 Å<sup>2</sup> (due to the monolayer condensing effect of the Cd<sup>2+</sup> ions present in the subphase), the large increase in the extent of polymerization seems to indicate, that steric restrictions encountered at the higher surface pressure of 25 mN/m are substantially reduced at 5 mN/m.

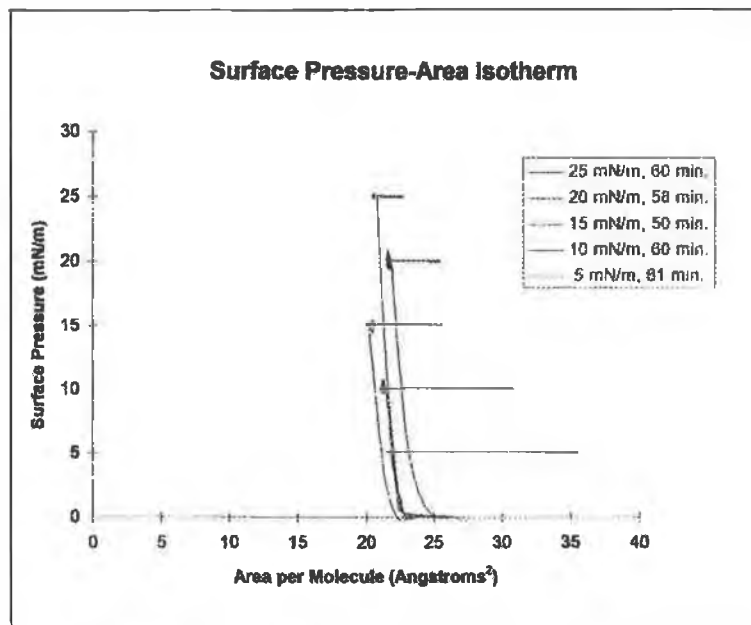
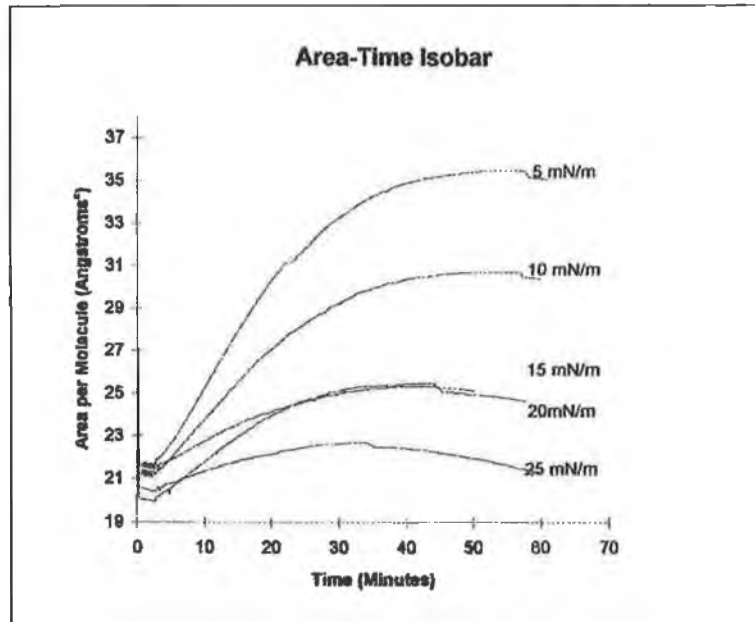


**Figure 3.13** The effect of surface pressure on the polymerization of TDA monolayers on a subphase of  $3 \times 10^{-4}$  M  $\text{CdCl}_2$  and  $5 \times 10^{-5}$  M  $\text{NaHCO}_3$ .

### Deposition of PTDA Monlayers

The stability of polymerized monolayer was such that the decrease in surface area over time at constant surface pressure was less than 4 % h<sup>-1</sup>. The polymerized Langmuir films could be deposited at 20 mN/m. Deposition was started after a stabilization period of 5 minutes at the selected deposition pressure. The meniscus was uniform throughout the transfer and excellent transfer ratios were observed. The PTDA films formed in this manner were red in color.

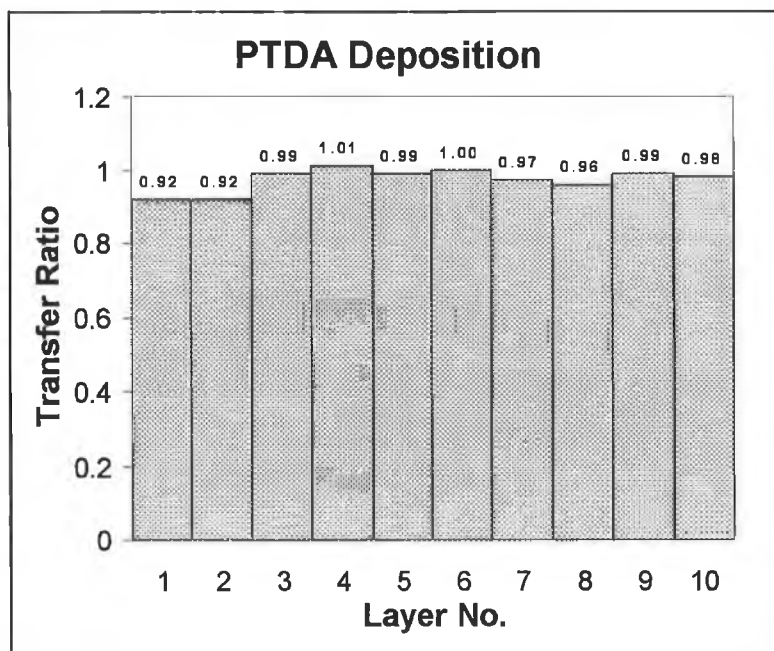


**Figure 3.14** Transfer ratios obtained for a TDA monolayer polymerized at the air-CdCl<sub>2</sub> subphase interface. Polymerization pressure: 10 mN/m. Deposition pressure: 20 mN/m. Dipping speed: 30 mm/min.

### 3.3.3 Capacitance Measurements

The presence of defect free TDA monolayer on the ITO slide is expected to passivate its conducting surface. The compact nature of the film should in theory prevent the permeation of ions and solvent molecules present in the contacting electrolyte solution. When the electrode is charged and electrostatic equilibrium is attained, the charge on the electrode is balanced by the charge at the monolayer-solution interface. The resulting charge separation can be described by two capacitors in series: the ideal compact capacity of the TDA monolayer,  $C_M$ , and the electrolyte concentration dependent capacity of the diffuse layer extending into the bulk electrolyte,  $C_{GC}$ .

When the interfacial capacity is measured, the total response ( $C_{dl}$ ) will be dominated by the smaller capacity as seen from equation 3.1.

$$\frac{1}{C_{dl}} = \frac{1}{C_M} + \frac{1}{C_{GC}} \quad (3.1)$$

Typically, the smaller capacity is that of the monolayer and  $C_{dl} \approx C_M$ . However in some cases (e.g., where the electrolyte concentration may be low thereby resulting in a relatively low value of  $C_{GC}$ ) the assumption that  $C_M \ll C_{GC}$  may not be valid and the contribution due to the diffuse layer capacitance,  $C_{GC}$ , must be taken in account. In this case, we assume that the double layer structure at the bare and coated electrode is similar and the interfacial capacitance measured for the bare ITO surface is taken as the value of  $C_{GC}$ .  $C_M$  is then calculated from the interfacial capacitance measured for the modified surface, using equation 3.1.

Capacitance measurements were carried out on monolayers of TDA deposited onto conducting ITO coated glass slides. Three techniques, cyclic voltammetry, chronoamperometry and AC impedance were used to determine the interfacial capacitance. The substrate was sampled in three different locations, twice at the monolayer coated ITO and once at the bare ITO as depicted in Figure 3.2. Both the monolayer capacitance and the dielectric constant within the monolayer could be estimated from the interfacial capacitance measurements as described below in subsection (iv).

### (i) Cyclic Voltammetry

Cyclic voltammograms were recorded at the bare and TDA modified ITO surface in 0.1 M LiClO<sub>4</sub>. The potential was scanned between 0 and 0.5 V vs. Ag/AgCl at scan rates between 0.05 and 1 V s<sup>-1</sup>.

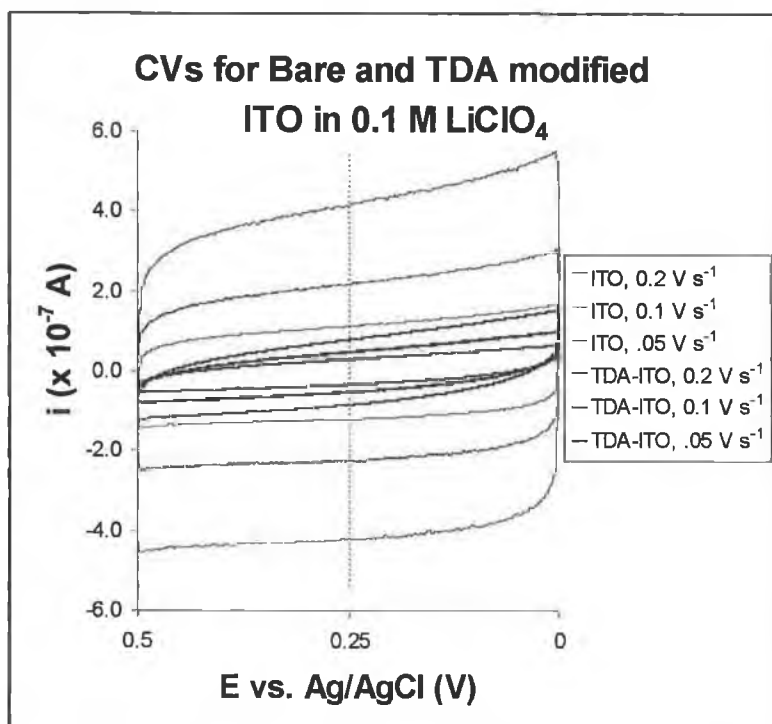


**Figure 3.15** Sample cyclic voltammograms of bare and TDA modified ITO recorded in 0.1 M LiClO<sub>4</sub>. From top to middle the traces are as follows: bare ITO, at scan rates of 0.2, 0.1 and 0.05 V s<sup>-1</sup> and TDA-ITO for the same scan rates. The vertical dotted line at 0.25 V indicates the potential at which  $i_{dl}$  was measured.

Figure 3.15 above shows typical traces observed as a function of scan rate. The double layer charging current (i.e., half the sum of the anodic and cathodic current), was measured at a potential of 0.25 V, and plotted versus the corresponding scan rate. Figure 3.16 shows the linear plots of  $i_{dl}$  vs.  $\nu$  obtained for the bare and TDA modified ITO surfaces. Given that the interfacial capacitance is related to the charging current and the scan rate according to following equation,

$$i_{dl} = \nu C_{dl} \quad (3.2)$$

the capacitance was determined from the slope of the curve, taking the electrode area to be  $0.16 \text{ cm}^2$ . It is evident that coating the ITO with a monolayer of TDA results in a significant reduction in the total capacitance for the system.

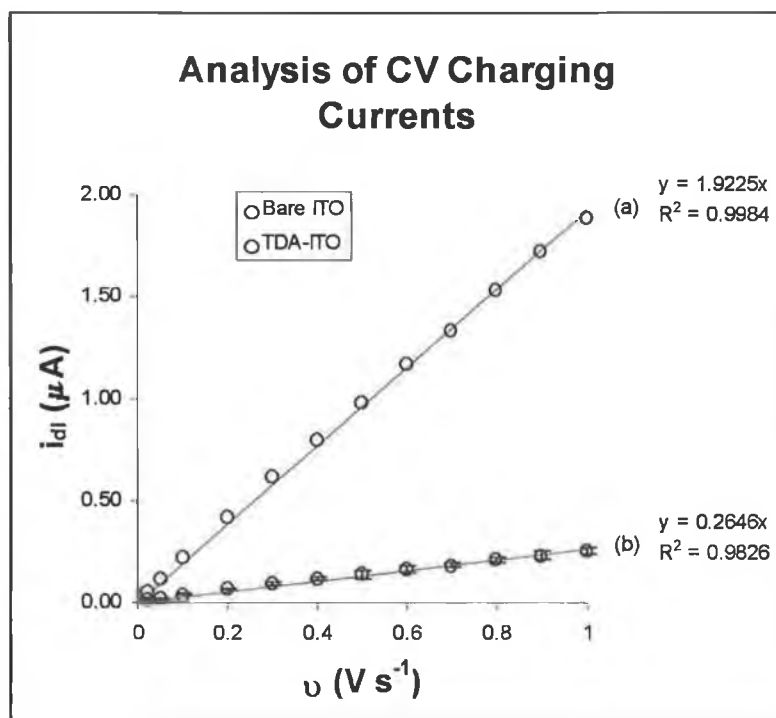


**Figure 3.16** Plot shows the scan rate dependence of the capacitive current for bare (a) and TDA-modified (b) ITO slide. The calculated capacitance values for the bare ITO and TDA modified ITO samples are  $12.0$  and  $1.7 \mu\text{F cm}^{-2}$  respectively.

## (ii) Chronoamperometry

Small amplitude potential pulse experiments of  $100 \text{ mV}$ , were carried out in  $0.1 \text{ M LiClO}_4$  at a base potential of  $0.25 \text{ V}$ . Figure 3.17 shows a current time transient typically obtained. The data were analyzed by plotting  $\ln i$  vs.  $t$  (see inset) in accordance with equation 3.3, which describes the exponential decay of the capacitive current that arises from the application a potential pulse  $\Delta E$ .

$$i_{dl}(t) = \frac{\Delta E}{R_U} \exp\left(\frac{-t}{R_U C_{dl}}\right) \quad (3.3)$$

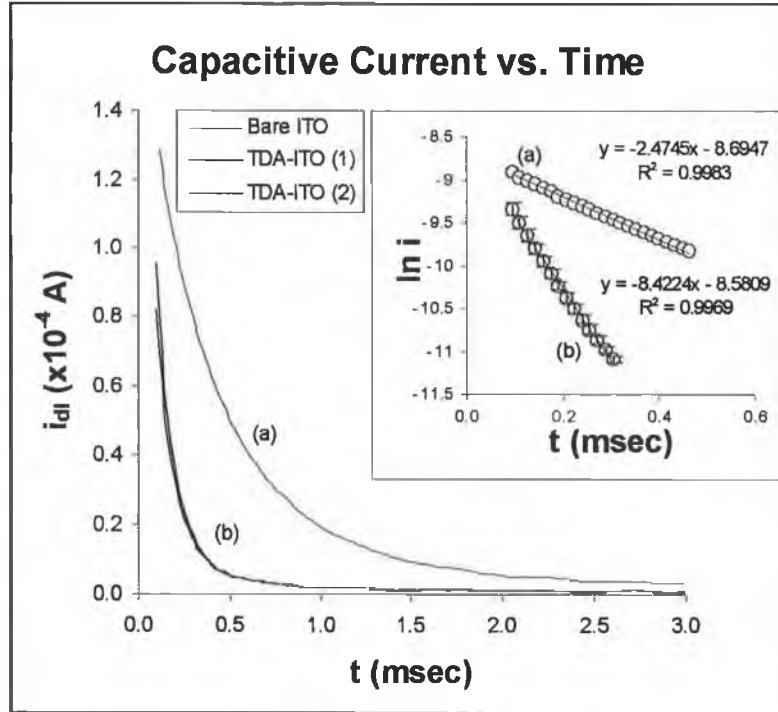


**Figure 3.17** Current-time transients recorded for the bare and modified ITO surfaces at 0.25 V in 0.1 M LiClO<sub>4</sub>, a potential step of 100 mV was applied. Inset shows the corresponding analysis of the experimental data. The calculated capacitance values are 4.2 and 1.4  $\mu\text{F cm}^{-2}$ , for the bare ITO (a) and TDA-ITO (b) samples.

Given that the semilog plot of  $\ln i$  vs.  $t$  is linear with an intercept of  $\ln (\Delta E/R_U)$  and a slope of  $(R_U C_{dl})^{-1}$ , the capacitance was calculated from equation 3.4 below

$$C_{dl} = \frac{-\exp(\text{int ercept})}{\Delta E * \text{Slope}} \quad (3.4)$$

### (iii) AC Impedance

AC impedance spectra for the bare and modified ITO surface were recorded in the frequency range  $10^4$  to 0.1 Hz at a potential of 0.25 V in 0.1 M LiClO<sub>4</sub>. The equivalent circuit used to model the interfacial region is one of a simple series combination of the electrolyte solution resistance,  $R_U$ , and the interfacial capacitance,  $C_{dl}$ . The total impedance measured,  $|Z|$ , is described in equation 3.5.

$$|Z| = R_U - j/\omega C_{dl} \quad (3.5)$$

At low frequencies the circuit behaves like a pure capacitor and the total impedance measured is approximated to

$$|Z| = \frac{1}{\omega C_{dl}} \quad (3.6)$$

Since the phase angle for a pure capacitor is  $-90^\circ$ , a good approximation of  $C_{dl}$  can be obtained at the maximum in Bode angle plot ( $\theta$  vs.  $\text{Log}(\omega)$ ) where the relationship in equation 3.6 applies. Figure 3.18 below shows the bode magnitude and angle plots obtained for the bare and modified ITO surface. The points highlighted on the Bode magnitude plot which coincide with the maximum in the corresponding Bode angle plot were used to evaluate the interfacial capacitance for the bare and modified ITO surfaces. Note also that at high frequencies ( $\text{Log}(\omega) > 4.5$ ) the impedance levels off and becomes independent of frequency. This is the region where the circuit behaves as a resistor and the observed impedance is due solely to  $R_U$  which is essentially the same for each sample.

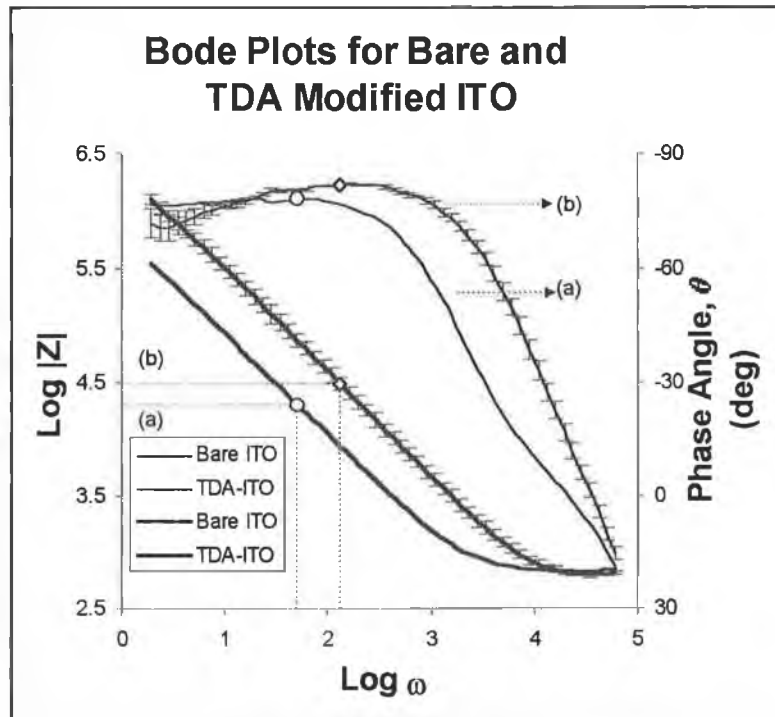


**Figure 3.18** Bode magnitude (heavy line) and angle (fine line) plots for (a) bare and (b) modified ITO samples recorded over the frequency range  $10^4$  to 0.1 Hz at a potential of 0.25 V in 0.1 M  $\text{LiClO}_4$ . The calculated capacitance values for the bare ITO and TDA modified ITO samples are 6.1 and  $1.5 \mu\text{F cm}^{-2}$  respectively.

It is also possible to display the data as a complex plane capacitance plot given the relations expressed in equations 3.7 and 3.8. In the complex plane capacitance plot the semicircle results from the series combination of  $R_U$  and  $C_{dl}$  and the intercept with the real axis yields the value of the interfacial capacitance.<sup>30</sup>

$$C' = \frac{Z''}{(|Z|)^2} \cdot \frac{1}{\omega} \quad (3.7)$$

$$C'' = \frac{Z'}{(|Z|)^2} \cdot \frac{1}{\omega} \quad (3.8)$$

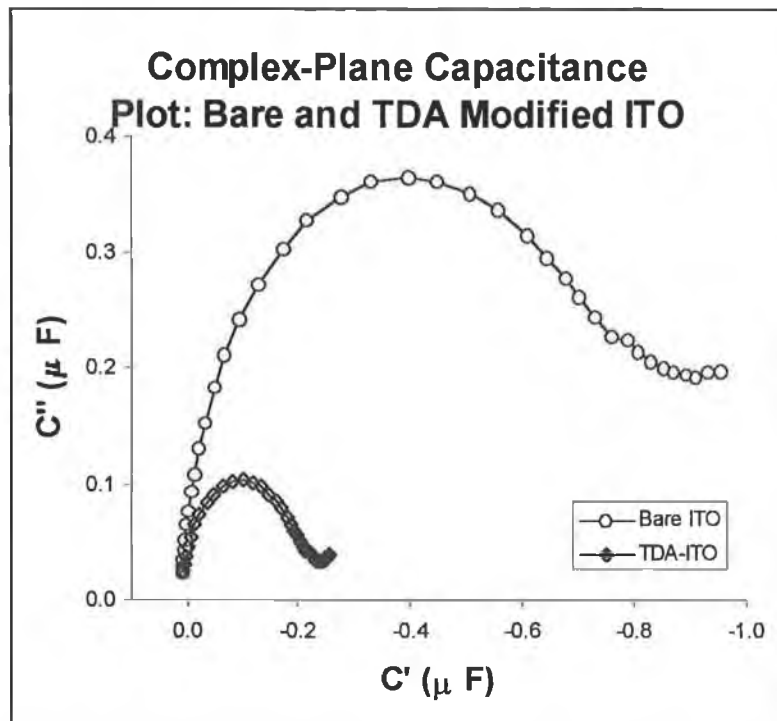


**Figure 3.19** Complex plane capacitance plots for the AC impedance data. The x-intercepts yield approximate capacitance values of 8.5, 2.4  $\mu\text{F}$  or 5.3 and 1.5  $\mu\text{F cm}^{-2}$ , for the bare ITO and TDA modified ITO samples. These values compare well with those calculated according to figure 3.18.

#### (iv) The evaluation of $C_M$ and $\epsilon$

Given the permittivity of free space,  $\epsilon_0$  ( $8.854 \times 10^{-12} \text{ F m}^{-1}$ ), the monolayer thickness,  $d$  ( $\sim 21 \text{ \AA}$ )<sup>23</sup>, and the electrode area,  $A$  ( $0.16 \text{ cm}^2$ ), one can evaluate the relative dielectric constant for the monolayer,  $\epsilon$ , from the monolayer capacitance in accordance with the Helmholtz model where,

$$C_M = \frac{\epsilon \epsilon_0}{d} \quad (3.9)$$

From the value of  $\epsilon$  obtained, an indication of the structural integrity of the monolayer may be gained. Table 3.1 below summarizes the results of the capacitance studies. The first two columns of data present the interfacial capacitance recorded for the bare and monolayer modified ITO samples. In the third column, the value of the monolayer dielectric is estimated for the case where the interfacial capacitance for the TDA modified surface approximates the TDA monolayer capacitance (i.e., the diffuse layer capacitance at the monolayer solution interface is so large that it does not contribute significantly to the inverse sum in equation 3.1). The monolayer capacitance quoted in the fourth column is calculated given equation 3.1 by assigning  $C_{GC}$  the value of the interfacial capacitance recorded for the bare ITO surface. The final column estimates  $\epsilon$  from the corrected value of monolayer capacitance.

**Table 3.1** Summary of Electrochemical results obtained

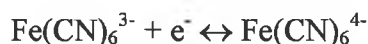
Technique	Bare ITO $C_{GC}$ ( $\mu\text{F cm}^{-2}$ )	PTDA-ITO $C_{dl}$ ( $\mu\text{F cm}^{-2}$ )	PTDA $\epsilon^d$	PTDA $C_M$ ( $\mu\text{F cm}^{-2}$ ) <sup>e</sup>	PTDA $\epsilon^f$
Cyclic Voltammetry <sup>a</sup>	12.0	1.7	3.9±0.3	1.9±0.2	4.6±0.4
Chronoamperometry <sup>b</sup>	4.2	1.4	3.3±0.2	2.1±0.2	4.9±0.5
AC Impedance <sup>c</sup>	6.1	1.5	3.7±0.5	2.1±0.4	4.9±0.9

<sup>a</sup> Electrolyte: 0.1 M LiClO<sub>4</sub>, potential scanned: 0 to 0.5 V,  $i_{dl}$  measured at 0.25 V,  $C_{dl}$  calculated from slope of  $i_{dl}$  vs.  $v$  plots. <sup>b</sup> Pulse width: 100 mV at 0.25 V,  $C_{dl}$  calculated from the intercept and slope of  $\ln i$  vs.  $t$  plots given eq 3.4. <sup>c</sup> Potential: 0.25 V, frequency range:  $10^4$  to  $10^{-1}$  Hz,  $C_{dl} = (\omega/Z)^{-1}$  at  $\theta_{max}$ . <sup>d</sup> Calculated from  $\epsilon = (C_M \times d)/\epsilon_0$  with  $d \approx 21 \text{ \AA}$  and  $C_M \approx C_{dl}$ . <sup>e</sup>  $C_M^{-1} = C_{dl}^{-1} - C_{GC}^{-1}$ , where  $C_{GC}^{-1}$  is the double layer capacitance for the bare ITO. <sup>f</sup> Calculated as in <sup>d</sup> but with  $C_M \neq C_{dl}$ . Note  $A = 0.16 \text{ cm}^2$ .

From the corrected values of  $C_M$  it can be seen that the interfacial capacitance is dominated by the smaller monolayer capacity. The value of monolayer capacitance obtained using the three electrochemical techniques agree remarkably well, with the average value being  $2.0 \mu\text{F cm}^{-2}$ . The corresponding average value monolayer dielectric, 4.8, is consistent with that expected for a hydrophobic layer and compares favourably to the dielectric constant of 2.3 quoted for bulk polyethylene.<sup>31</sup> This observation suggests that the layer forms an effective barrier to the ions and solvent molecules of the contacting aqueous electrolyte solution.

### 3.3.4 Permeation Studies

The permeability of the TA monolayer to the electroactive complex ferricyanide,  $\text{Fe}(\text{CN})_6^{3-}$ , was investigated using cyclic voltammetry.  $\text{Fe}(\text{CN})_6^{3-}$  undergoes a reversible one electron reduction reaction to form ferrocyanide



Cyclic voltammograms were recorded between 0.7 and -0.2 V in 0.1 M  $\text{LiClO}_4$  solutions containing 5 mM  $\text{Fe}(\text{CN})_6^{3-}$ . The left hand side of Figure 3.20 show cyclic voltammograms recorded in blank electrolyte (0.1 M  $\text{LiClO}_4$ ) prior to potential cycling in the presence of the redox active probe, the right hand side shows the current response of the probes species at the bare and TDA modified ITO surfaces. A clear reduction in the current response was observed after modifying the surface with a monolayer. If The TDA monolayer was defect free, then there should be no response observed as the thickness of the layer which is an estimated at 21 Å would generally be considered too large to support electron tunneling. The sigmoidal current response observed at the TDA modified surface is presumably due to imperfections in the film structure possibly as a result of the domain like manner in which the TDA molecules assemble at the air-water interface. The large peak to peak separation for the  $\text{Fe}(\text{CN})_6^{3-/4-}$  couple at the bare ITO surface is possibly due to the effects of IR drop (as a result of the resistive nature of the semiconductor coating) coupled with slow electron transfer from the ITO to the redoxactive probe.

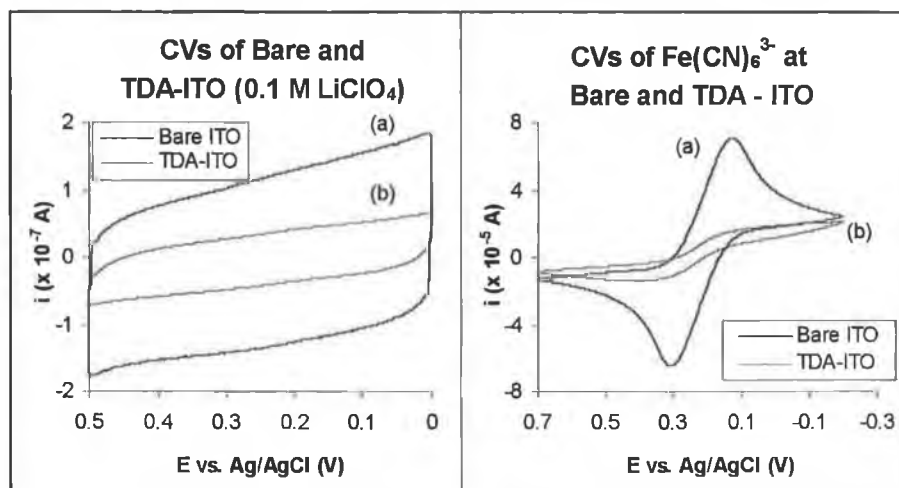


**Figure 3.20** Current responses for 5 mM  $\text{Fe}(\text{CN})_6^{3-}$  at bare (a) and TDA-modified (b) ITO surfaces. Electrolyte: 0.1 M  $\text{LiClO}_4$ ; Scan rate: 50  $\text{mV s}^{-1}$ .

### 3.4 CONCLUSIONS

The pH studies carried out on the TDA monolayers, reveal that the film expands as the subphase pH increases. The collapse pressure for the TDA monolayer was found to be directly related to the degree of monolayer ionization, and it is estimated from  $\pi_C$  vs. pH curves that the  $pK_a$  for the acid groups within the TDA monolayer is approximately 8. The positive shift relative to the bulk  $pK_a$  value is a result of hydrogen bonding stabilization and a lower dielectric constant within the TDA monolayer.

Condensed monolayers of TDA formed on cadmium containing subphases can be subsequently polymerized by UV irradiation to yield polymer TDA monolayers. It was found that depending on the method of formation, the PTDA monolayers produced, exhibit different  $\lambda_{max}$  values. Films that are polymerized after LB deposition yield the blue form of the polymer which absorbs at 629 and 580 nm. On exposure to ethanol, or by heating above 80 °C, these films readily convert to the red form of the polymer, which absorbs at 547 and 504 nm. In contrast, films that are polymerized at the air-water interface, under constant surface pressure prior to LB transfer, yield the red form of the polymer. Prepolymerization under constant surface pressure provides the molecules with the necessary degree of freedom to reorganize as the reaction proceeds. Although, it does result in expansion of the monolayer, the polymerized monolayer can be recompressed to its original area without collapse. This suggests that the polymer structure maintains a certain degree of flexibility, and may indicate that the polymer formed possesses a domain-like structure. If this is in fact the case, then it could have serious repercussions in terms of stability/safety, as the drug could potentially leak through gaps in the film structure.

Capacitance measurements were carried out on PTDA films formed on conducting ITO coated glass substrates. The monolayer capacitance was determined to be  $2.0 \pm 0.2 \mu\text{F cm}^{-2}$ . From the value of monolayer capacitance, the dielectric constant was estimated to be 4.8 which suggests that the PTDA polymer forms an effective barrier to the ions and water molecules of the electrolyte solution. The polymer's permeability to the larger inorganic complex ferricyanide was also examined. The reduction of  $\text{Fe}(\text{CN})_6^{3-}$  is severely hindered by the presence of the

polymer at the ITO surface, confirming the capacitance results that the polymer forms a barrier that is essentially impermeable to the complex.

In hindsight, it seems unlikely that the structural rearrangement required to cause a change in TDA monolayer permeability could possibly occur. Molecular transport through the monolayer would only become feasible if the polymer side chains were to separate sufficiently, a process which would be energetically unfavourable given the highly associated, dense nature of the TDA polymer. As regards the PTDA monolayers, it is inconceivable that the electrostatic repulsion created upon ionization of terminal carboxylic acid groups, would be capable of inducing monolayer permeability.

Although the LB polymers of TDA possessed some desirable properties they are ultimately unsuitable candidates for the manufacture of organized pH responsive polymers. It was therefore decided that alternative approach was required and possibility of using Self-Assembled Monolayers (SAMs) was explored. The following chapter describes research carried out on the final monolayer system, that of thioctic acid, which forms thinner more fluid monolayers, that should prove more conducive to structural rearrangement.

### 3.5 REFERENCES

- [1] Wegner, G *Makromol. Chem.* **1972**, *154*, 35.
- [2] Wegner, G., *Chimia*, **1975**, *28*, 475.
- [3] Baughman, R. H. *J. Polym. Sci. Polym. Phys. Ed.* **1973**, *11*, 603.
- [4] Tieke, B.; Wegner, G.; Naegele, D.; Ringsdorf, H. *Angew. Chem. Int. Ed. Engl.* **1976**, *15*, 764.
- [5] Tieke, B.; Graf, H.-J.; Wegner, G.; Naegele, B.; Ringsdorf, H.; Banerjee, A.; Day, D.; Lando, J. B. *Colloid Polym. Sci.* **1977**, *255*, 521.
- [6] Tieke, B.; Lieser, G. *J. Colloid Interface Sci.* **1982**, *88*, 471.
- [7] Tieke, B.; Lieser, G.; Weiss, K. *Thin Solid Films* **1983**, *99*, 95.
- [8] Day, D.; Ringsdorf, H. *J. Polym. Sci. Polym. Lett. Ed.*, **1978**, *16*, 205.
- [9] Tieke, B.; Weiss, K. *J. Colloid Interface Sci.* **1984**, *101*, 129.
- [10] Day, D.; Ringsdorf, H. *Makromol. Chem.* **1979**, *180*, 1059.
- [11] Shand, M. L.; Chance, R. R.; LePostollec, M.; Schott, M. *Phys. Rev.* **1982**, *B25*, 4431.
- [12] Kaneko, F.; Dresselhaus, M. S.; Rubner, M. F.; Shibata, M.; Kobayashi, S. *Thin Solid Films* **1988**, *160*, 327.
- [13] Lieser, G.; Tieke, B.; Wegner, G. *Thin Solid Films* **1980**, *68*, 77.
- [14] Lim, K. C.; Heeger, A. J. *J. Chem. Phys.* **1985**, *82*, 522.
- [15] Lio, A.; Reichert, A.; Nagy, J. O.; Salmeron, M.; Charych, D. H. *J. Vac. Sci. Technol. B* **1996**, *14*, 1481.
- [16] Mino, N.; Tamura, H.; Ogawa, K. *Langmuir* **1992**, *7*, 2336.
- [17] Hub, H.; Hupfer, B.; Koch, H.; Ringsdorf, H. *Angew. Chem. Int. Ed. Engl.* **1980**, *19*, 938. O'Brien, D. F.; Whitesides, T. H.; Klingbiel, R. T. *J. Polym. Sci. Polym. Lett. Ed.*, **1981**, *19*, 95. Lopez, E.; O'Brien, D. F.; Whitesides, T. H. *J. Am. Chem. Soc.* **1982**, *104*, 305.
- [18] Hub, H.; Hupfer, B.; Koch, H.; Ringsdorf, H. *J. Macromol. Sci. Chem.* **1981**, *A15*, 701.
- [19] Tomioka, Y.; Tanaka, N.; Imazeki, S. *J. Chem. Phys.* **1989**, *91*, 5694.
- [20] Ogawa, K. *J. Phys. Chem.* **1989**, *93*, 5305.
- [21] Ogawa, K. *J. Phys. Chem.* **1991**, *95*, 7109.
- [22] Deckert, A. A.; Horne, J. C.; Valentine, B.; Kiernan, L.; Fallon, L. *Langmuir* **1995**, *11*, 643.
- [23] Higashino, H.; Mizoguchi, E.; Ogawa, K. *Jpn. J. Appl. Phys.* **1997**, *36*, 319.
- [24] Ives, D. J. G.; Janz, G. J. (eds.) *Reference Electrodes*, Academic Press, New York, **1961**.
- [25] Lindén, M.; Rosenholm, J. B. *Langmuir* **1995**, *11*, 4499.
- [26] Roberts, G. *Langmuir-Blodgett Films*, Plenum Press, New York, **1990**.
- [27] Homes-Farley, S. R.; Reamey, R. H.; Mc Carthy, T. J.; Deutch, J.; Whitesides, G. M. *Langmuir* **1985**, *1*, 725. Bain, C. D.; Whitesides, G. M. *Langmuir* **1989**, *5*, 1370. Creager, S. E.; Clarke, J. *Langmuir* **1994**, *10*, 3675.
- [28] Solov'ev, A. A.; Katz, E. *J. Electroanal. Chem.* **1990**, *277*, 377.
- [29] Olmsted, J., III; Strand, M. *J. Am. Chem. Soc.* **1983**, *87*, 4790.
- [30] Gileadi, E. *Electrode Kinetics For Chemists, Chemical Engineers & Materials Scientists*, VCH, **1993**, pg 433.
- [31] Lanza, V. L.; Herrman, D. B.; *J. Polym. Sci.* **1958**, *28*, 622.

---

## **CHAPTER 4**

# **Formation and Characterization of Self-Assembled Thioctic Acid Monolayers**

---

## 4.1 INTRODUCTION

The final monolayer system studied was that of thioctic acid, a disulphide compound, that forms monolayers by spontaneous adsorption onto gold. Although this system is not polymer based, it is chemically immobilized to the substrate and behaves somewhat like a polymer, in that the molecules are locked into position thereby forming a stable monolayer. As in the previous two systems studied, the thioctic acid monolayer contains terminal carboxylic acid groups and the pH dependent permeability of the layer is our main focus. Due to the asymmetry of the compound, and the shorter chain length, the resulting monolayer is expected to be more permeable and to lend itself more to structural rearrangement on ionization.

Electrochemical experiments performed provide an insight into the effects of pH on mass transport across these layers. By carrying out permeation studies electrochemically one is looking at the process of molecular release in reverse. The diffusion of molecules/ions through the monolayer to the underlying electrode surface is studied and interactions between the probe molecule and the layer can be investigated. The permeability of the thioctic acid monolayer was studied on two levels. First, by looking at the monolayers capacitance, the extent to which solvent molecules and electrolyte ions permeate the monolayer is evaluated. Second, by looking at the redox properties of larger complexes/molecules in solution the presence of the monolayer and the effect of its ionization on the response to such probes is studied.

Many mercaptan derivatives undergo self-assembly to form organized surface-confined monolayers with reproducible morphologies. Since the performance of monolayers as effective barriers depends both on stability and structural integrity, these monolayer properties can be characterized effectively using a variety of electrochemical techniques. As a general introduction, examples of similar studies into monolayer capacitance and permeation are reviewed.

### 4.1.1 Capacitance Studies

As mentioned previously in Section 1.3, capacitance measurements can be used to evaluate various monolayer properties e.g., packing quality, pinhole density and film thickness. The monolayer capacitance provides an insight into the inner structure of the film such as the degree of solvent and ion penetration and the relative dielectric constant of the monolayer.<sup>1</sup> The dielectric constant is a measure of the resistive force the medium exerts against an external electrical field. High values arise because of film penetration by solvent and electrolyte, which leads to a lower film resistance or lower potential drop across the film.<sup>2</sup> The capacitance of a monolayer depends on the dielectric property of the terminal groups.<sup>3</sup> An increase in the disorder or the hydrophilic nature of the monolayer (e.g., upon ionization) may also account for the increased electrolyte penetration that results in higher capacitance values. Typically, when the monolayer is tightly packed, its capacitance is independent of the solution composition, since no ions or solvent molecules partition into the film.

Preliminary studies carried out by Cheng and Brajter-Toth<sup>1</sup> showed that the capacitance of a thioctic acid monolayer depended on the solution composition, suggesting that these monolayers are permeable to the electrolyte solution. The larger capacitance values observed for the TA system (compared to that reported for a C<sub>6</sub>-hydroxythiol monolayer), also supports the penetration of electrolyte and solvent ions into the TA monolayer. Further studies on mixed monolayers revealed a similar trend.<sup>2</sup> Capacitance values for the pure TA monolayers were larger than those for the mixed monolayers indicating that the TA films allow the solvent and electrolyte to partition into the layer more easily than the more hydrophobic mixed monolayers. From the measured capacitance they calculated that the theoretical potential drop across both the pure TA monolayer and the pure hexanethiol monolayers and found that the potential drop was lower in the case of the TA monolayer. As a result, faster electrochemical kinetics of electroactive probes in solution were observed for the less resistive TA monolayers (see Section 4.1.2).

Smith and White<sup>4</sup> have provided a theoretical basis for relating the differential interfacial capacitance of an electrode surface derivatized with a monolayer film containing pH-sensitive groups to the fractional degree of acid/base dissociation. Figure 4.1 shows how the potential of the modified electrode system varies from the

electrode surface to the bulk solution. A linear potential drop occurs between the metal and the plane of acid dissociation and a nonlinear potential drop occurs on the electrolyte side of the interface in accordance with Gouy-Chapman theory (see Chapter 1, pg 26). The magnitude of the potential drop depends on the electrode potential and the monolayer and solution capacitances. In their model, the total interfacial capacitance is a function of the monolayer capacitance,  $C_M$ , the potential dependent diffuse layer capacitance,  $C_s$ , and the degree of protonation,  $C(f)$ :

$$1/C_T = 1/C_M + 1/[C_s + C(f)] \quad (4.1)$$

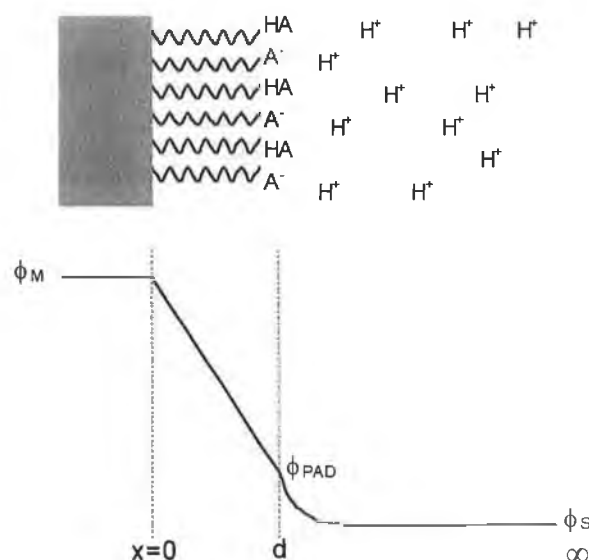


**Figure 4.1** Schematic representation of an adsorbed monolayer of an acid/base pair in contact with an electrolyte solution, and the corresponding potential distribution. The acid groups of all the molecules are assumed to lie in a common plane, the “plane of acid dissociation” (PAD), located a distance  $d$  from the electrode surface.  $\phi_M$ ,  $\phi_{PAD}$ ,  $\phi_S$  denote the electrostatic potential at the metal surface, the plane of acid dissociation, and in the bulk solution respectively. Adapted from Ref. [4].

From the variation in differential capacitance with applied potential and solution pH, they predicted the presence of maxima and/or minima in the voltammetric response to these monolayers, and developed a basis for quantitative analyses of acid/base surface chemistry.

As stated in Section 2.3.2, the  $pK_a$  of molecules in monolayer systems can differ greatly from the reported dissociation constants for the same compound in aqueous solution. Unfortunately, there is no simple relationship between bulk and monolayer values, and various techniques such as contact angle measurement,<sup>5</sup> surface potential measurements,<sup>6</sup> IR and Raman spectroscopic methods<sup>7</sup> have employed to determine surface  $pK_a$  values. Crooks *et al.*<sup>8</sup> presented a method for the *in situ* electrochemical measurement of surface  $pK_a$  values as a function of electrode potential. The results they obtained for surface-confined bases agreed qualitatively with the theoretical predictions developed by Smith and White.<sup>4</sup> A plot of capacitance versus potential for the base form of a 4-mercaptopyridine monolayer exhibited a minimum at +0.2 V vs. Ag/AgCl, KCl<sub>Sat</sub>, which corresponds to the potential of zero charge, PZC. On protonating the monolayer the PZC shifted to more negative values and a new capacitance minimum appeared at -0.1 V corresponding to the PZC for the fully protonated monolayer. A plot of capacitance vs. pH at the PZC of the deprotonated monolayer exhibited a maximum at a solution pH of 3.6. They calculated the theoretical value for the surface  $pK_a$  to be one pH unit higher than the solution pH, i.e., 4.6 at +0.2 V. They emphasize that since the surface  $pK_a$  is a strong function of electrode potential, the experimental value reported is only correct at +0.2 V. At more positive potentials the surface  $pK_a$  shifts to lower values (<4.6) while at negative potentials it shifts in the opposite direction (>4.6). It is significant to note that they calculated the theoretical surface  $pK_a$  to be one unit higher than the solution pH. No details are provided, but given that they apply the theory of Smith and White, it appears that they calculated the degree of monolayer protonation from the experimental observed capacitance maximum at pH 3.6 using the relation:

$$C(f) = (F^2 \Gamma_T / 2.3 RT) f(1-f) \quad (4.2)$$

Based on the data presented, solving for  $f$ , the fraction of molecules in the deprotonated state one obtains two possible solutions,  $f = 0.9$  and  $f = 0.1$ . Taking  $f = 0.9$ , the Henderson-Hasselbach equation yields a theoretical surface  $pK_a$  of  $3.6 - 1 = 2.6$ . However, taking  $f = 0.1$  the surface  $pK_a$  is  $3.6 + 1 = 4.6$ . Since both solutions yield  $pK_a$  values that are higher than the bulk  $pK_a$  of the compound, the

reason for choosing one solution is not apparent. Due to the uncertainty regarding the degree of monolayer protonation (which translates as a difference in surface  $pK_a$  of 2 units), it seems that despite theoretical predications, the accurate determination of the surface  $pK_a$  of the 4-mercaptopyridine monolayer systems cannot be unambiguously determined using capacitance measurements alone. However, if pH dependent permeation studies were carried out in conjunction with the capacitance measurements, then a clearer picture might emerge.

Savinell *et al.*<sup>3</sup> found that the capacitance of the  $C_5$ -carboxylic acid monolayers was independent of solution pH while that of thioctic acid increased directly with solution pH. They suggested this pH-dependency was due to the structure of the thioctic acid monolayer, which allowed ions and solvent to penetrate the monolayer more easily. The pH-independent capacitance observed for the  $C_5$ -carboxylic acid contradicts the theoretical predictions of Smith and White.<sup>4</sup> However, it is possible that the electrolyte concentration (0.1 M) used caused the electrolyte content of the film to be high at all pH making the film capacitance independent of the electrolyte concentration. Also, according to the Stern model at potentials far from the PZC the capacitance is independent of electrolyte concentration, so maybe the potential at which they carried out their measurements (-0.4 V vs. Hg/Hg<sub>2</sub>SO<sub>4</sub>, or 0.0188 V vs. Ag/AgCl, KCl<sub>sat</sub>) was too far from the PZC to observe the effects predicted by Smith and White. However, their research does confirm that the nature of the terminal group in the monolayer influences the capacitance. For compounds of the same chain length, the capacitance of the monolayer modified electrodes increased with an increase in the polarity of the ionic end group.

#### 4.1.2 Permeation Studies

The screening the self-assembled monolayers with different probes is necessary in order to properly characterize the film integrity. One useful approach to quantify both the structural integrity of the monolayers (blocking characteristics) and changes caused by the presence or absence of chemical or thermal triggers (switchable changes) is cyclic voltammetry. In this approach, one monitors the current response for an electroactive solution phase probe under a wide variety of experimental conditions. The presence of structural defects can be recognized by either a higher

current than would be expected for electron tunneling through a uniform defect free monolayer, or a change in the shape of the cyclic voltammogram.

Using cyclic voltammetry the degree of passivation can be determined from the voltammetric response<sup>9, 10</sup> :

- A peak shaped current-voltage response is characteristic of semi-infinite linear diffusion. The peak current scales linearly with square root of the scan rate, indicating that there are relatively large areas of bare electrode accessible to the probe molecule, i.e., the electrode is unpassivated.
- A sigmoidal current-voltage response is characteristic of radial diffusion to pinholes in an otherwise impermeable film. The presence of these defects permit the unimpaird penetration of probe molecules through the monolayer. To observe this response the pinholes must be small and widely dispersed relative to the diffusion layer thickness. Under these circumstances, the defects act as an array of inlaid disk microelectrodes and at long timescales the current is independent of scan rate (provided that the diffusion fields do not coalesce). As the number of defects increases, linear diffusion becomes dominant and peak shaped CVs, reminiscent of traditional macroelectrode behaviour, are observed.
- An exponential current-voltage response is characteristic of electron tunneling, where probe molecules cannot penetrate the compact monolayer and as a result can only be reduced/oxidized by electrons tunneling through the film. In this case the electrode is completely passivated. The current (the magnitude of which is massively reduced compared to unpassivated electrode), is controlled by the properties of the monolayer.

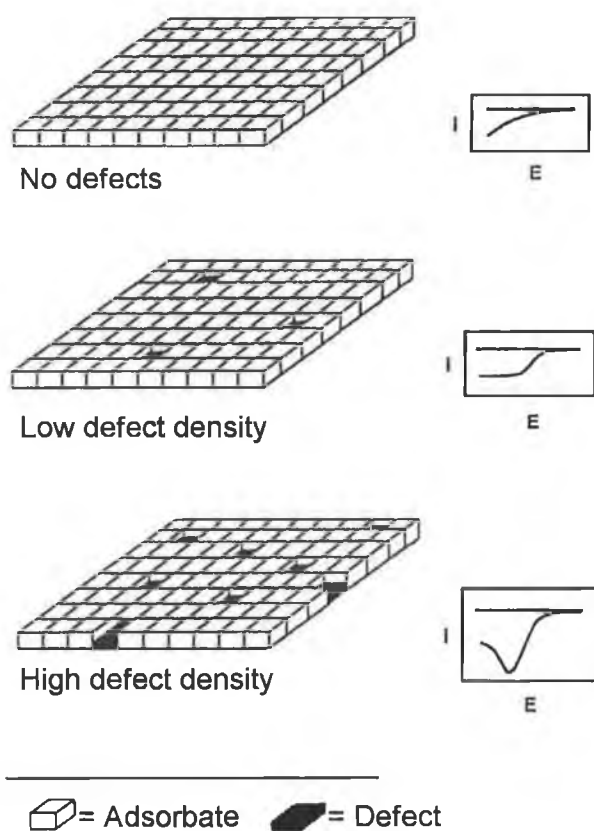


**Figure 4.2** The essential features of theory are qualitatively summarized by the cyclic voltammetry responses shown on the right. Adapted from Ref. [9].

A number of permeation studies have been reported in the literature. Rubinstein *et al.*<sup>11</sup> emphasized the usefulness of electrochemical techniques in the evaluation of the structural integrity of organized *n*-octadecyl trichlorosilane and *n*-octadecyl mercaptan monolayers. The inhibition of the electrochemical oxidation of a covered gold surface, and the electrochemical behaviour of the  $\text{Fe}(\text{CN})_6^{4-/3-}$  couple at monolayer coated electrodes, were employed as quantitative measures of the total pinhole area and of the pinhole size and distribution. The average values of pinhole diameter and spacing were estimated using the theory of Amatore *et al.*<sup>12</sup> to be  $\sim 5\text{-}10$  nm and  $50\text{-}100$  nm respectively. They demonstrated that the microscopic pinholes in the highly ordered monolayers behaved as arrays of extremely small microelectrodes, and could be used to facilitate the determination of large heterogeneous electron-transfer rate constants. Using AC impedance, they calculated the apparent and standard heterogeneous rate constants ( $k_{\text{app}}$  and  $k^0$ , respectively) and the diffusion coefficient,  $D$  for the  $\text{Fe}(\text{CN})_6^{4-/3-}$  couple at the bare and modified

electrode surfaces. Their results showed good agreement in the values of both  $k^0$  ( $\sim 10^{-2} \text{ cm s}^{-1}$ ) and  $D$  ( $\sim 10^{-6} \text{ cm}^2 \text{ s}^{-1}$ ) between the bare and modified electrodes for  $k_{app}$  values spread over more than two orders of magnitude ( $10^{-2}$ - $10^{-5} \text{ cm s}^{-1}$ ). The capacitance and the relative dielectric constant for the compact, hydrophobic monolayers were found to be  $\sim 1.0 \mu\text{F cm}^{-2}$  and 2.82 respectively, in good agreement with previously reported values.<sup>13</sup>

Crooks *et al.*<sup>14</sup> discussed the molecular discrimination by electrostatic interactions between an adsorbed layer and a dissolved redox species. They found that self-assembled monolayers of aminothiols, (4-ATP), prevented adsorption of anthraquinone-2,6-disulfonate (AQDS) at high pH but that electrostatically binding occurred at low pH. The adsorbed AQDS could be removed by simply increasing the pH of the contacting solution. The principle of pH-dependent binding is general for a number of amine, carboxylic acid and pyridine terminated mercaptan derivatives adsorbed to gold surfaces. These monolayers impart a pH-dependent electrostatic-based recognition capability to a gold electrode. Solution phase CV's showed that, while the presence of the monolayer affected the electron transfer kinetics of the AQDS probe (large increase in the peak separation), the monolayer did not possess any significant barrier properties. The formal potential values at the monolayer modified electrodes, at pH 2 and pH 7, were not significantly different from the corresponding values at the bare gold electrode. They tested the effect of the 4-ATP modified electrode on the electrochemistry of a positively charge probe  $\text{Ru}(\text{NH}_3)_6^{3+}$  and found that the reduction of this probe at bare and modified electrodes was reversible at pH 2 and 7. In addition, no adsorption of  $\text{Ru}(\text{NH}_3)_6^{3+}$  was observed. It appears that the protonated monolayer did not effect the response of the positively charged probe. This is somewhat surprising, since one would expect that the charged monolayer, which electrostatically binds the negatively charged probe, would by the same rationale repel the positively charged probe and diminish its response. It may be that the monolayer coverage is insufficiently dense to effect the electroactivity of the probe. Differences in the size of the probe molecules might also account for the differences in the way the monolayer affects their solution phase electrochemistry.

Bilewicz and Majda<sup>15</sup> described mixed LB monolayers of long chain amphiphilic molecules and ubiquinone. The long chain amphiphilic molecules passivated the

electrode while the ubiquinone molecules acted as a gate sites channeling access to the electrode surface. Using the LB technique, they immobilized ubiquinone at a controlled surface concentration, thereby controlling the number of gate sites at the electrode surface. The presence of ubiquinone removed the passivating character of the monolayer allowing the redox response of the  $\text{Ru}(\text{NH}_3)_6^{3+/2+}$  couple to be observed. The reduction potential for  $\text{Ru}(\text{NH}_3)_6^{3+}$  was  $-0.41$  V vs. SCE in  $0.5$  M KCl ( $-0.3658$  V vs. Ag/AgCl,  $\text{KCl}_{\text{sat}}$ ), and confirms that reduction of the ruthenium complex was not mediated by the quinone moiety. As shown in Figure 4.2, as the surface concentration of ubiquinone decreased (from  $2.5 \times 10^{-15}$  to  $1.9 \times 10^{-17}$  mol  $\text{cm}^{-2}$ ) the shape of the voltammogram became sigmoidal suggesting spherical diffusion of the  $\text{Ru}(\text{NH}_3)_6^{3+}$  probe.

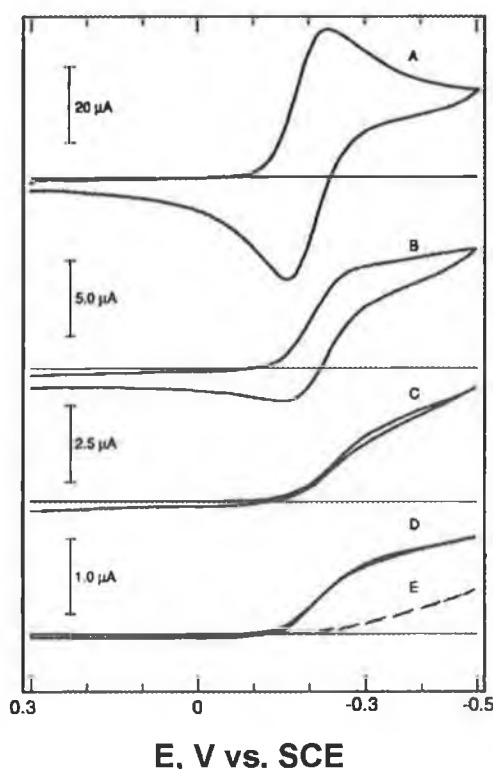


**Figure 4.3** Cyclic voltammograms of  $\text{Ru}(\text{NH}_3)_6^{3+}$  ( $1.0$  mM in  $0.5$  M KCl) at a bare electrode (A) and those coated with  $\text{Q}_{10}/\text{C}_{18}\text{SH}/\text{C}_{18}\text{OH}$  LB monolayers ( $x_{\text{C}_{18}\text{SH}} : x_{\text{C}_{18}\text{OH}} = 2.3$ , LB transfer pressure,  $20$  mN/m). Surface concentrations of  $\text{Q}_{10}$  (in mol/ $\text{cm}^2$ ): B,  $2.5 \times 10^{-15}$ ; C,  $5.4 \times 10^{-17}$ ; D,  $1.9 \times 10^{-17}$ ; E,  $0$ . A =  $0.40$   $\text{cm}^2$ ,  $v = 50$  mV/s. Taken from Ref. [15].

At the lowest surface concentration, the plateau current of the  $\text{Ru}(\text{NH}_3)_6^{3+}$  reduction was independent of scan rate. Plots of the  $\text{Ru}(\text{NH}_3)_6^{3+}$  limiting current per ubiquinone site vs. surface concentration revealed that the mass-transport rate to the ubiquinone centres increased as the surface density decreased. This is consistent with the reduction of  $\text{Ru}(\text{NH}_3)_6^{3+}$  occurring at individual ubiquinone sites. It seems that the isoprenoid chain of ubiquinone forms a channel of sufficiently large diameter which spans the thickness of the  $\text{C}_{18}\text{SH}/\text{C}_{18}\text{OH}$  monolayer, and allows  $\text{Ru}(\text{NH}_3)_6^{3+}$  to approach the electrode. Using the equation derived by Amatore *et al.*<sup>12</sup>, they calculated the apparent heterogeneous rate constant of  $\text{Ru}(\text{NH}_3)_6^{3+}$  reduction, from the shift of the half wave potential relative to the formal potential measured at a clean gold electrode. Although the  $k_{\text{app}}$  ( $79 \pm 1.3 \text{ cm s}^{-1}$ ) they obtained supports the unhindered access of the ruthenium complex, realistically, it is doubtful that  $k_{\text{app}}$  could be that large. It is likely, that mass transport restrictions, due to the inlaid character of the modified electrode, leads to an overestimation of  $k_{\text{app}}$ .

Brajter-Toth *et al.*<sup>1</sup> self-assembled thioctic acid onto gold. They characterized the modified electrode to determine the quality of packing and the effect of solution pH on the response to two probes,  $\text{Fe}(\text{CN})_6^{3-}$  and  $\text{Ru}(\text{NH}_3)_6^{3+}$ . Their results showed that the electrode was both permeable and stable and that the charge on the monolayer controlled the response to species in solution. For  $\text{Fe}(\text{CN})_6^{3-}$  at low pH and  $\text{Ru}(\text{NH}_3)_6^{3+}$  at neutral and high pH, the peak separation and cathodic peak currents were essentially the same at the monolayer modified and bare Au electrodes. Therefore, the presence of the film did not affect the kinetics of the probes, which suggests that the monolayer was reasonably permeable and that probe diffusion was unimpeded. The positive shift in the negative formal potential of the  $\text{Ru}(\text{NH}_3)_6^{3+/2+}$  couple at neutral and high pH for the TA-modified gold electrode pointed to the existence of attractive interactions between the ionized monolayer and the probe. This was confirmed by adsorption of  $\text{Ru}(\text{NH}_3)_6^{3+}$  from these solutions. In contrast, the response of the  $\text{Fe}(\text{CN})_6^{3-}$  molecule was severely suppressed at neutral pH, and effectively eliminated at high pH, where the dissociated carboxylic acid groups of the monolayer impede the diffusion of the negatively charged probe. Consequently, at high pH, selective permeability is achieved; the negatively charged terminal groups of the monolayer screen the response of the anionic probe while favouring the response of the cationic probe. Interestingly, at low pH they found that the permeability of the

monolayer to  $H^+$  ions, caused a significant decrease in the response to the  $Ru(NH_3)_6^{3+}$  cation due to electrostatic repulsion. Therefore, by changing the solution pH, it is possible through coulombic interactions at the monolayer-solution interface, to reversibly alter the permeability of the monolayer to charged molecules in solution.

Cheng and Brajter-Toth<sup>2</sup> formed mixed monolayers of thioctic acid and hexanethiols with different degrees of surface hydrophobicity. The hydrophilic TA monolayers showed fast kinetics for the hydrophilic probes,  $Fe(CN)_6^{3-}$  and  $Ru(NH_3)_6^{3+}$ , while for the more hydrophobic monolayers, an increased hexanethiol composition slowed down the kinetics of these probes. As mentioned earlier in Section 4.1.1, capacitance measurements revealed that pure TA monolayers had the lowest film resistance of the mixed monolayers studied. The increased permeability of the TA monolayer, due to its lower resistance, can therefore account for the differences in monolayer response. Slower kinetics were consistently observed for the more hydrophobic probes (Catecholamines and quinones) at the modified electrodes, irrespective of the monolayer composition. The fact that no improvement in response to the probes was observed on increasing the monolayer hydrophobicity suggests that in the absence of unfavourable interactions between the probe and the monolayer, the monolayer resistance is a significant factor in the overall response. Although it is possible that other factors (such as size and the electron transfer mechanism) may complicate the response of the hydrophobic probes compared to the hydrophilic probes at the modified electrode surface.

Chailapakul and Crooks<sup>9</sup> studied monolayer films with a nanoporous structure formed by spontaneous coadsorption onto gold. The electron-transfer-retarding alkanethiol framework molecules passivated the gold surface while the shorter aromatic mercaptan template molecules induced molecular sized defects within the passivating framework. The approach of using mixed monolayers to control the response of solution phase species, is similar to that used by Majda.<sup>15</sup> The chemical nature of the template and framework molecules, and their ratio in the deposition solution, control the size, number and chemical characteristic of the defect sites, which in turn controls permeation of the probe molecules.

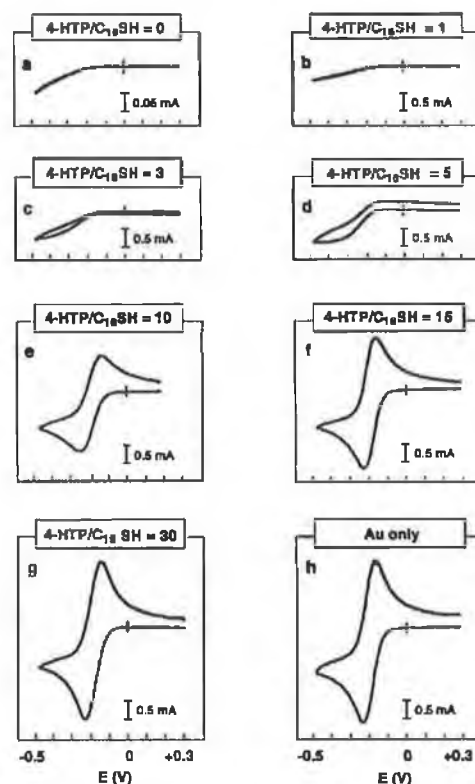


**Figure 4.4** Cyclic voltammograms for perforated monolayers formed by immersing an Au surface in ethanol solutions containing various ratios of 4-HTP/C<sub>16</sub>SH (HS(C<sub>6</sub>H<sub>4</sub>)OH/HS(CH<sub>2</sub>)<sub>15</sub>CH<sub>3</sub>). The concentration ratio is given above each cyclic voltammogram. The data were obtained in an aqueous electrolyte solution consisting of 5 mM Ru(NH<sub>3</sub>)<sub>6</sub><sup>3+</sup> and 1.0 M KCl. The scan rate was 0.1 V s<sup>-1</sup>. Taken from Ref. [9].

Figure 4.3 shows that as the number of defect sites increased, a clear progression from electron tunneling through the monolayer, to electron transfer at the electrode surface is observed.

Nakashima *et al.*<sup>16</sup> Formed self-assembled monolayer of a phosphate lipid, bis(11-mercaptoundecyl)phosphoric acid, on gold electrodes via chemisorption from ethanol solutions. They examined the electrochemistry of cationic (methylviologen, MV) and zwitterionic (dipropanesulphonate-4,4'-bipyridium) redox active markers. They compared the blocking ability of the lipid monolayers to conventional thiol based monolayers of similar chain length.

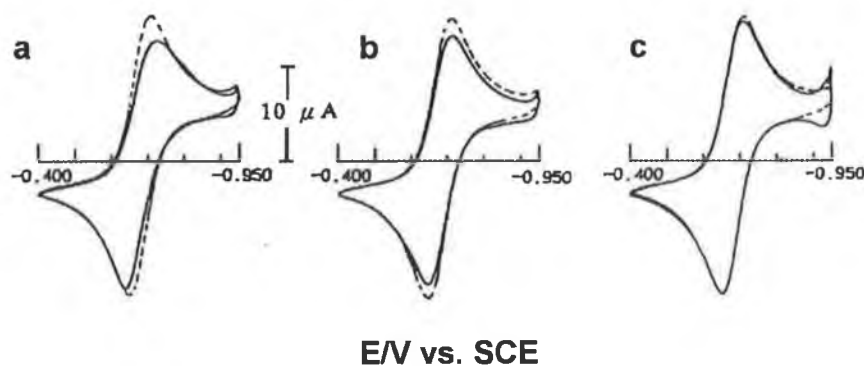


**Figure 4.5** Cyclic voltammograms of SAMs of HS(CH<sub>2</sub>)<sub>11</sub>CH<sub>3</sub> (curve a), HS(CH<sub>2</sub>)<sub>11</sub>OH (curve b) and HS(CH<sub>2</sub>)<sub>11</sub>COOH (curve c) on gold electrodes which were prepared by 24 h adsorption from 10 mM ethanolic solutions of each thiol compound. Dotted lines show CVs at a bare electrode surface. The solutions were 2 mM MV in 0.1 M KCl (pH 7.0). Scan rate, 200 mV s<sup>-1</sup>. Taken from Ref. [16].

Surprisingly, as shown above in Figure 4.5, the conventional thiol monolayers were unable to block the electrochemistry of probes studied. In contrast, the phosphate lipid monolayers formed under identical conditions, exhibited pH-responsive ion-gating behaviour. At low pH, access of the cationic probe was prohibited, while at high pH, ionization of the phosphoric acid groups in the monolayer enabled the unimpeded access of the probe molecule. The gating behaviour was explained by coulombic interaction between the terminal phosphoric acid group of the monolayer and the redox-active species in solution. It may be that the phosphoric acid groups are bulkier than the carboxylic acid functionality and so when protonated restrict access to the electrode. They suggested that the pH-responsive permeation may also be due to structural changes within the monolayer, caused by the change in solution pH, but the detection and characterization of such conformational changes has yet to be addressed. It was also found that the modified electrode responded to the presence of Ca<sup>2+</sup> which could be detected by a change in response for MV at high pH. Chelation of the phosphate terminal group with the divalent ion results in a decrease in the negative charge-density of the surface, hence decreasing the electrostatic interaction between MV and the monolayer.

Willner *et al.*<sup>17</sup> modified gold electrodes with thiolate monolayers that possess amine groups of different bulk p*K*<sub>a</sub> values. The redox probe pyrrolquinoline revealed reversible electrochemical properties only in the presence of positively-charged monolayer-modified electrodes, owing to its electrostatic attraction at the

monolayer/electrode interface. The transition from reversible to irreversible behaviour was observed at different pH values depending on the  $pK_a$  value of the monolayer. The protonation/deprotonation of monolayers containing terminal acid/base groups is generally observed over a broad range in pH, due to the polyelectrolyte effect of neighbouring groups within the monolayer assembly.<sup>18</sup> In contrast to this general result, Willner found that the pH-switching of the electrochemical activity occurred in a relatively narrow pH range and was observed at one unit lower than the reported  $pK_a$  value of the respective monolayer.<sup>8</sup> They suggested that in order to enable the quasi-reversible electron transfer with the redox probe, the surface charge density of the monolayer had to be enhanced. This was achieved by lowering the solution pH by 1 unit with respect to the  $pK_a$ . However, Willner neglects to mention that the  $pK_a$  values quoted by Crooks *et al.*<sup>8</sup> are valid only at +0.2 V vs. Ag/AgCl, KCl<sub>sat</sub>. According to Crooks, the  $pK_a$  of these systems are strongly potential dependent, varying by approximately 6 pH units within the range of  $\pm 1$  V vs. the PZC. This potential induced shift is due to the fact that the ionizable group is strongly coupled electrostatically to the electrode via the pyridine ring. Therefore, it is important to consider the impact of the formal potential of the redox active probe. If there is a uniform variation in  $pK_a$  with potential, then the  $pK_a$  would be increased by approximately 0.8 units (1 pH unit/0.333 V) at -0.0678 V relative to +0.2 V. Such an effect would mean that the difference between the bulk pH and the switching pH of the monolayer would be almost 2 units. It seems that the only reasonable conclusion to be drawn is that the pH at which the values of the peak separation and peak currents reach a plateau represent a fully protonated monolayer.

There is also considerable uncertainty in the estimation of the degree of monolayer protonation at intermediate pH values, i.e., away from the  $pK_a$ . If the protonation/deprotonation curve for monolayer systems follows that of a solution phase species, then the Henderson-Hasselbach equation suggests that at a pH one unit lower than the  $pK_a$ , the monolayer would be 90 % protonated, making the surface charge density of the monolayer significantly higher. On the other hand, if the protonation/deprotonation of monolayers occurs over a relatively broad pH range as discussed by Solov'ev,<sup>18</sup> then the monolayer could be protonated to any degree within

the limits of 50-90 %. At present it is not known how protonation of monolayers proceeds.

Krysinski *et al.*<sup>10</sup> tested the passivating behaviour of octadecanethiol monolayers on gold using cyclic voltammetry. Three probes, namely,  $\text{Ru}(\text{NH}_3)_6^{3+}$ ,  $\text{Fe}(\text{CN})_6^{4-}$  and BQ (benzoquinone), that have different heterogeneous rate constants and different hydrophobic/hydrophilic character, were chosen for their study. The integrity of the monolayer was investigated by recording the current-voltage characteristics of the monolayer in the presence of the selected probes. Using cyclic voltammetry, they showed that the passivating properties of the monolayer depended on the identity of the probe. From the quasi-reversible CV's observed for bare gold, they calculated the standard heterogeneous rate constant for each probe and compared it to the value determined from the exponential-type CV's observed for modified gold. They found that although BQ was significantly less kinetically reversible under the experimental conditions, it was far less affected by the presence of the monolayer ( $k^0$  decreased from  $9.7 \times 10^{-4}$  to  $1.4 \times 10^{-5} \text{ cm s}^{-1}$ ) when compared to the other two probes  $\text{Ru}(\text{NH}_3)_6^{3+}$  and  $\text{Fe}(\text{CN})_6^{4-}$ . The smaller decrease was presumably due to its hydrophobic nature, which enables the molecule to at least partially partition into the monolayer, compared to the hydrophilic probes which are excluded from the low dielectric monolayer interior. They observed a significant decrease in the standard heterogeneous rate constant,  $k^0$ , for both the  $\text{Fe}(\text{CN})_6^{4-}$  and  $\text{Ru}(\text{NH}_3)_6^{3+}$  probes (by  $\sim 10^3$  times for  $\text{Ru}(\text{NH}_3)_6^{3+}$ , and  $\sim 10^4$  times for  $\text{Fe}(\text{CN})_6^{4-}$ ), and a substantial decrease in the anodic transfer coefficient,  $\alpha_a$ , for  $\text{Fe}(\text{CN})_6^{4-}$ . Assuming the radii for the two probes are similar, they calculated the Gibbs energies of transfer of the two probes and found that the transfer of  $\text{Fe}(\text{CN})_6^{4-}$  required 80% more energy than that of  $\text{Ru}(\text{NH}_3)_6^{3+}$ , based on the difference in charge alone. This it seems, would explain the observed differences in response for the two hydrophilic probes. It is perhaps significant to note that the values of  $k^0$ , obtained for  $\text{Fe}(\text{CN})_6^{4-}$  and  $\text{Ru}(\text{NH}_3)_6^{3+}$  at the bare gold electrode were very similar ( $1.5 \times 10^{-2}$  and  $1.8 \times 10^{-2} \text{ cm s}^{-1}$  respectively), which disagrees with the report of Crooks *et al.*<sup>9</sup> who state that the heterogeneous rate constant for  $\text{Fe}(\text{CN})_6^{3-}$  is one thousand times smaller than  $k^0$  for  $\text{Ru}(\text{NH}_3)_6^{3+}$ . Also Rubinstein *et al.*<sup>11</sup> studied alkanethiol monolayers of the same chain length and reported that the  $k^0$  observed at the modified and bare electrode surfaces were of the

same order of magnitude ( $\sim 10^{-2}$  cm s<sup>-1</sup>). They calculated  $k^0$  for the Fe(CN)<sub>6</sub><sup>4-/3-</sup> couple from the apparent rate constants by taking into consideration the presence of defects.

The above studies demonstrate that permeation of ions/molecules through monolayer systems is quite complex, and depends on a range of factors such as the size, hydrophobicity charge density of the solute and the structure, hydrophobicity, and charge of the monolayer.

## 4.2 EXPERIMENTAL

### 4.2.1 Materials/Reagents

Thioctic acid (97 %) was purchased from Lancaster Synthesis (Morecambe, UK). Lithium perchlorate (95+ %) and potassium chloride (98+ %) obtained from Aldrich (Gillingham, UK) were used to make up electrolyte solutions. Hexaamineruthenium (III) trichloride (32.68 % Ru) was purchased from Johnson Matthey Chemicals (Royston, UK). Potassium ferrocyanide and potassium ferricyanide (99+ %) were obtained from Aldrich. Sodium dihydrogen phosphate (99 %) and disodium hydrogen phosphate (98.5 %), supplied by Merck (Darmstadt, Germany), were used to alter the electrolyte pH. All chemicals were used as received. Aqueous solutions were freshly prepared from ultrapure water (resistivity  $\geq 18 \text{ M}\Omega \text{ cm}$ ), obtained from a Milli-Q filtering system (Millipore Corp., USA). All solutions were degassed thoroughly with nitrogen prior to use.

### 4.2.2 Instrumentation

Electrochemical measurements were performed using a CH Instruments Model 660 Electrochemical Workstation (CH Instruments Inc., Cordova, USA) in a single-compartment, three-electrode, glass electrochemical cell containing the unmodified/modified gold working electrode, a platinum counter electrode and an Ag/AgCl reference electrode (BAS, Stockport, UK). All potentials are reported with respect to this reference electrode whose potential is 44.2 mV more positive than SCE.<sup>19</sup>

### 4.2.3 Preparation of Gold Electrodes

Prior to their use, the gold disk electrodes (BAS, diameter 0.16 cm, geometric area  $20.1 \times 10^{-3} \text{ cm}^2$ ) were polished successively with alumina slurries of 0.3 and 0.05  $\mu\text{m}$  particle diameter (Buehler Ltd., Lake Bluff, USA). The alumina was then removed by sonication in a ultrasound bath for 5 minutes. The electrode was then

electrochemically cleaned by cycling the potential between -0.2 and +1.5 V in 0.1 M H<sub>2</sub>SO<sub>4</sub> at 100 mV s<sup>-1</sup>. The electrochemical or microscopic area was estimated by measuring the charge corresponding to the reduction of the gold oxide layer. The surface roughness was determined by dividing this value by the geometric area determined by chronoamperometry in a solution of 0.1 M KCl containing 3 mM K<sub>3</sub>Fe(CN)<sub>6</sub> ( $D = 0.763 \pm 0.005 \times 10^{-5} \text{ cm}^2 \text{ s}^{-1}$ ).<sup>20</sup> The roughness factor for the electrodes used were typically between 2-2.5. Faradaic responses were analyzed with respect to the geometric area (0.0201 cm<sup>2</sup>), capacitances values are reported with respect to the electrochemical area.

#### 4.2.4 Modification of Gold Electrodes

Monolayers were prepared by immersing freshly cleaned electrodes in ethanol solutions containing 0.1 % (w/v) thiocetic acid (TA). Following a deposition period of ~24 h the modified electrodes were rinsed thoroughly in ethanol and finally water to remove any physically adsorbed TA. The modified electrodes were then soaked in 0.1 M electrolyte prior to electrochemical measurements.

## 4.3 RESULTS & DISCUSSION

### 4.3.1 Self-Assembly of Thioctic Acid Monolayers

By spontaneous adsorption from solution, thioctic acid (TA) forms organized carboxylic acid terminated monolayers on gold surfaces.<sup>1</sup> The disulphide group of TA physisorbs to the gold surface. The firm attachment of TA to gold is a result of the strong chemisorption of the molecule, due to the formation of two thiolate bonds with gold after S-S bond cleavage (see Figure 4.6 below). The reaction of disulphide with gold is considered to proceed by an oxidative addition mechanism.<sup>21</sup> The precise orientation and molecular packing of the adsorbed TA molecules on gold is not known, which makes it difficult to estimate the film thickness. The length of the thioctic acid molecule in its extended form, as measured from space-filling molecular models is 9.1 Å.<sup>22</sup> Given that extensive studies on *n*-alkylthiols monolayers have shown that the molecules in a compact monolayer lie at a tilt of 30° from the surface normal the thickness of thioctic acid monolayers is expected to be approximately 8 Å.<sup>2</sup>

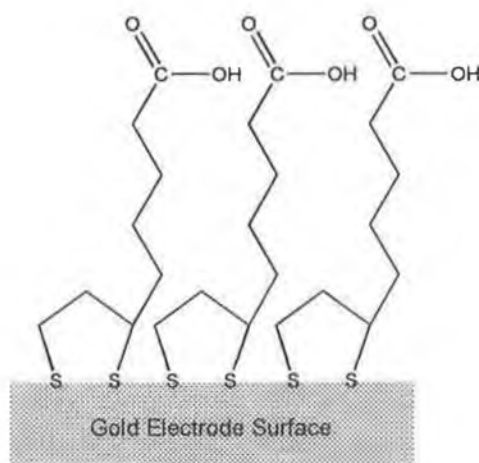


**Figure 4.6** Schematic diagram of an idealized thioctic acid monolayer self-assembled on a gold electrode.

As shown in Figure 4.6, the hydrophobic alkyl chains of neighbouring thioctic acid molecules interact laterally, and extend outwards due to the favourable interactions between the hydrophilic terminal carboxylic acid group and the contacting aqueous

solution. Based on its molecular structure (i.e., the absence of a second alkyl chain in this asymmetric molecule) the monolayer is expected to be less closely packed than corresponding alkanethiol, and is expected to allow some degree of solvent and electrolyte penetration. The monolayer surface charge is influenced by the contacting solution pH due to the protonation/deprotonation reactions.

### 4.3.2 Capacitance Measurements

Capacitance measurements are extremely valuable as a diagnostic test for the presence/absence of an adsorbed monolayer, especially when the monolayer is itself electroinactive. When an electrode is charged and electrostatic equilibrium is attained, the charge on the electrode is balanced by the charge in solution. The double layer capacitance is a result of this charge separation in the metal solution interphase. The interfacial capacitance of a clean bare electrode surface is a function of the electrode material, its potential and the contacting electrolyte solution. As seen from Chapter 1, the charge separation is described by Stern model as two capacitors in series: that of the compact Helmholtz layer,  $C_H$ , and that of the diffuse layer extending into the solution phase,  $C_{GC}$ .

$$\frac{1}{C_{dl}} = \frac{1}{C_H} + \frac{1}{C_{GC}} \quad (4.3)$$

When a monolayer is adsorbed to the gold surface the interfacial region is modified and a change in the interfacial capacitance is observed. The presence of an adsorbed TA monolayer on the gold electrode surface is easily detected by capacitance measurements in blank electrolyte. Figure 4.7 shows the traces obtained when a clean gold electrode and TA modified electrode are cycled between  $\pm 0.3$  V in 0.1 M LiClO<sub>4</sub>.

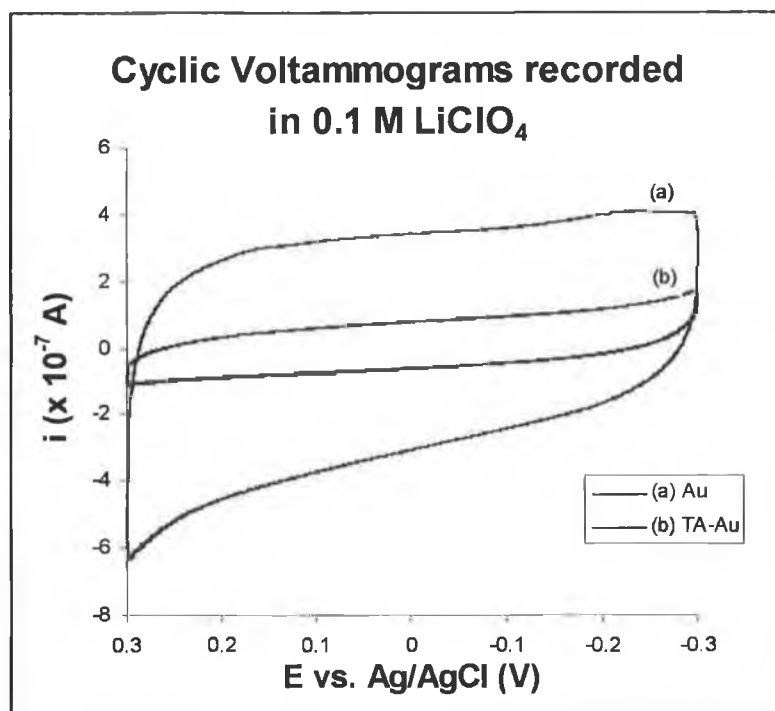


**Figure 4.7** Potential cycling in 0.1 M LiClO<sub>4</sub>. Trace (a) obtained for a clean bare gold electrode. Trace (b) obtained for a thioctic acid modified gold electrode. Scan rate: 100 mV s<sup>-1</sup>. Electrode area: 2.01 × 10<sup>-2</sup> cm<sup>2</sup>.

The charging current observed for the modified surface is greatly reduced in comparison to that observed at the bare electrode. The interfacial capacitance for the monolayer modified surface is described by modified version of the Stern model where  $C_H$  is replaced by  $C_M$ , the monolayer capacitance. When the interfacial capacity is measured the total response ( $C_{dl}$ ) will be dominated by the smaller term in the sum, which is typically  $C_M$ .

By studying monolayer capacitance it is possible to gain valuable information concerning the barrier properties of the layer to ions in solution. The TA monolayer behaves as an idealized dielectric material and the monolayer dielectric constant,  $\epsilon$ , can be calculated from  $C_M$  in accordance with the Helmholtz model:

$$C_M = \frac{\epsilon \epsilon_0}{d} \quad (4.4)$$

where  $\epsilon_0$  is the permittivity of free space and  $d$  is the monolayer thickness. From the value of  $\epsilon$ , an indication of the monolayer integrity can be obtained. Since changes in

surface charge density at the monolayer/solution interface can influence the measured interfacial capacity, capacitance measurements can also be useful in evaluating the dissociation constant of surface confined acids/bases. In this study, the dielectric constant,  $\epsilon$ , and dissociation constant,  $pK_a$ , for the adsorbed TA monolayer were determined from interfacial capacitance measurements.

### **(i) Evaluation of Monolayer Capacitance and Dielectric Constant**

The total interfacial capacitance,  $C_{dl}$ , of the TA modified electrode was measured electrochemically using cyclic voltammetry, chronoamperometry and AC impedance as described in Chapter 3. All capacitance measurements were carried out in 0.1 M  $LiClO_4$  at the bare and modified electrodes.

Cyclic voltammograms were recorded at scan rates between 20 and 200  $mV s^{-1}$ . The potential was scanned between 0 and 0.5 V and the double layer charging current,  $i_{dl}$ , was taken as the average of the anodic and cathodic currents at 0.25 V. In accordance with equation 3.2, the slope of the linear plot of  $i_{dl}$  vs.  $\nu$  yielded the value of  $C_{dl}$ .

Small amplitude potential pulse experiments of 100 mV were carried out at a base potential of 0.25 V. The resulting charging current which decays exponentially with time was followed for 2 msec. The current-time transients recorded were analyzed according to equation 3.3, by plotting the  $\ln i_{dl}(t)$  vs.  $t$ . The y-intercept of the linear semilog plot yielded the solution resistance,  $R_U$ , which was used to evaluate  $C_{dl}$  from the slope, using equation 3.4.

AC impedance measurements were performed at 0.25 V at frequencies between  $10^5$  and  $10^{-1}$  Hz. Using equation 3.6, the capacitance for the bare and modified ITO surfaces was evaluated from the value of the total impedance measured at the maximum in the Bode angle plot (i.e., where the interfacial region behaves like a pure capacitor).

The monolayer capacitance was then determined from the measured interfacial capacitance. Generally, at high electrolyte concentrations the diffuse layer capacitance,  $C_{GC}$ , is much higher than the monolayer capacitance,  $C_M$ , and its contribution to the total interfacial capacitance,  $C_{dl}$ , is minimal. In this case the monolayer capacitance can be approximated by the measured interfacial capacitance.

However, if the value of  $C_{GC}$  is lower (depends on the variation in the diffuse layer capacitance with electrolyte concentration) or  $C_M$  is higher (e.g., for a leaky incomplete monolayer) then the assumption that  $C_M \ll C_{GC}$  may not be valid and the contribution due to  $C_{GC}$  must be taken in account. In this case, taking the measured capacitance for the bare gold electrode as the value of  $C_{GC}$ ,  $C_M$  is calculated from the interfacial capacitance measured for the modified electrode using equation 4.3.

As the concentration dependence of  $C_{GC}$  was not investigated here, its contribution to  $C_{dl}$ , at an electrolyte concentration of 0.1 M was not evaluated experimentally and it is necessary to consider both cases. Using equation 4.4, the dielectric constant for the monolayer was calculated from the value of  $C_M$  for each case, given the permittivity of free space,  $\epsilon_0$  ( $8.854 \times 10^{-12}$  F m<sup>-1</sup>) and taking the estimated monolayer thickness,  $d$ , of  $\sim 8$  Å.

Table 4.1 below summarizes the results obtained. The first two columns of data present the interfacial capacitances recorded for the bare and monolayer modified gold electrodes. In the third column, the value of the  $\epsilon$  is estimated for the case where the interfacial capacitance for the TA modified surface approximates the TA monolayer capacitance (i.e., the diffuse layer capacitance at the monolayer solution interface is so large that it does not contribute significantly to the inverse sum in equation 4.3). The monolayer capacitance quoted in the fourth column is calculated given equation 4.3 by assigning  $C_{GC}$  the value of the interfacial capacitance recorded for the bare Au surface (column 1) and the final column estimates  $\epsilon$ , from the corrected value of monolayer capacitance.

**Table 4.1** Results of capacitance measurements.

Technique	Au: $C_{GC}$ ( $\mu\text{F cm}^{-2}$ )	TA-Au $C_{dl}$ ( $\mu\text{F cm}^{-2}$ )	TA-Au $\epsilon^d$	TA-Au $C_M$ ( $\mu\text{F cm}^{-2}$ ) <sup>e</sup>	TA-Au $\epsilon^f$
Cyclic Voltammetry <sup>a</sup>	21.3	6.8	6.1	9.9	9.0
Chronoamperometry <sup>b</sup>	23.5	10.2	9.2	18.0	16.3
AC Impedance <sup>c</sup>	24.3	8.3	7.5	12.6	11.4

<sup>a</sup> Potential scanned: 0 to 0.5 V,  $i_{dl}$  measured at 0.25 V,  $C_{dl}$  calculated from slope of linear  $i_{dl}$  vs.  $v$  plots. <sup>b</sup> Pulse width: 100 mV at 0.25 V,  $C_{dl}$  calculated from slope of linear  $\ln i_{dl}$  vs.  $t$  plots. <sup>c</sup> Potential: 0.25 V, Frequency range:  $10^5$  to  $10^1$  Hz,  $C_{dl} = (\omega/Z)^{-1}$  at  $\theta_{MAX}$ . <sup>d</sup> Calculated given that  $\epsilon = (C_M \times d)/\epsilon_0$  and  $d \approx 8$  Å, for the case where  $C_{dl} \approx C_M$ . <sup>e</sup>  $C_M^{-1} = C_{dl}^{-1} - C_{GC}^{-1}$ . <sup>f</sup> Calculated as before, for the case where  $C_{dl} \neq C_M$ .

The capacitance values determined for bare gold are all in good agreement. Typically for clean bare gold,  $C_{GC}$  is expected to be around  $22 \mu\text{F cm}^{-2}$ .<sup>3</sup> The high values of  $\epsilon$  determined relative to n-alkylthiols based systems and the TDA system studied in Chapter 3 suggest that solvent and ions penetrate the monolayer. This is not unexpected, as the structure of the TA molecule would result in the formation of monolayer that is quite fluid in nature. The large reduction in  $\epsilon$  compared to that of bulk water suggests that the monolayer is relatively coherent, since if the film was leaky, then a much higher value dielectric constant would be expected.

The variation in the value of the interfacial capacitance for the TA modified surface, measured by the individual techniques may be due to differences in the timescale of the experiments. Although, the close agreement in the capacitance values for the bare gold surface would seem to eliminate the possibility that the experimental timescale influences the measured capacitance.

#### **(ii) Determination of Surface $pK_a$ from $C_{dl}$**

As described earlier, Smith and White<sup>4</sup> developed a theory that related the capacitance of electrodes modified with ionizable monolayers to the fraction of molecules in the protonated/deprotonated state. Therefore, analysis of the capacitance data obtained as a function of pH should in theory yield the surface  $pK_a$  of the TA monolayer. The variation in interfacial capacitance was monitored as a function of electrode potential between  $\pm 0.4$  V at high and low pH using AC impedance. Impedance measurements were carried out in the frequency range  $10^4$  to  $10^{-1}$  Hz. Since the Bode angle plot (phase angle vs.  $\text{Log } \omega$ ) is a more sensitive test of the capacitance of a system than the Bode magnitude plot ( $\log Z$  vs.  $\log \omega$ )<sup>23</sup>, the capacitance at each potential/pH was calculated at the maximum in the Bode angle plot which coincides with the inflection point of the Bode magnitude plot as shown in Figure 4.8.

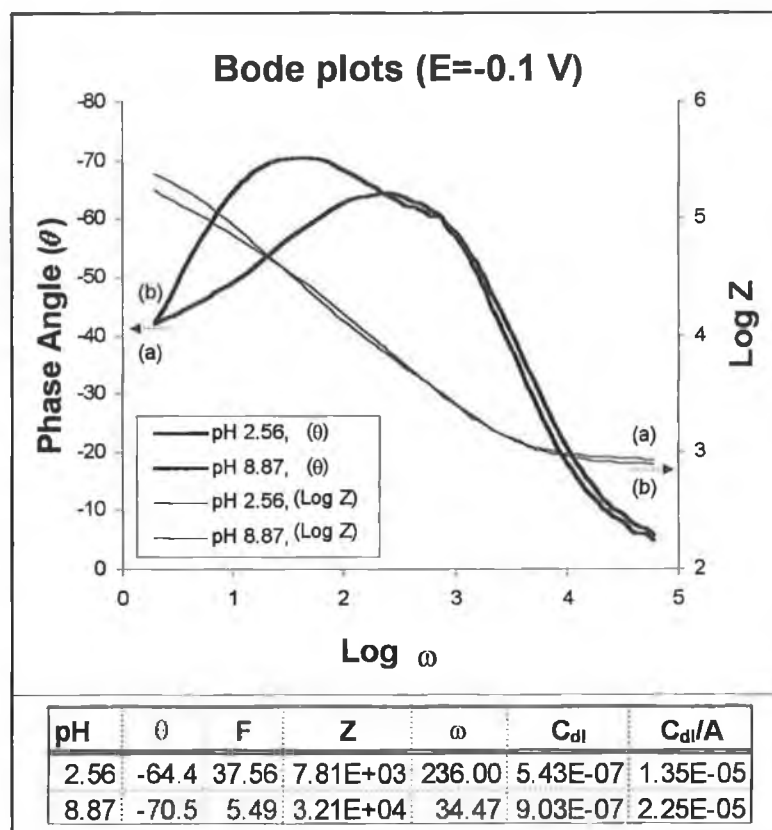


**Figure 4.8** Bode angle (heavy line) and magnitude (fine line) plots for impedance measurements carried out at a potential of -0.1 V for (a) the protonated (pH 2.56) and (b) ionized TA monolayer (pH 8.87).  $C_{dl}$  was calculated from the values of Z and  $\omega$  at the  $\theta_{Max}$  given equation 3.6.

The capacitance values obtained were plotted as a function of potential for pH 2.56 and pH 8.87. Figure 4.9 overleaf shows, that for both the protonated (pH 2.56) and deprotonated (pH 8.87) TA monolayers, a capacitance maximum was observed at a potential of -0.1 V. The value of the capacitance maximum increased dramatically from 13.5 to 22.4  $\mu\text{F cm}^{-2}$  on ionization of the monolayer. The PZC for the monolayer observed at a potential of -0.1 V, is significantly shifted in a negative direction relative to the PZC for bare gold (+0.2 V), this is to be expected due to the negatively charge of deprotonated monolayer.

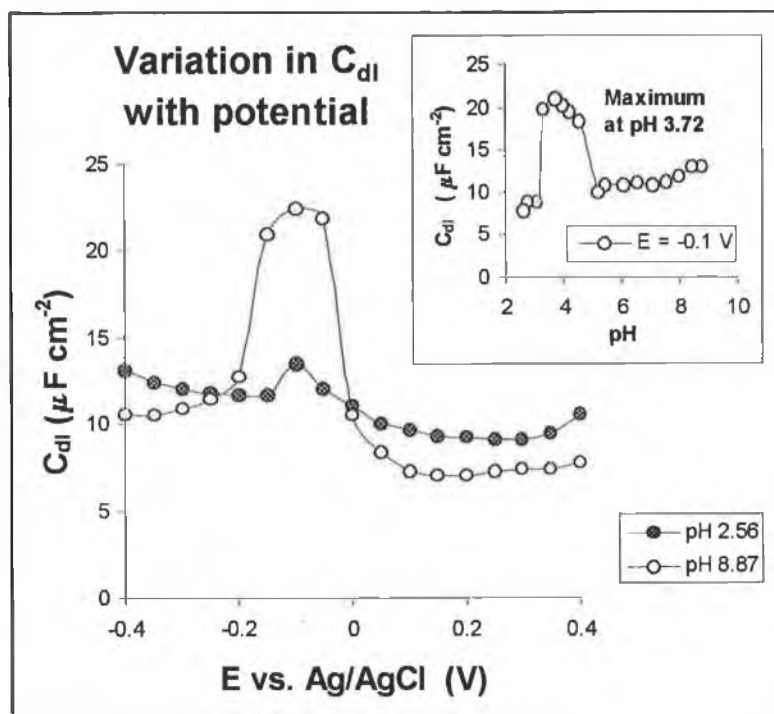


**Figure 4.9** Electrolyte: 0.01 M  $\text{Na}_2\text{HPO}_4$  + 0.01 M  $\text{NaH}_2\text{PO}_4$ ; pH adjusted with  $\text{H}_2\text{SO}_4$  or  $\text{NaOH}$ . Frequency range:  $10^4$  to  $10^{-1}$  Hz. AC amplitude: 5 mV. Potential window: +0.4 to -0.4 V. Capacitance values were calculated from  $(\omega/Z)^{-1}$  at the maximum phase angle.

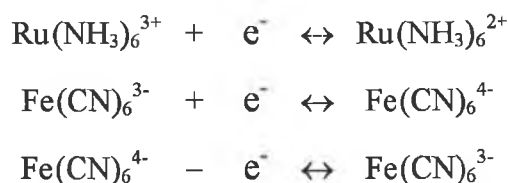
Impedance measurements as a function of pH were carried out at the PZC of the modified electrode. The insert of Figure 4.9 shows the variation in capacitance with pH at a fixed potential of -0.1 V. At pH 3.72, a local maximum in the capacitance of  $21.0 \mu\text{F cm}^{-2}$  was observed, which is a result of a maximum in the  $C(f)$ , the degree of protonation.<sup>4</sup> From this value, taking the surface coverage,  $\Gamma_T$ , to be  $2 \times 10^{-10} \text{ mol cm}^{-2}$  (theoretical value for a dense monolayer) the fraction of molecules in the deprotonated state  $f$ , was determined using equation 4.2.  $f$  was determined to be 0.93 or 0.07, resulting in a calculated  $\text{p}K_a$  of  $3.72 \pm 1.12$ . This value is significantly lower than the  $\text{p}K_a$  of 5.4, quoted for the dissociation constant for thioctic acid in aqueous solution.<sup>24</sup> Interestingly, the observed maximum occurs over a relatively narrow range in pH; between pH 3.09 and pH 5.18. Previous reports have suggested that the dissociation of carboxylic acid groups within monolayer systems occurs over a much broader pH range (due to hydrogen bonding stabilization) compared to the relatively narrow range observed in the solution phase.<sup>25, 26</sup> The relative narrowness of the titration curve observed here may indicate that the monolayer is less densely packed.

It is evident that while a capacitive maximum is observed for the TA monolayer in accordance with the theoretical predictions of Smith and White, the relationship between the observed capacitance value and monolayer protonation does not hold for this system. This may be due to the fact that the terminal carboxylic acid group of the thioctic acid molecule is not in conjugation with the gold electrode and so its  $pK_a$  remains essentially potential independent.

### 4.3.3 Permeation Studies

The permeability of the TA monolayer to complexes in solution was investigated electrochemically using a variety of techniques. The objective of the permeability studies was to analyze how the presence of the monolayer in its protonated and dissociated form influences the electrode's response to the probe molecules. By monitoring the electrochemistry of the probe molecules, it was anticipated that any changes in monolayer permeability, occurring upon deprotonation, would be detected.

The probes used in this study; potassium ferricyanide, potassium ferrocyanide and ruthenium hexaamine,  $\text{Fe}(\text{CN})_6^{3-}$ ,  $\text{Fe}(\text{CN})_6^{4-}$  and  $\text{Ru}(\text{NH}_3)_6^{3+}$  respectively, are all simple one outer-sphere electron redox couples:



Potassium ferrocyanide was used only in the AC impedance measurements where it is necessary to have equal concentrations of both redox species in solution at equilibrium. Figure 4.10 below outlines basic redox reaction scheme and the sign convention used in this study:

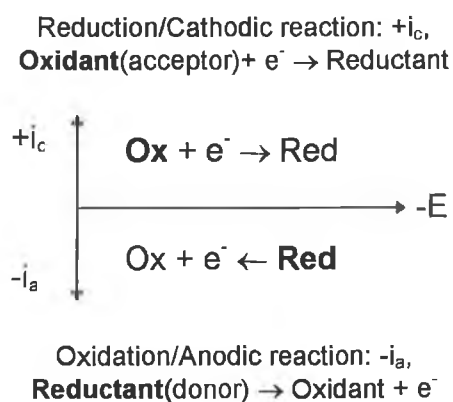


Figure 4.10 Overview of a simple one electron redox process.

The probes were selected on the basis of three important criteria; firstly they all undergo pH independent electron transfer; secondly, they are all hydrophilic in nature, which facilitates the variation of electrolyte pH and thirdly they are all of comparable size. For comparative purposes both negatively and positively charged probes were chosen.

The response of TA modified electrodes to the above solution phase species was monitored at low pH where the layer is expected to be protonated (pH 2) and high pH (pH 7/8), where the layer is expected to be ionized. The effect of the TA monolayer, and its degree of protonation on the diffusion coefficient,  $D$ , and the standard rate constant,  $k^0$ , for the probe molecules was investigated. The measurement of these properties enables one to evaluate the barrier properties of the layer and allows the possibility of pH dependent permeation to be investigated.

### (i) Cyclic Voltammetry

Cyclic voltammograms of  $\text{Fe}(\text{CN})_6^{3-}$  and  $\text{Ru}(\text{NH}_3)_6^{3+}$  were recorded at the bare and TA modified electrodes at high and low pH. Figure 4.11 shows characteristic current-potential responses observed at a scan rate of  $50 \text{ mV s}^{-1}$  for both probes at high pH. There is little change in the response of the positively charged complex,  $\text{Ru}(\text{NH}_3)_6^{3+}$  at the bare and TA modified electrode. The presence of the monolayer did not alter the formal potential ( $-0.191 \text{ V}$ ) of the  $\text{Ru}(\text{NH}_3)_6^{3+/2+}$  redox couple. As is evident from Figure 4.11, at high pH the current observed for the negatively charge probe,  $\text{Fe}(\text{CN})_6^{3-}$ , at the modified electrode was considerably reduced compared to that observed at the bare electrode, the peak shaped response is lost and a sigmoidal response is observed.

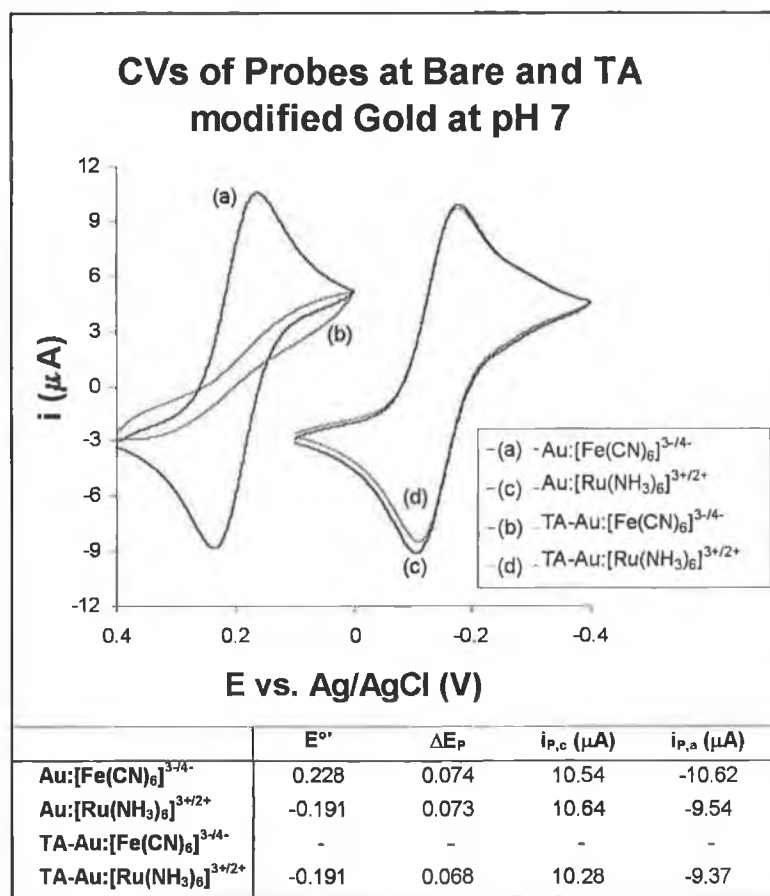


**Figure 4.11** Current responses for 3 mM  $\text{Fe}(\text{CN})_6^{3-}$  (LHS) and  $\text{Ru}(\text{NH}_3)_6^{3+}$  (RHS) for bare gold (Au) and thioctic acid modified gold (TA-Au) at pH 7. Scan rate:  $50 \text{ mV s}^{-1}$ . The response for  $\text{Fe}(\text{CN})_6^{3-}$  is clearly repressed at the TA-Au surface.

The effect of scan rate on the current response was investigated. The peak current for reversible reactions involving a freely diffusing reactant, is defined by the Randles Sevčik equation:

$$i_p = 0.4463 nF (nF / RT)^{1/2} A D^{1/2} \nu^{1/2} C^* \quad (4.4)$$

Figure 4.13 and Figure 4.14 overleaf show cyclic voltammograms for  $\text{Fe}(\text{CN})_6^{3-}$  and  $\text{Ru}(\text{NH}_3)_6^{3+}$ , recorded as a function of scan rate in the range 10 to 50  $\text{mV s}^{-1}$ , for the bare and TA modified electrodes at pH 7. The background corrected cathodic peak currents,  $i_{p,C}$ , were measured and plotted as a function of the square root of the scan rate as shown below in Figure 4.12, in accordance with equation 4.4. The diffusion coefficients were evaluated from the slopes as follows

$$D = \left( \frac{\text{Slope}}{0.4463 nF (nF / RT)^{1/2} A C^*} \right)^2 \quad (4.5)$$

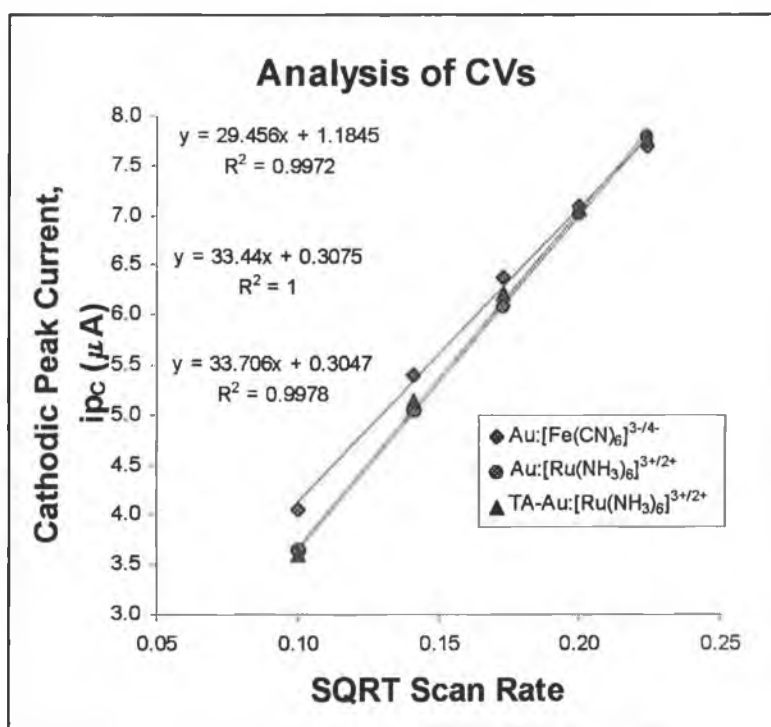
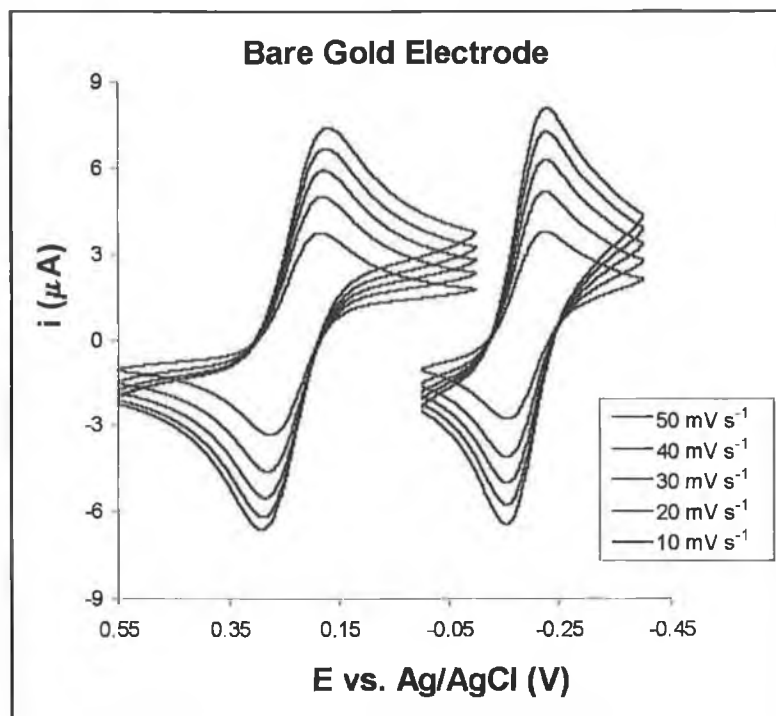
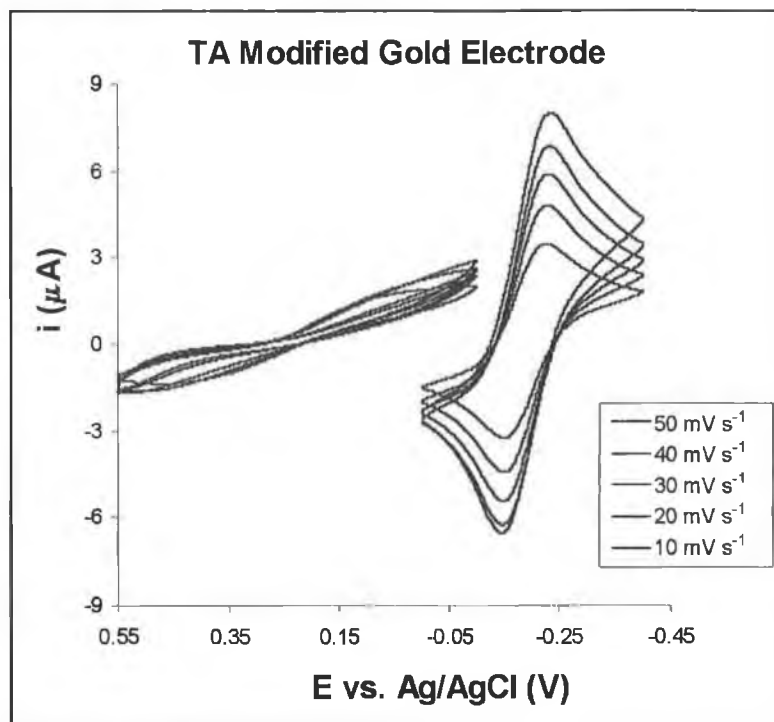


Figure 4.12 Randles Sevčik plots for solutions of 3mM  $\text{Fe}(\text{CN})_6^{3-}$  and  $\text{Ru}(\text{NH}_3)_6^{3+}$  in 0.02 M  $\text{NaH}_2\text{PO}_4$  + 0.08 M  $\text{Na}_2\text{HPO}_4$  (pH 7).



**Figure 4.13** Cyclic Voltammograms recorded for  $\text{Fe}(\text{CN})_6^{3-}$  (LHS) and  $\text{Ru}(\text{NH}_3)_6^{3+}$  (RHS) at a bare gold electrode as a function of scan rate. Electrolyte: 0.02 M  $\text{NaH}_2\text{PO}_4$  + 0.08 M  $\text{Na}_2\text{HPO}_4$  (pH 7).



**Figure 4.14** Cyclic Voltammograms recorded for  $\text{Fe}(\text{CN})_6^{3-}$  (LHS) and  $\text{Ru}(\text{NH}_3)_6^{3+}$  (RHS) at a TA modified gold electrode as a function of scan rate. Electrolyte (pH 7): 0.02 M  $\text{NaH}_2\text{PO}_4$  + 0.08 M  $\text{Na}_2\text{HPO}_4$ .

An estimation of the standard rate constant,  $k^0$ , for the redox couples was determined from the variation in peak to peak separation with scan rate, using the Nicholson technique (see Table 1.1 and equation 1.1).<sup>27</sup> Although the cyclic voltammograms indicate that the redox probes were chemically reversible, the  $59/n$  V peak to peak separation expected for complete electrochemical reversibility was never observed.

Table 4.2 summarizes the results obtained. In the case of  $\text{Ru}(\text{NH}_3)_6^{3+}$  chemical reversibility was observed at the bare and modified surfaces. The magnitude of the peak currents obtained were similar suggesting that the presence the monolayer does not impede the diffusion of  $\text{Ru}(\text{NH}_3)_6^{3+}$  to the underlying gold surface. Although the probe is allowed unhindered access to the monolayer interior, the lower value of  $k^0$  observed for  $\text{Ru}(\text{NH}_3)_6^{3+}$  at the modified electrode suggests that electron transfer is affected by the presence of the layer. A reduction in the rate of electron transfer could be due to an increase in the electron transfer distance. It is possible that the presence of the layer reduces the distance of closest approach for the  $\text{Ru}(\text{NH}_3)_6^{3+}$  complex. Although the complexes diffuses freely through the alkyl chains of the monolayer, the dithiolane ring of the TA molecule may hinder its access to the underlying gold surface and electron transfer must therefore occur over a greater distance. Given that  $k^0$  is proportional to  $\exp(-\beta d)$ , where  $\beta$  is distance dependant tunnelling parameter and  $d$  is the electron transfer distance, it is possible to estimate the increase in  $d$  on monolayer modification. The observed decrease in  $k^0$  from  $10.9 \times 10^{-3}$  to  $5.5 \times 10^{-3} \text{ cm s}^{-1}$  translates as an increase in the electron transfer distance of  $0.68 \text{ \AA}$ , which suggests that electron transfer is occurring from within the monolayer. Had electron transfer occurred out at the monolayer-solution interface then a rate constant of the order  $10^{-5} \text{ cm s}^{-1}$  would be expected.

**Table 4.2** Analysis of CV data.

Cyclic Voltammetry	Au: $\text{Ru}(\text{NH}_3)_6^{3+}$	TA-Au: $\text{Ru}(\text{NH}_3)_6^{3+}$	Au: $\text{Fe}(\text{CN})_6^{3-}$	TA-Au: $\text{Fe}(\text{CN})_6^{3-}$
$E^{0i}$ (V)	-0.191	-0.191	0.228	-
Slope ( $\times 10^{-5} \text{ C}^{3/2} \text{ s}^{-1/2} \text{ J}^{-1/2}$ ) <sup>a</sup>	3.344	3.371	2.946	-
$D$ ( $\times 10^{-6} \text{ cm}^2 \text{ s}^{-1}$ ) <sup>b</sup>	4.3	4.3	3.3	-
$k^0$ ( $\times 10^{-3} \text{ cm s}^{-1}$ ) <sup>c</sup>	10.9±0.1	5.5±0.1	2.46±0.1	-

<sup>a</sup> From plots of  $i_{p,c}$  vs.  $v^{1/2}$  (eq. 4.4). <sup>b</sup> Calculated from eq. 4.5, using  $A = 2.01 \times 10^{-2} \text{ cm}^2$ . <sup>c</sup> Calculated using eq. 1.1 with the approximation  $\gamma^{\alpha} = 1$ .

The lower rate constant observed for  $\text{Fe}(\text{CN})_6^{3-}$  compared to  $\text{Ru}(\text{NH}_3)_6^{3+}$  at the bare gold electrode suggests that the  $\text{Fe}(\text{CN})_6^{3-/4-}$  reaction is kinetically less facile than that of  $\text{Ru}(\text{NH}_3)_6^{3+/2+}$ . The  $\text{Fe}(\text{CN})_6^{3-}$  response was extremely irreversible at the TA modified electrode and the evaluation of the diffusion coefficient for the negatively charged complex was not possible using cyclic voltammetry at these low scan rates. The sigmoidal shape of the cyclic voltammograms obtained for  $\text{Fe}(\text{CN})_6^{3-}$  at high pH, for the TA modified electrodes suggests that the presence of the ionized monolayer blocks the mass transfer of the negative probe to the gold electrode. Since this effect was not observed for the positively charged probe which is of comparative size, it seems reasonable to conclude that this effect is principally due to the electrostatic repulsion between the negatively charged carboxylate groups at the surface of the TA monolayer and the negatively charged complex, which prevents diffusion of the complex through the monolayer to the underlying Au surface.

The response observed for the negatively charged  $\text{Fe}(\text{CN})_6^{3-}$  probe at the ionized monolayer was always sigmoidal in character, verifying that electron transfer occurs as result of the diffusion of  $\text{Fe}(\text{CN})_6^{3-}$  to defect sites within the monolayer. An exponentially shaped response is typically observed when a monolayer forms an effective barrier, thereby forcing electron transfer to occur out at the monolayer/solution interface. Since such a response was not observed for the TA system, the presence of the monolayer does not effectively passivate the electrode surface. Defects are present at a low level and appear to be of a molecular dimension, i.e., large enough to enable the complex pass unimpeded by electrostatic repulsion yet small enough to produce a sigmoidal response. Therefore, although a reasonably coherent monolayer is formed, electron transfer to a solution phase species is possible through a small number of defects.

## (ii) Sampled Current Voltammetry

Using sampled current voltammetry, the kinetic parameters associated with heterogeneous electron transfer,  $k^0$  and  $\alpha$ , were evaluated. The potential region investigated was from 0 to -0.4 V for  $\text{Ru}(\text{NH}_3)_6^{3+}$ , and between 0.5 and -0.1 V for  $\text{Fe}(\text{CN})_6^{3-}$ . The sampling times were 49.5 and 59.5 msec for  $\text{Ru}(\text{NH}_3)_6^{3+}$  and  $\text{Fe}(\text{CN})_6^{3-}$ , respectively. For comparative purposes, Figure 4.15 shows an overlay of the current responses for the two probes at the modified and bare surfaces. It is evident that at high pH on the TA modified surface the response to  $\text{Fe}(\text{CN})_6^{3-}$  is severely affected. From the observed limiting currents, the diffusion coefficients for both  $\text{Ru}(\text{NH}_3)_6^{3+}$  and  $\text{Fe}(\text{CN})_6^{3-}$  at the bare electrode and for  $\text{Ru}(\text{NH}_3)_6^{3+}$  at the TA modified electrode, could be calculated using the modified Cottrell equation.

$$i_{\text{lim}} = \frac{nFAD_0^{1/2}C_0^*}{\pi^{1/2}(\tau - \tau')^{1/2}} \quad (4.6)$$

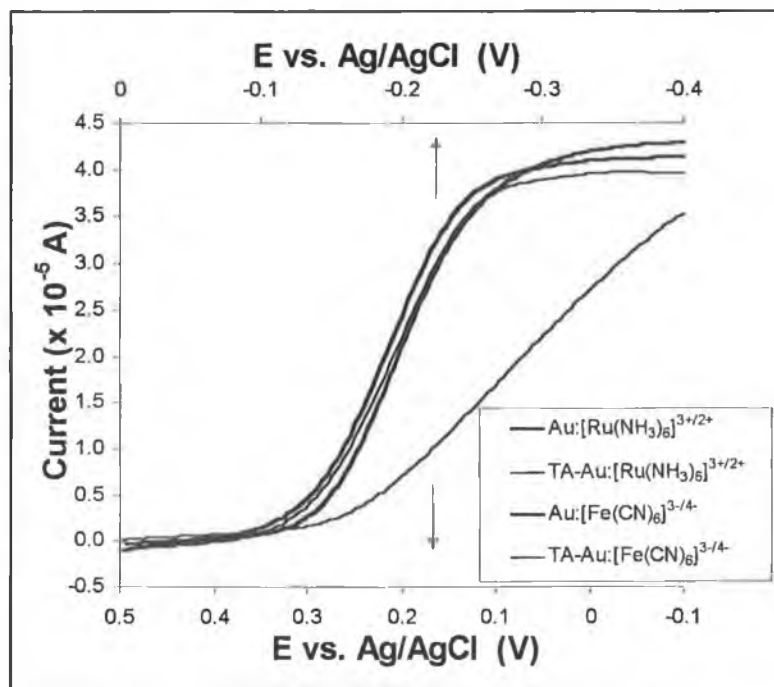


**Figure 4.15** Sampled current voltammograms obtained for 3mM  $\text{Fe}(\text{CN})_6^{3-}$  and  $\text{Ru}(\text{NH}_3)_6^{3+}$  in 0.01 M  $\text{NaH}_2\text{PO}_4$  + 0.09 M  $\text{Na}_2\text{HPO}_4$  (pH 8). From the LHS the curves are as follows:  $\text{Ru}(\text{NH}_3)_6^{3+}$ , bare and TA modified gold (upper x-axis,  $\tau - \tau' = 49.5$  msec),  $\text{Fe}(\text{CN})_6^{3-}$ , bare and TA modified gold (lower x-axis,  $\tau - \tau' = 59.5$  msec).

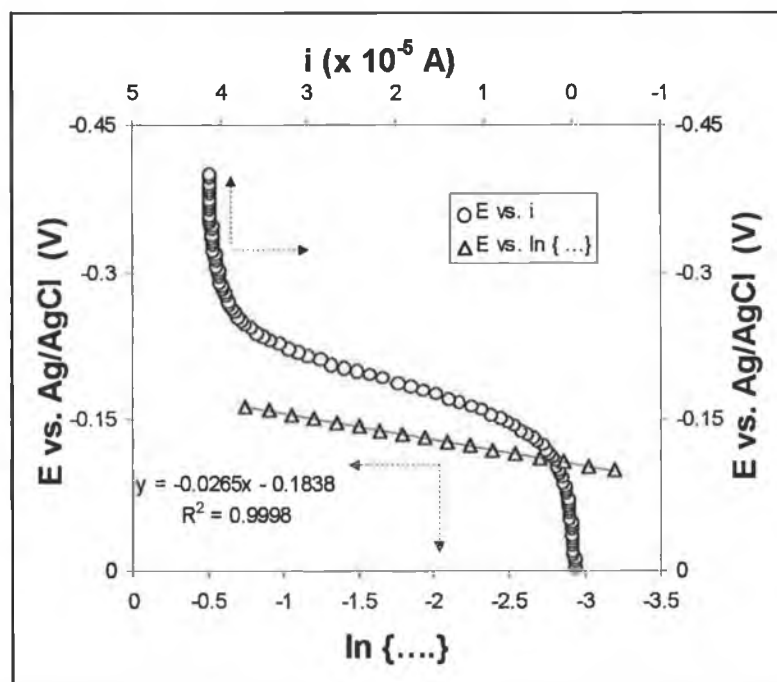


**Figure 4.16** Analysis of the rising portion of a sampled current voltammogram obtained for 3mM  $\text{Ru}(\text{NH}_3)_6^{3+}$  at a bare gold electrode. The SCV trace is overlaid to illustrate the portion of the curve that is analyzed.

As shown in Figure 4.16 the analysis of the rising portion of the SCV in accordance with equation 4.7, (where  $X$  is the ratio of the current at potential  $E$  to the anodic limiting current, and  $\xi$  is a dimensionless parameter  $[(nF/RT)/(E-E^0)]$ ), yields a linear plot of slope  $RT/(\alpha \mp nF)$  and intercept  $E^*$ .

$$E = E^* \mp \frac{RT}{\alpha \mp nF} \ln \left\{ X \left[ \frac{1.75 + X^2 [1 + \exp(\pm \xi)]^2}{1 - X [1 + \exp(\pm \xi)]} \right]^{1/2} \right\} \quad (4.7)$$

The value of  $\alpha$  was obtained directly from the slope and the value of  $k^0$  was calculated from the intercept given that:

$$E^* = E^{oi} \pm \frac{RT}{\alpha \mp nF} \ln \left\{ \frac{4 k^0 (\tau - \tau')^{1/2}}{\sqrt{3} D^{1/2}} \right\} \quad (4.8)$$

The analyzed experimental data, summarized in Table 4.3, reveal that the presence of the monolayer does not affect the standard rate constant for electron transfer in the

case of the positively charged  $\text{Ru}(\text{NH}_3)_6^{3+}$ . The value of  $k^0$  obtained by SCV is considered to be more accurate, than that obtained from the peak to peak separation method of Nicholson. In agreement with the data obtained from the cyclic voltammetry, the reduction of  $\text{Fe}(\text{CN})_6^{3-}$  on bare gold is kinetically less facile compared to  $\text{Ru}(\text{NH}_3)_6^{3+}$ .

Although the values of  $D$  obtained from the SCV experiments are higher than those observed from the CV experiments they are of the same order of magnitude,  $10^{-6} \text{ cm}^2 \text{ s}^{-1}$ . The values of  $k^0$  also agree to an order of magnitude of  $10^{-3} \text{ cm s}^{-1}$ . The value of the transfer coefficient,  $\alpha$ , was determined to 0.92 and 0.85 for  $\text{Ru}(\text{NH}_3)_6^{3+}$  and  $\text{Fe}(\text{CN})_6^{3-}$  respectively.  $\alpha$  is an indication of the symmetry of a reaction and is related to the shape of the free energy barrier and to the position of the activated complex along the reaction coordinate. Generally, for reversible systems obeying Butler-Volmer kinetics, the predicted value of  $\alpha$  is  $\sim 0.5$ . The large values of  $\alpha$  obtained in this study are not unusual for coated electrodes and highlight the failure of classical kinetics to accurately describe many electrochemical systems.

**Table 4.3** Analysis of SCV data.

Sampled Current Voltammetry	Au: $\text{Ru}(\text{NH}_3)_6^{3+}$	TA-Au: $\text{Ru}(\text{NH}_3)_6^{3+}$	Au: $\text{Fe}(\text{CN})_6^{3-}$	TA-Au: $\text{Fe}(\text{CN})_6^{3-}$
$i_{\text{lim}} (\times 10^{-5} \text{ A})^a$	4.11	4.01	3.81	-
$\tau - \tau'$ (ms)	49.5	49.5	59.5	59.5
Slope <sup>b</sup>	-0.027	-0.028	-0.030	-
Intercept (V) <sup>b</sup>	-0.184	-0.185	0.219	
$k^0 (\times 10^{-3} \text{ cm s}^{-1})^c$	7.04±0.02	7.23±0.02	3.38±0.02	-
$\alpha^d$	0.92	0.92	0.85	-
$D (\times 10^{-6} \text{ cm}^2 \text{ s}^{-1})^e$	7.7	7.4	8.00	-

<sup>a</sup> From experimental data. <sup>b</sup> From plot of eq. 4.7. <sup>c</sup> Calculated from eqs. 4.7 & 4.8, with  $D_{\text{Lit}}(\text{Fe}(\text{CN})_6^{3-}) = 7.6 \times 10^{-6} \text{ cm}^2 \text{ s}^{-1}$  [20],  $D_{\text{Lit}}(\text{Ru}(\text{NH}_3)_6^{3+}) = 7.1 \times 10^{-6} \text{ cm}^2 \text{ s}^{-1}$  [28]. <sup>d</sup> Calculated from slope. <sup>e</sup> Calculated from  $i_{\text{lim}}$  using eq. 4.6, with  $A = 2.01 \times 10^{-2} \text{ cm}^2$ .

### (iii) Chronoamperometry

Diffusion coefficients were also measured using chronoamperometry. The potential was stepped in a negative direction from a potential where no reduction occurs to one where diffusion is rate limiting, i.e., from 0.0 to -0.4 V in the case of  $\text{Ru}(\text{NH}_3)_6^{3+}$  and from 0.5 to -0.1 V in the case of  $\text{Fe}(\text{CN})_6^{3-}$ . The current decays were followed for 10 seconds and analyzed in accordance with equation 4.9 by plotting  $i_c(t)$  vs.  $t^{-1/2}$ .

$$i_c(t) = \frac{nFA D_o^{1/2} C_o^*}{(\pi t)^{1/2}} \quad (4.9)$$

Linear plots were obtained for both probes at the bare and TA modified electrode surfaces, and the diffusion coefficients were determined from the slopes, given that

$$D_o = \left( \frac{\text{Slope}(\pi)^{1/2}}{nFA C_o^*} \right)^2 \quad (4.10)$$

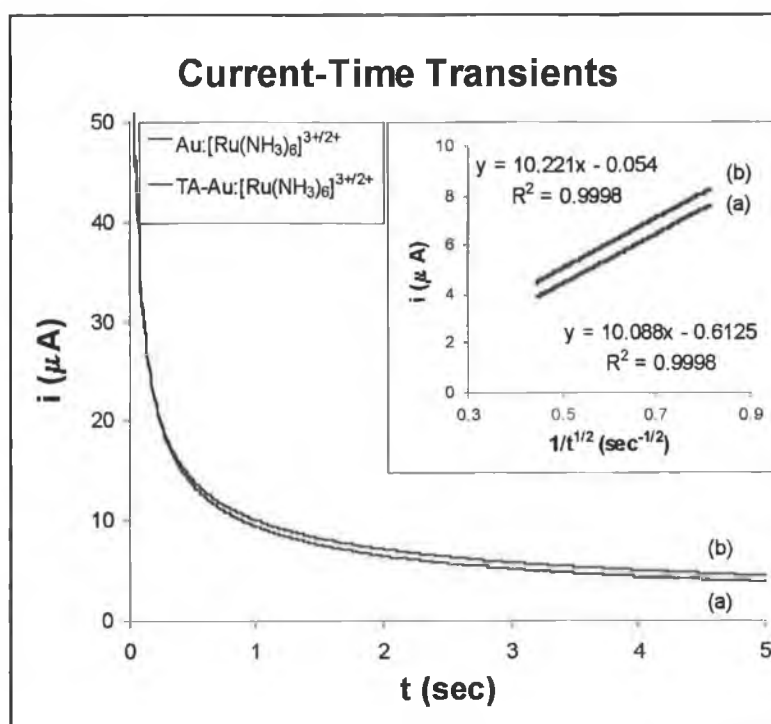


**Figure 4.17** Current-time transients observed for 3 mM  $\text{Ru}(\text{NH}_3)_6^{3+}$  at (a) bare and (b) TA modified gold electrodes. Electrolyte: 0.1 M  $\text{LiClO}_4$  + 0.01 M  $\text{NaH}_2\text{PO}_4$  + 0.09 M  $\text{Na}_2\text{HPO}_4$  (pH 8); The potential was stepped from 0 to -0.4 V. The inset shows analysis of the chronoamperometric data.

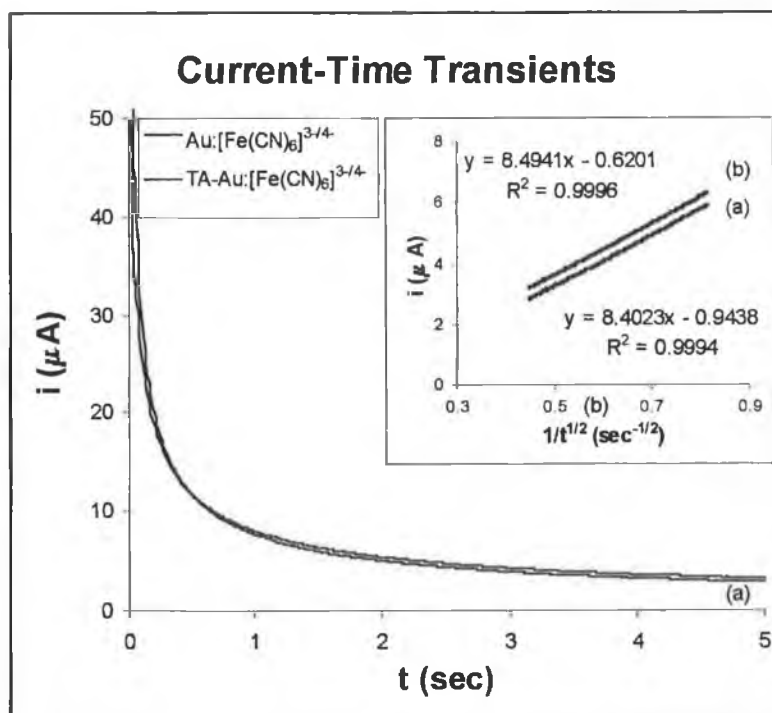


**Figure 4.18.** Current-time transients observed for 3 mM  $\text{Fe}(\text{CN})_6^{3-}$  at bare and TA modified gold electrodes. Electrolyte: 0.1 M  $\text{LiClO}_4$  + 0.01 M  $\text{NaH}_2\text{PO}_4$  + 0.09 M  $\text{Na}_2\text{HPO}_4$  (pH 8). The potential was stepped from 0.5 to -0.1 V. The inset shows analysis of the chronoamperometric data.

Figure 4.17 and Figure 4.18 show the results obtained for  $\text{Ru}(\text{NH}_3)_6^{3+}$  and  $\text{Fe}(\text{CN})_6^{3-}$  for both the bare and TA modified gold surfaces at pH 8. From Table 4.4 below, it is clear that quite surprising results were obtained, The diffusion coefficients for both probes remained essentially unchanged by the presence of the ionized TA monolayer. While this is to be expected for the positively charged  $\text{Ru}(\text{NH}_3)_6^{3+}$ , based on the results from the sample current voltammetry experiments, it is entirely unexpected for the negatively charged  $\text{Fe}(\text{CN})_6^{3-}$  which previously exhibited irreversible behaviour at ionized TA monolayer. These results indicate that the charged monolayer does not block the access of the probe to the monolayer interior, suggesting that defects are present within the monolayer.

**Table 4.4** Analysis of CA data.

Chronoamperometry	Au: $\text{Ru}(\text{NH}_3)_6^{3+}$	TA-Au: $\text{Ru}(\text{NH}_3)_6^{3+}$	TA-Au: $\text{Fe}(\text{CN})_6^{3-}$	TA-Au: $\text{Fe}(\text{CN})_6^{3-}$
Slope ( $\times 10^{-6} \text{ C s}^{-1/2}$ ) <sup>a</sup>	10.088	10.221	8.402	8.494
$D$ ( $\times 10^{-6} \text{ cm}^2 \text{ s}^{-1}$ ) <sup>b</sup>	9.44	9.69	6.55	6.69

<sup>a</sup> From  $i_c(t)$  vs.  $t^{1/2}$  plots. <sup>b</sup> Calculated from eq. 4.6, with  $A = 2.01 \times 10^{-2} \text{ cm}^2$ .

#### (iv) Effect of pH on Response of $\text{Fe}(\text{CN})_6^{3-}$

It was evident from the experimental data that the presence of the monolayer and its dissociation had the greatest effect on the negatively charged probe. Since the permeation studies point to discrimination on the basis of charge and electrostatic effects it was decided to monitor the response of the TA modified electrode to the probe as function of pH. It was hoped that from this experiment an indication of the value of the surface  $pK_a$  could be obtained. A solution of 5 mM  $\text{Fe}(\text{CN})_6^{3-}$  was prepared with 0.1 M  $\text{LiClO}_4$  as the electrolyte and contained 0.1 M phosphate buffer (equimolar  $\text{NaH}_2\text{PO}_4/\text{Na}_2\text{HPO}_4$ , pH 6.59). The solution pH was brought up to pH 10.30 with a small volume 2 M  $\text{NaOH}$ . A cyclic voltammogram was recorded at  $50 \text{ mV s}^{-1}$  within the potential where electroactivity of the probe is expected to occur, then  $\text{H}_2\text{SO}_4$  was added to decrease the pH. The solution was allowed to equilibrate for 2 minutes and a second CV was recorded. The process was repeated until a pH of 1.83 was reached. The volume change during the titration was less than 4 % and so the concentration of the solution was not significantly altered. Figure 4.20 overleaf, shows the cyclic voltammograms recorded as a function of pH. The variation in the peak to peak separation and the formal potential with solution pH is shown graphically below in Figure 4.19.

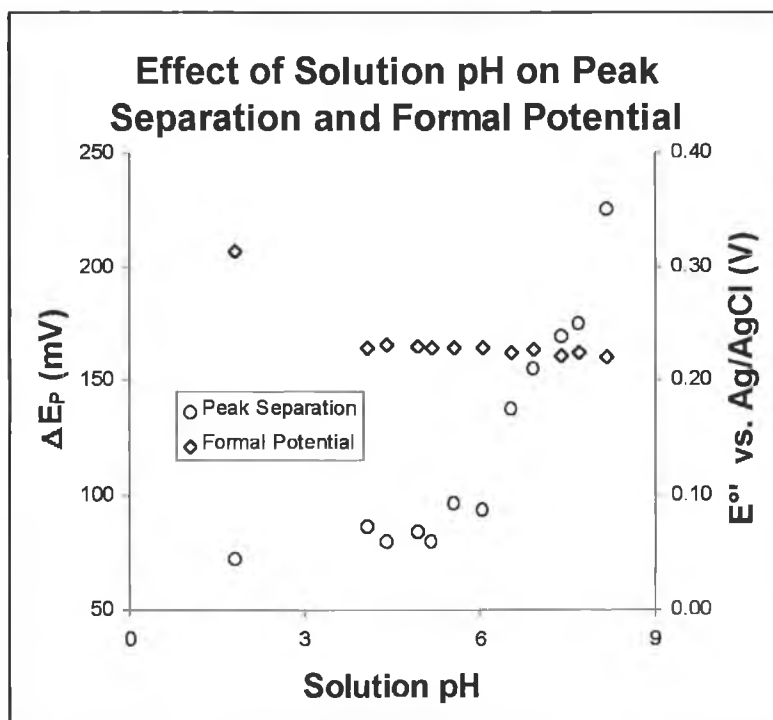
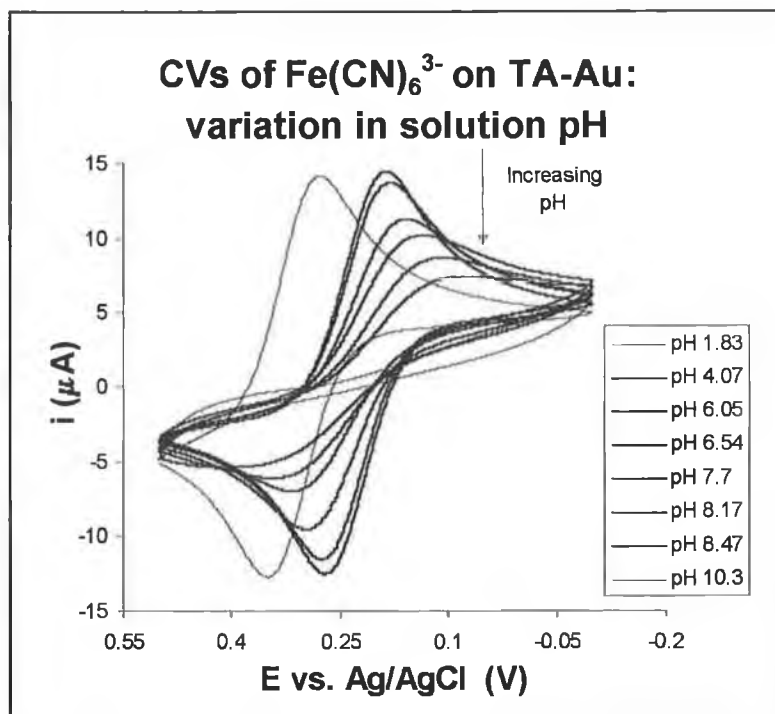
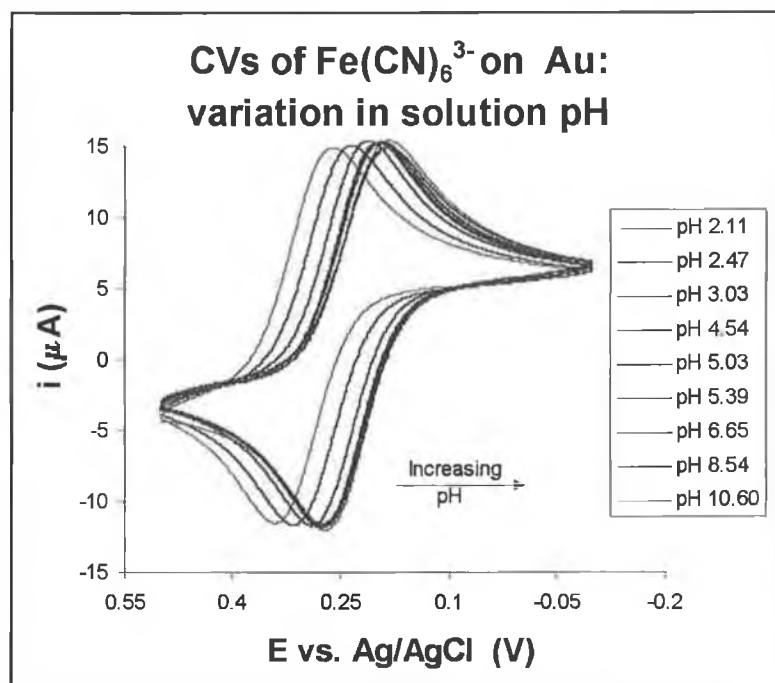


Figure 4.19 The pH Variation of  $\Delta E_p$  and  $E^\circ$  for  $\text{Fe}(\text{CN})_6^{3-}$  based on the cyclic voltammograms displayed overleaf in figure 4.20.



**Figure 4.20** CVs recorded as a function of pH for 5 mM  $\text{Fe}(\text{CN})_6^{3-}$  at a TA modified electrode. Electrolyte: 0.1 M  $\text{LiClO}_4$  + 0.05 M  $\text{NaH}_2\text{PO}_4$  + 0.05 M  $\text{Na}_2\text{HPO}_4$ ; pH adjusted with  $\text{NaOH}/\text{H}_2\text{SO}_4$ ; Scan rate:  $50 \text{ mV s}^{-1}$ . The trace on the extreme left is at pH 1.83. The effects of ionization are first observed at pH 6.05.



**Figure 4.21** CVs recorded as a function of pH for 5 mM  $\text{Fe}(\text{CN})_6^{3-}$  at bare Au electrode. Conditions as detailed in figure 4.20. The first three traces from the extreme left were recorded at pH 2.11, 2.47 and pH 3.03 respectively. From pH 4.54 through to pH 10.60 the traces overlap.

From the variation in peak to peak separation,  $\Delta E_p$ , with pH shown in Figure 4.19, it is evident that the response of the modified electrode depends on the degree of monolayer protonation. The  $\Delta E_p$  begins to gradually increase on going from pH 1.83 to pH 6, after which point the  $\Delta E_p$  increases more dramatically with pH. At a solution of pH 10 the response is totally repressed and a sigmoidal shaped response is observed. The formal potential,  $E^\circ$ , of the  $\text{Fe}(\text{CN})_6^{3-/4-}$  remains essentially constant between pH 4 and 8.47 for as long as a peak shaped response is observed. Between pH 4 and 2,  $E^\circ$  shifts positive by almost 85 mV. The same shift is observed at a bare gold electrode and is therefore not attributed to the presence of the TA monolayer.

Based on the above data it would seem that the solution pH, at which the degree of monolayer ionization begins to effect the reversibility of the solution phase probe is higher than expected. Given that the permeation studies carried out, indicate that electrostatic effects control the permeation of the negatively charged probe, then from the value of surface  $pK_a$  ( $3.72 \pm 1.12$ ) determined by capacitance measurements in Section 4.3.2.(ii), one would expect the response to  $\text{Fe}(\text{CN})_6^{3-}$  to be substantially reduced at solution pH 5. It was not feasible to determine the  $pK_a$  of the monolayer from the  $\Delta E_p$  vs. pH curve displayed in Figure 4.19 as the relationship between monolayer ionization and peak separation was not evident. It was not possible to fit the data as the peak to peak separation did not increase with ionization in a linearly, exponential or logarithmical fashion. Interestingly, in contrast to the capacitance studies as a function of pH, the effect of monolayer ionization on the peak separation occurred over a relatively broad pH range.

### (v) AC Impedance

In theory, AC impedance measurements of small amplitude can provide a separation in frequencies between the kinetic and mass transfer control allowing evaluation of kinetic parameters free of mass transport complication. For AC impedance measurements it is necessary to have equal concentrations of both redox species in solution at equilibrium. A 5mV ac amplitude was applied to a solution containing 3 mM  $\text{Fe}(\text{CN})_6^{3-}$  and 3 mM  $\text{Fe}(\text{CN})_6^{4-}$  at 0.226 V (i.e., the formal potential for the redox couple). The frequency range studied was from  $10^5$  to  $10^{-1}$  Hz. Figure 4.22 shows Nyquist plots of the data obtained.

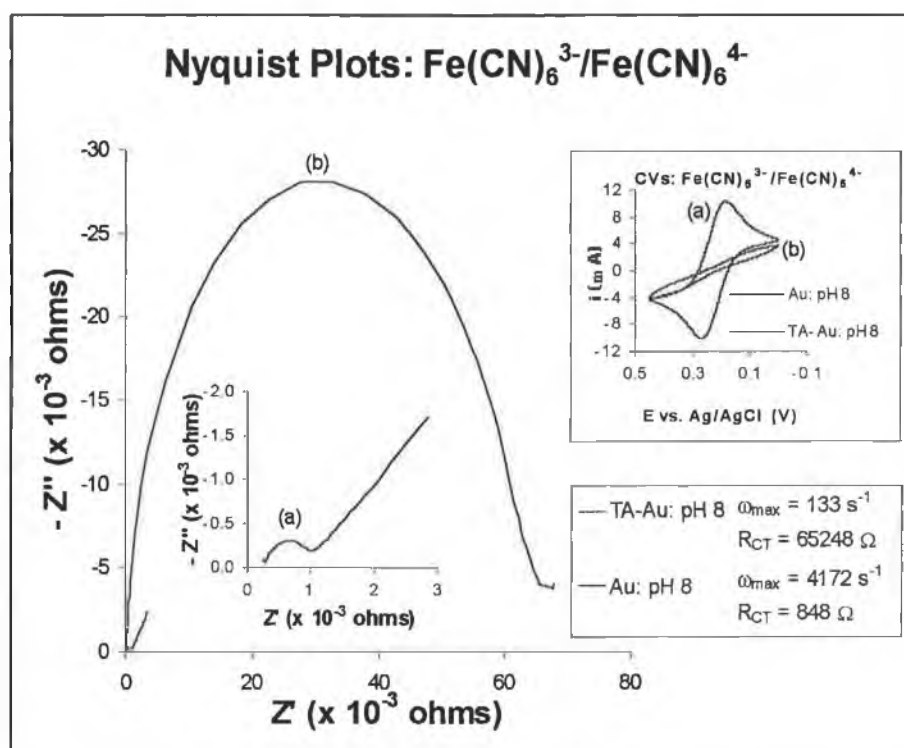


**Figure 4.22** Nyquist plots obtained for 3.0 mM  $\text{Fe}(\text{CN})_6^{3-}$  + 3.0 mM  $\text{Fe}(\text{CN})_6^{4-}$  at the (a) bare and (b) TA modified gold electrodes. Electrolyte (pH 8): 0.1 M  $\text{LiClO}_4$  + 0.01 M  $\text{NaH}_2\text{PO}_4$  + 0.09 M  $\text{Na}_2\text{HPO}_4$ ; Frequency range:  $10^5$  to  $10^{-1}$  Hz. AC amplitude: 5 mV. Measurement potential: 0.226 V. The insert at top RHS shows the solution phase CV's recorded at a scan rate of  $20 \text{ mV s}^{-1}$  prior to the impedance measurements.

Table 4.5 above summarizes the calculations based on the interpretation of the Nyquist plots based Randles equivalent circuit, which model the system as the series combination of  $R_{CT}$ , the resistance due to the heterogeneous electron transfer (the

smaller the rate of electron transfer the larger  $R_{CT}$ ) and  $Z_w$ , the Warburg impedance, (a frequency dependent reactance due to the mass transfer between the bulk solution and the electrode surface) in parallel with  $C_{dl}$  and combined with  $R_U$ .

$$k^0 = \frac{2RT}{n^2 F^2 A C^* R_{CT}} \quad (4.11)$$

$$D = \left( \frac{4RT}{\sqrt{2} n^2 F^2 A \sigma C^*} \right)^2 \quad (4.12)$$

**Table 4.5** Analysis of AC Impedance data.

AC Impedance	Bare Au	TA-Au
$R_U (\Omega)^a$	245.8	245.8
$R_U + R_{CT} (\Omega)^a$	1,094	65494
$R_{CT} (\Omega)^a$	848.2	65248.2
$\omega_{max} (s^{-1})^a$	4,172.66	133.39
intercept $(\Omega)^a$	927	-
$C_{dl} (\mu F cm^{-2})^b$	7.03	2.86
$k^0 (cm s^{-1})^c$	$5.20 \times 10^{-3}$	$6.76 \times 10^{-5}$
$\sigma (\Omega s^{-1/2})$	17,190	-
$D (cm^2 s^{-1})^d$	$1.32 \times 10^{-7}$	-

<sup>a</sup> Values taken from Nyquist plots of data. <sup>b</sup>  $C_{dl} = (R_{CT} \times \omega_{max})^{-1}$ .

<sup>c</sup> Calculated using eq. 4.11. <sup>d</sup> Calculated using eq. 4.12.

The first thing to note is that for the ionized monolayer surface, the charge transfer resistance is so large that the region corresponding to the mass transport is absent. When frequencies lower than 0.1 Hz were investigated, the response became extremely erratic and the 45° Warburg line typically observed for diffusion control was absent making it impossible to accurately determine the diffusion coefficient. The second noteworthy effect is the strength of impedance measurements over other techniques for the evaluation of the small  $k^0$ . AC impedance was the only process which permitted the evaluation of  $k^0$  for  $Fe(CN)_6^{3-}$  for the TA modified electrode at high pH. The standard rate constant for the bare and modified electrodes could be easily determined given the value of the charge transfer resistance,  $R_{CT}$ , which is obtained from the Nyquist plot. The value of  $k^0$  obtained for  $Fe(CN)_6^{3-}$  at pH 8,

$6.76 \times 10^{-5} \text{ cm s}^{-1}$ , was almost two orders of magnitude lower than at the bare gold electrode confirming that the redox reaction at the ionized monolayer surface was extremely irreversible. The relative decrease in  $k^0$ , translates as an increase in the electron transfer distance of approximately  $4.34 \text{ \AA}$ , further confirming that the charge on the monolayer impedes the diffusion of  $\text{Fe}(\text{CN})_6^{3-}$  through to the underlying electrode. The capacitance values calculated from the maximum value of  $Z''$  in the semicircle region of the Nyquist plot, for both the bare and TA modified electrodes, were considerably lower in value to those obtained from the capacitance measurements carried out in  $0.1 \text{ M LiClO}_4$  (see Section 4.3.2). This may be due to differences in the electrolyte/solution composition. The lower capacitance values would also explain why the value of the diffusion coefficient is an order of magnitude lower than expected. The diffusion coefficient is calculated from the Warburg coefficient,  $\sigma$ , which is related to the capacitance, as shown in Figure 1.17, by the following relation:

$$R_U + R_{CT} - 2 \sigma^2 C_{dl} \quad (4.13)$$

For a larger capacitance, one would obtain a lower value of  $\sigma$ , which would result in a larger diffusion coefficient. The value of  $k^0$  for the bare gold surface compares favourably with that obtained from the sampled current voltammogram experiments.

## 4.4 CONCLUSIONS

The permeation studies for the TA modified gold reveal that changes in response observed as a function of pH are not due to changes in monolayer permeability on ionization. The diffusion coefficient and standard rate constant determined for  $\text{Ru}(\text{NH}_3)_6^{3+}$  show that the modified electrode response is unaffected by the charge on the surface of the monolayer. The same is true of  $\text{Fe}(\text{CN})_6^{3-}$ , a complex of similar size but opposite charge, at low pH. Unfortunately, it seems that TA forms monolayers that are essentially permeable to the complexes studied. At low pH, both probes were allowed unimpeded access to the underlying electrode. Although pH dependent permeation of the layer was observed for the  $\text{Fe}(\text{CN})_6^{3-}$ , the electrochemical analyses show that the reduction in current response observed consistently at high pH, was due to coulombic repulsion between the ionized carboxylic acid terminated monolayer and the negatively charged probe, which prevented access to the underlying electrode. There was no evidence to suggest that a pH induced alteration in the structure of the monolayer affected the permeability of the above probe. That is not to say that pH induced structural changes within the monolayer do not occur. Since no change was observed in the case of  $\text{Ru}(\text{NH}_3)_6^{3+}$  it is possible that the probes chosen for this study were too small in size. Based on the results of this study alone, one cannot eliminate the possibility that ionization causes increased permeability due to swelling of the layer. Further investigations into the effect of probe size on permeation would be required before such a conclusion is reached.

The study of  $\text{Fe}(\text{CN})_6^{3-}$  response as a function of pH demonstrated that ionization of TA molecules within the monolayer occurs at a higher pH than in bulk solution. The fact that the  $\text{p}K_a$  of a compound shifts when incorporated into monolayers (presumably due to changes in the dielectric medium that the molecules experiences), will additionally complicate the design of pH-dependent release systems. It is apparent that the choice of compound for such a system cannot be made on the basis of its bulk  $\text{p}K_a$  alone. The shift in  $\text{p}K_a$  will have to be taken into

account and since at present there is no available correlation between bulk and surface dissociation constants the choice will have to be determined empirically.

It was hoped that the shorter chain length and asymmetry of the thioctic acid molecule would result in the formation of monolayers which would be more disposed to structural rearrangement compared with the previously studied monolayers systems of eicosenoic acid and tricosadiynoic acid. However, the results from this study show that the TA monolayers formed were essentially permeable to the complexes studied. The monolayers permeability to larger molecules may in fact be pH dependent. It is apparent from this study that permeability in monolayer systems is by no means a straight forward process, numerous factors control the diffusion of compounds through these layers. It would therefore be more beneficial to concentrate efforts on the design of a system for a specific drug/class of drug. That way a better, more educated choice of monolayer material can be made, as the size and hydrophobicity of the drug in question would be taken into account. In any case, it is clear from the above results, that pH induced release is not suitable for the release of similarly charged drugs (i.e., acidic drugs in the case of a carboxylic acid monolayer, and basic drugs in the case of an amine monolayer). Unlike disordered polymer systems the surface charge density of ionized monolayer is much greater, and ultimately effects the diffusion of charged molecules to a greater extent. This is perhaps the most significant conclusion to be drawn from the study, and will dictate the application of these systems in the area of drug delivery. The situation regarding neutral lipophilic drugs may be more favourable.

## 4.5 REFERENCES

- [1] Cheng, Q.; Brajter-Toth, A. *Anal. Chem.* **1992**, *64*, 1998.
- [2] Cheng, Q.; Brajter-Toth, A. *Anal. Chem.* **1995**, *67*, 2767.
- [3] Dalmia, A.; Liu, C. C.; Savinell, R. F. *J. Electroanal. Chem.* **1997**, *430*, 205.
- [4] Smith, C. P.; White, H. S. *Langmuir* **1993**, *9*, 1.
- [5] Homes-Farley, S. R.; Reamey, R. H.; Mc Carthy, T. J.; Deutch, J.; Whitesides, G. M. *Langmuir* **1985**, *1*, 725. Bain, C. D.; Whitesides, G. M. *Langmuir* **1989**, *5*, 1370.
- [6] Betts, J. J.; Pethica, B. A. *Trans. Faraday Soc.* **1956**, *52*, 1581. Caspers, J.; Goormaghtigh, E.; Ferreira, J.; Basseur, R.; Vanden-Branden, J.; Ruyschaert, J.-M. *J. Colloid Interface Sci.* **1983**, *91*, 546.
- [7] Bagg, J.; Haber, M. D.; Gregor, H. P. *J. Colloid Interface Sci.* **1966**, *22*, 138. Mullen, K. I.; Wang, D.-X.; Crane, L. G.; Carron, K. T. *Anal. Chem.* **1992**, *64*, 930.
- [8] Bryant, M. A.; Crooks, R. M. *Langmuir* **1993**, *9*, 385.
- [9] Chailapakul, O.; Crooks, R. M. *Langmuir* **1993**, *9*, 884.
- [10] Krysinski, P.; Brzostowska-Smolka, M. *J. Electroanal. Chem.* **1997**, *424*, 61.
- [11] Sabatani, E.; Rubinstein, I.; Maoz, R.; Sagiv, J. *J. Electroanal. Chem.* **1987**, *219*, 365.
- [12] Amatore, C.; Savéant, J. M.; Tessier, D. *J. Electroanal. Chem.* **1983**, *147*, 39.
- [13] Polymeropoulos, E. E.; Sagiv, J. *J. Chem. Phys.* **1978**, *69*, 1836.
- [14] Sun, L.; Johnson, B.; Wade, T.; Crooks, R. M. *J. Phys. Chem.* **1990**, *94*, 8869.
- [15] Bilewicz, R.; Majda, M. *J. Am. Chem. Soc.* **1991**, *113*, 5464.
- [16] Nakashima, N.; Taguchi, T. *Colloids Surf.* **1995**, *A103*, 159.
- [17] Katz, E.; Lion-Dagan, M.; Willner, I. *J. Electroanal. Chem.* **1996**, *408*, 107.
- [18] Solov'ev, A. A.; Katz, E. *J. Electroanal. Chem.* **1990**, *277*, 377.
- [19] Ives, D. J. G.; Janz, G. J. (eds.) *Reference Electrodes*, Academic Press, New York, **1961**.
- [20] Von Stackelberg, M.; Pilgram, M.; Toome, V. *Z. Elektrochem.* **1953**, *57*, 342.
- [21] Ulman, A. *An Introduction To Ultrathin Organic Films. From Langmuir-Blodgett To Self Assembly*, Academic Press Inc. San Diego, CA **1991**.
- [22] Tsutsumi, H.; Furumoto, S.; Morita, M.; Matsuda, Y. *J. Electrochem. Soc.* **1992**, *139*, 1522.
- [23] Gileadi, E. *Electrode Kinetics For Chemists, Chemical Engineers & Materials Scientists*, VCH, **1993**, p. 435.
- [24] Wagner, A. F.; Folkers, K. *Vitamins and Coenzymes*, Interscience, New York, **1964**, p. 244.
- [25] Wang, J.; Frostman, L. M.; Ward, M. D. *J. Phys. Chem.* **1992**, *96*, 5224.
- [26] Cheng, Q.; Brajter-Toth, A. *Anal. Chem.* **1996**, *68*, 4180.
- [27] Nicholson, R. S. *Anal. Chem.* **1965**, *37*, 1351.
- [28] Bard, A. J.; Crayston, J. A.; Kittleson, G. P.; Shea, T. V.; Wrighton, M. S. *Anal. Chem.* **1986**, *58*, 2321.

## FINAL CONCLUSIONS AND FUTURE PROSPECTS

The objective of this research was to determine if it is fundamentally possible to achieve pH modulated release from monolayer systems. The investigations focused on the formation of monolayers and by studying the electrochemical properties of the films the permeation of the films to ions, solvent molecules and larger complexes was explored. Electrochemical techniques, while extremely useful for the permeation studies, are limited by the type of probe compound available. Other means of studying permeability are essential to complement the work. Broader approaches, such as the use of colorimetric/fluorimetric diagnostic tests to monitor permeation through monolayers mounted on porous supports, would provide further insight into the issue of molecular diffusion.

The area of drug release is so case specific that many factors have to be taken in to consideration when designing a release system, e.g., the size, charge, and  $pK_a$  of drug molecule, its interaction with the components of the system, and the effects of indigenous biological components on the system. The complexity of the task necessitates a more collaborative approach, and it would be far more beneficial to focus efforts on the design a system for a particular application, in conjunction with the pharmaceutical industry.

Realistically, it seems unlikely following our investigations, that pH induced structural changes within ordered polymer systems will modulate drug release. The compact TDA monolayers formed were essentially impermeable and since they do not possess the degree of freedom necessary for rearrangement/expansion upon ionization, will remain impermeable. On the hand, the less dense TA layers remained permeable regardless of the extent of monolayer ionization. Despite the attempts to imitate biological membranes through the fabrication of monolayer systems, the systems studied lack the fluidity necessary for a change in structure. It seems that disordered hydrogels and ionizable polymers, disadvantages aside, possess a structure that is better disposed to rearrangement, expansion and the molecular release.